A Novel High-Throughput In-Cell Western Assay for the Quantitative Measurement of Signaling Dynamics in DNA Damage Signaling Networks – Cell Decision Processes in Response to DNA Double Strand Breaks

by

Andrea R. Tentner

B.A. Biological Sciences
University of Chicago, 2003

Submitted to the Department of Biological Engineering in Partial Fulfillment of the Requirements for the Degree of

Master of Science in Biological Engineering
at the
Massachusetts Institute of Technology
[June 2006]
February 2006

Signature of Author: _____
Department of Biological Engineering
January 6, 2006

Certified by: _____
Michael B. Yaffe
Howard S. and Linda E. Stern Associate Professor of Biology and Biological Engineering
Thesis Supervisor

Accepted by: _____
Alan Grodzinsky
Professor of Electrical, Mechanical, and Biological Engineering
Chairman, Committee for Graduate Students

A Novel High-Throughput In-Cell Western Assay for the Quantitative Measurement of Signaling Dynamics in DNA Damage Signaling Networks – Cell Decision Processes in Response to DNA Double Strand Breaks

by

Andrea R. Tentner

Submitted to the Department of Biological Engineering on January 6, 2006 in Partial Fulfillment of the Requirements for the Degree of Master of Science in Biological Engineering

Abstract

Following exposure to DNA damage, cells initiate a stress response involving multiple protein kinase signaling cascades. The DNA damage response results in one of several possible cell-fate decisions, or cellular responses: induction of cell-cycle arrest, initiation of DNA repair, activation of transcriptional programs, and either apoptosis, necrosis or cell senescence. The mechanisms by which cells make these decisions, and how cell fate depends upon variables such as DNA damage type and dose, and other environmental factors, is unknown. The process by which cells select among alternate fates following such stimuli, or "cues" is likely to involve a dynamic, multi-variate integration of signals from each of the kinase signaling components. A major goal of signal transduction research is to understand how information flows through signal transduction pathways downstream of a given cue, such as DNA damage, and how signals are integrated, in order to mediate cellular responses.

Mathematical modeling approaches are necessary to advance our understanding of these processes. Indeed, statistical mining and modeling of large datasets, consisting of quantitative, dynamic signaling and response measurements, is capable of yielding models that identify key signaling components in a given cue-response relationship, as well as models that are highly predictive of cellular response following novel cues that perturb the same network.

We have validated a novel assay system that allows for the high throughput collection of quantitative and dynamic signaling data for 7 protein kinases or phospho-proteins known to be "hubs" in the DNA damage response and/or general stress response networks, including ATM, Chk2, H2AX, JNK, p38, ERK and p53. This novel high-throughput In-cell Western assay is based on

immuno-fluorescent staining and detection of target proteins in a "whole cell" environment, performed and visualized in a 96-well plate format. This assay allows for the detection and measurement of up to 7 target proteins in triplicate, over up to 3 treatment regimes, or up to 21 signals for a single treatment, simultaneously. Pre-processing steps, and steps involved in the protocol itself are significantly fewer (and require smaller amount of most reagents and biological material), as compared to traditional signal measurement methods, such as quantitative Western analysis and kinase assays.

We have used this novel high-throughput In-cell Western assay to investigate the DNA damage response after the specific induction of DNA double strand breaks (DSB). We have measured the dynamics of seven "hub" proteins modified with activating phosphorylations (as a surrogate measure of protein activity) that span major branches of the DNA damage, stress, and death signaling networks, following the specific induction of DNA double strand breaks. Signaling proteins measured include ATM, Chk2, H2AX, JNK, p38, ERK and p53. In parallel with these signaling measurements, we have quantitatively measured corresponding phenotypic responses, such as cell cycle profile and apoptosis.

In future work, we will use a Partial Least Squares (PLS) regression analysis approach to construct a statistical model using this data, which is predictive of the cellular responses included in our measurements, following perturbation of this branch of the DNA damage response network. This analysis should reveal key signaling components involved in the decision-making process (possible molecular targets for the improvement of cancer therapy regimens that rely upon the induction of DSB, e.g. the topoisomerase inhibitor, cisplatin), and provide a basis for constructing new, and improving existing, physico-chemical models of this branch of the DNA damage response network.

Thesis Supervisor: Michael B. Yaffe and Forest White
Title: Howard S. and Linda E. Stern Associate Professor of Biology and Biological Engineering and Assistant Professor of Biological Engineering

Table of Contents

I. Introduction

Signal transduction networks are extremely complex. They consist of highly inter-connected and redundant signaling pathways, which are constantly receiving input from intra- and extra-cellular cues. These overlapping and redundant pathways allow a cell to integrate a large amount of information regarding its extra-cellular environment and its intra-cellular status in order to make important decisions regarding its fate. Such cell decisions may depend on multiple "cues" such as extra-cellular growth factors or intracellular viral antigens. The relationship between any received cue and the phenotypic response of the cell resulting from that cue is determined by the overall state of the signal transduction network at the time the cue is received. In other words the state of the network determines how information flows through it.

A major goal of research in signal transduction is to understand how information flow through a network results in a given outcome. In order to understand the cell decision process, it is necessary to follow information flow ("signals") through various network states following perturbations to that network ("cues") and to record the resultant corresponding phenotypes ("responses"). From this data, it should be possible to extract the features of the information flow that were influential in mediating those phenotypes.

Many signaling molecules participate in signal transduction networks, and it is not possible or necessary to measure them all. Instead it is more efficient to measure the signals in the network that are most likely to carry critical information that will influences the decision-making processes. For certain cue-response pairs, many of the influential signaling molecules may be known. For example, Akt is a critical signaling molecule in mediating survival ("response") after exposure of cells to insulin ("cue") (Janes, Albeck et al. 2003).

I. Mathematical Modeling as an Approach to Biological Problems

The relationship between the signaling information and the resultant phenotypes is complex and non-intuitive, and analysis of data relating network states to outcomes requires mathematical modeling approaches. Partial least squares regression analysis (PLS) has been applied to data extraction problems in fields ranging from meteorology to sociology. PLS is capable of finding statistically significant inter-relationships between dependent and independent variables in multivariate data-sets when the number of independent variables is large and relationships are no longer intuitive. PLS is effective at "reducing dimensionality"; that is, PLS identifies a few factors or combinations of factors that are important in the determination of the dependent variable, out of a very large number of input parameters in the model. PLS can be thought of as a modification or extension of multiple linear regression analysis (MLR), but differs from MLR in several ways (Tobias). MLR gives a linear relationship between a dependent variable and a large number of independent variables, producing a

weighting matrix of factors relating the dependent variable to the independent variables that is of the same rank as the number of input independent variable (the manifest factors). If the number of independent variables is greater than the number of observations in the data set, this type of regression analysis will tend to over-fit the data as not all manifest factors accounting for the variation in the sample used to train the model will significantly account for variation in the population from which the sample was drawn. Thus the model will well fit the training data, but may lack predictive ability for new data. In the case where the number of independent variables is greater than the number of observations in the data set, PLS is a more appropriate analysis technique. PLS is capable of finding a reduced set of underlying, or latent, factors, that may also be combinations of manifest factors, and that account for most of the manifest variation in response (Tobias; Janes, Kelly et al. 2004). These latent factors are expected to significantly account for the variation in the dependent variables and the covariation between these inter-independent variable variations and the dependent variable in the sample data and in the population from which the sample data was taken. A model constructed using PLS is therefore expected to have predictive capabilities for new data under these conditions (Tobias).

PLS and MLR analyses require large amounts of quantitative, reproducible data as input. A caveat on the predictive capability of a model constructed using PLS is that the original model must be sufficiently trained to accommodate such predictions. That is, in order for the model's predictive ability to be robust, it must encompass signaling data from cues that highly perturb the network and result in highly variable response phenotype in order to stretch the dynamic range of each of the measured network signaling and response components(Gaudet, Janes et al. 2005).

Since many proteins participate in signal transduction networks downstream of any given cue that mediates a response, the trajectory of their activity between the time of the cue and the mediated response is important in determining what that response will be. Thus, it is necessary to collect quantitative, dynamic data regarding the activity of the important molecules in the signal transduction network following various cues that perturb the network to lead to differential phenotypes. In addition, the model will also require quantitative data regarding the corresponding phenotypic outcome. In such a model, the signaling data are the independent variables and the responses are the dependent variables.

Janes et al. pioneered the application of PLS to biological problems in their analysis of a data set of protein measurements in the context of TNF-induced apoptosis (Janes, Albeck et al. 2003). Janes et al. developed a heterogeneous set of assays capable of measuring levels and/or activities of 20-30 intracellular signals thought to be important in the cytokine response network under study (Janes, Albeck et al. 2003; Janes, Kelly et al. 2004). These included kinase assays, quantitative westerns, and antibody arrays. Many assays

concentrated on direct measurement of kinase activity or on indirect measurement of the same by measurement of levels of kinase modified with activating phosphorylations, since protein kinases are some of the most important molecular mediators in signal transduction events and are expected to carry much of the information that is influential in cell decision processes.

Janes et al rigorously showed that these assays generated data that was quantitative and reproducible both over time, and between assays (Janes, Kelly et al. 2004; Gaudet, Janes et al. 2005). With these data, Janes et al. constructed extremely accurate predictive models of apoptotic response to various cytokine cues in HT-29 cell lines. These models exceeded the expectations of the investigators, and were capable even of predicting the apoptotic response of a different cell type to various cytokine cues (a model trained on the HT-29 cell line signal-response is able to predict HeLa cell line response) as well as the apoptotic response of this cell type to a cue of a completely different character (a model trained on cytokine/mitogen stimulation is able to predict response to an invading pathogen such as adenovirus).

II. Project Goals

In the current project, we had two major goals:

- To develop an In-cell Western (ICW)-based assay system that will allow the measurement of signaling dynamics in a high throughput, quantitative and reproducible manner
- To use this assay system to study the signaling dynamics specifically involved in the cellular response to DNA double strand breaks (DSB) and to collect data for future construction of a predictive statistical model using the PLS methods

III. DNA damage response

DNA damage is an intracellular "cue" that results in perturbation of signal transduction networks and leads to cell fate decisions. Following exposure to DNA damage, cells initiate a stress response involving multiple protein kinase signaling cascades (Fig. 1). The DNA damage response results in one of several possible cell-fate decisions: induction of cell-cycle arrest, initiation of DNA repair, activation of transcriptional programs, and either apoptosis, necrosis or cell senescence (Khanna and Jackson 2001; Zhou and Bartek 2004). The mechanisms by which cells make these decisions are not known.

It is widely accepted that DNA damage causes cancer (Khanna and Jackson 2001; Kastan and Bartek 2004). In addition, intentional damage to the DNA of tumor cells is used to treat cancer (Baldwin and Osheroff 2005), and the inadvertent damage to non-tumor cells is partially responsible for the side effects associated with cancer treatment (Allan and Travis 2005). Cellular DNA is

constantly being damaged as a result of attack by endogenous and exogenous sources (e.g. oxygen radicals produced in metabolic processes and environmental ionizing radiation respectively) and as a result of normal DNA replication. Therefore, a greater understanding of how information flow through DNA damage signaling networks mediates cell decision processes regarding fate is highly relevant to the prevention and effective treatment of human cancer.

DNA can be damaged in many ways, leading to a variety of lesions that are thought to have specific sensors. Signals arising from these specific sensors are integrated into the general DNA damage signaling network. Most treatments used to induce DNA damage (clinically or experimentally) produce a broad spectrum of lesions, and so responses to general types of treatments have been better characterized than responses to specific lesions. The cellular response to ionizing radiation (IR) and ultraviolet radiation (UV) are perhaps the best studied.

The Serine/Threonine PI(3) Kinase-like kinases (PIKKs) ATM (Ataxia-telangiectasia mutated) and ATR (Ataxia-telangiectasia and RAD3-related) are among the most proximal players in response to IR and UV-induced DNA damage (Tibbetts, Brumbaugh et al. 1999; Klein, Muijtjens et al. 2000), possibly even serving to directly sense DNA damage (Khanna and Jackson 2001; Kastan and Bartek 2004). Following IR treatment, ATM, which exists in the nucleus as a resting homodimer, is the PIKK that is preferentially activated in a multi-step process that is necessary for full activation (Tibbetts, Brumbaugh et al. 1999). This process involves intermolecular auto-phosphorylation on Ser-1981, dissociation of ATM-homodimers, and localization of monomeric ATM to sites of damage on the DNA (Bakkenist and Kastan 2003). Activated ATM in turn serves to activate the downstream effector kinase Chk2 on Thr-68 (Matsuoka, Rotman et al. 2000; Zhou, Chaturvedi et al. 2000; Bartek and Lukas 2003). ATM also participates in the activation of the p53 transcription factor by phosphorylation of p53 on Ser-15 (Caspari 2000). Following UV treatment, ATR is preferentially activated (Tibbetts, Brumbaugh et al. 1999). Under normal cellular conditions, ATR is found in complex with ATRIP (ATR-interacting protein), a small interacting protein with a considerable affinity for replication protein A (RPA) (Cortez, Guntuku et al. 2001; Unsal-Kacmaz and Sancar 2004). Unlike ATM, the intrinsic kinase activity of ATR is not greatly increased following DNA damage. The increased functional activity of ATR under these conditions is, instead, likely to be the result of the localization of ATR to sites of DNA damage, via the affinity of complexed ATRIP, for RPA that coats ssDNA at sites of DNA damage either before or after processing of the lesion (Zou and Elledge 2003). Once activated, ATR serves to phosphorylate the downstream effector kinase Chk1 on Ser-317 and Ser-345 (Lopez-Girona, Tanaka et al. 2001; Zhao and Piwnica-Worms 2001). The small Chk1-interacting protein, Claspin, is required for the ATR-mediated phosphorylation and activation of Chk1 (Lee, Gold et al. 2005). Claspin binds RPA and chromatin; it binds to Chk1 when it has been dually phosphorylated on Ser-864 and Ser-895 and it is likely required to bring Chk1 into close proximity with ATR (Jeong, Kumagai et al. 2003). ATR is also

activated in response to IR, although probably later and not as strongly as ATM; in the absence of ATM, ATR can partially compensate for its function by phosphorylating and activating downstream targets of ATM (Cliby, Roberts et al. 1998; Kim, Lim et al. 1999). Additionally, ATR localizes to sites of collapsed replication forks, and seems to be required for regulation of normal cell cycle progression (Cobb, Schleker et al. 2005). In the absence of ATR, ATM is unable to compensate, and ATR(-/-) mutants are embryonic lethal (Klein, Muijtjens et al. 2000).

Chk1 and Chk2 play a key role in mediating cell cycle arrest in G1 and G2/M following DNA damage by phosphorylating CDC25 family members. Chk1 is thought to mediate a G1 arrest through phosphorylation of CDC25A, targeting it for ubiquitination and degradation (Bulavin, Amundson et al. 2002; Ho, Siu et al. 2005). Phosphorylation of CDC25B or CDC25C by Chk1 and Chk2 also results in a 14-3-3 binding site and cytoplasmic sequestration required for the induction of a G2/M arrest following IR (O'Connell, Walworth et al. 2000). Chk1 and Chk2 (in addition to ATM and ATR) also phosphorylate p53 (Caspari 2000). p53 participates in the long term maintenance of cell cycle arrest, by transcriptionally upregulating the cdk inhibitor p21 and other factors, as well as the induction of apoptosis (Vousden 2000; Appella and Anderson 2001; Yoon, Chen et al. 2003; Yoon and Yang 2004). It has been shown recently by the Yaffe lab and the Fornace lab that the p38 SAPK pathway is activated following UV treatment, and it has been proposed that p38 activation of MAPKAPK2/Chk3 acts as another branch in the DNA damage response, in analogy to the ATM-Chk2 and ATR-Chk1 branches. Indeed, MAPKAPK2/Chk3 shares a high functional similarity to the other Chk effector kinases in mediating cell cycle arrest following UV (Manke, Nguyen et al. 2005). MAPKAPK2/CHK3 has been shown to phosphorylate CDC25B/C following UV, generating the 14-3-3 binding site necessary for cytoplasmic sequestration, and it has been shown that loss of MAPKAPK2/Chk3 results in an inability to sustain a G2/M or a G1/S checkpoint following UV-induced DNA damage (Manke, Nguyen et al. 2005).

Rapid response of the DNA damage signaling network is mediated by post-translational modifications which lead to rapid activation, localization and degradation of various signaling components (Appella and Anderson 2001; Kastan and Bartek 2004). Maintenance of these initial responses (e.g. the maintenance of a cell cycle checkpoint in order to allow for on-going DNA repair) requires transcriptional up-regulation of signaling components; transcriptional upregulation of p21, for example, is required for maintenance of the G1 checkpoint (Appella and Anderson 2001; Yoon, Chen et al. 2003; Kastan and Bartek 2004; Yoon and Yang 2004).

Although some DNA damaging chemotherapeutic agents (particularly topoisomerase inhibitors, such as doxorubicin (DOX)) cause other types of DNA damage to a certain extent, it is thought that the ability of these agents to kill cancer cells is due mainly to their ability to induce DNA double strand breaks

(DSB) (Khanna and Jackson 2001; Baldwin and Osheroff 2005). Here, we used calicheamicin (CLM), an enediyene antibiotic agent that is capable of specifically inducing DSB without other known types of DNA damage (Elmroth, Nygren et al. 2003; Prokop, Wrasidlo et al. 2003), to study cellular signaling and response pathways downstream of this type of DNA lesion.

IV. Calicheamicin (CLM)

Calicheamicin (CLM) is a naturally occurring enediyne anti-cancer antibiotic that was first discovered in the fermentation broth of Micromonospora echinospora ssp. Calichensis (Fig. 2A) (Liang)). CLM potently and specifically induces DNA double strand breaks (DSB). The mechanism for the specificity of the lesion created by CLM has been extensively investigated. Attack of the central sulfur atom of the CLM tri-sulfide group by a nucleophile (such as glutathione) results in a conformational change in the structure of the CLM molecule. This conformational change places strain on the 10-membered enediyene-containing ring, which is completely relieved when the enediyene undergoes the Bergman cyclization reaction (Fig. 2B) (Nicolaou, Smith et al. 1993). An intermediate of this cyclization reaction is a highly reactive benzenoid diradical that, when CLM is docked to DNA is a site-specific manner, abstracts hydrogen atoms from one DNA strand at the C-5' position of the 5' cytidine in 5'-TCCT-3', and from the C-4' position of the nucleotide on the complementary strand three base pairs removed on the 3'side. This results in the cleavage of both strands of DNA (Nicolaou, Smith et al. 1993). The chemical structure of the DNA lesion remaining on each of the DNA strands following CLM attack is determined by the position at which it has been attacked (4' C on one strand, 5' C on adjacent strand). 4'-deoxyribose chemistry frequently leads to strand breaks and abasic sites on the DNA and 5'-deoxyribose chemistry can lead to strand breaks with bulky lesions (M.S. DeMott, private communication) (Lopez-Larraza, Moore et al. 2001; Chen, Bohnert et al. 2004). Once the reaction has taken place, the CLM enediyne function is lost; thus no further DNA may be cleaved.

CLM appears capable of inducing DSB far more specifically than other methods of DSB induction used either experimentally to study the DSB response or clinically to treat various cancers, with some sources citing percentages of CLM-induced DNA damage in the form of DSB as high as 95% (Lopez-Larraza, Moore et al. 2001). The relative rates of DNA double strand break (DSB) and DNA single strand break (SSB) induction for several DNA damaging agents are listed in Table 1 (Nicolaou, Smith et al. 1993; Banath and Olive 2003; Ismail, Nystrom et al. 2005).

Table 1

DNA damaging agent	SSB:DSB
Calicheamicin	2:1
Bleomycin	5:1
X-rays	20:1
γ-IR	100:1
4-nitro-quinoline-N-oxide	100:1
Hydrogen peroxide	1000:1

This specificity for DSB induction is desirable experimentally as it allows the signaling response to DSB to be evaluated independent of the signaling response to other DNA lesions such as single strand breaks (SSB) and base damage, or the signaling response to damage to other cellular components such as proteins and lipids.

In vitro, CLM treatment of a wide range of cell lines results in strong DSB response and cell cycle arrest (Elmroth, Nygren et al. 2003) as well as a potent induction of cell death. CLM has highly variable levels of cytotoxicity depending on cell-line, with IC50s ranging from femtomolar (fM) to micromolar (μM) concentrations in a panel of 11 tumor cells lines tested (Nicolaou, Smith et al. 1993). It also shows preferential cytotoxicity in tumor cell lines over normal cell lines. In a panel of 4 normal cell lines tested, including bone marrow and dermal fibroblast cells that frequently experience bystander effects from chemotherapeutic regimens, measured IC50s were micromolar (μM) and higher. This preference may prove clinically useful. Cell death following CLM treatment seems to proceed largely by apoptosis (Nicolaou, Smith et al. 1993), though it has also been observed in some cell types that death can occur by mitotic catastrophe; this involves the accumulation of aneuploid cells that undergo several abnormal mitoses without cell division before dying (in vitro and in vivo observation) (Mekid, Tounekti et al. 2003).

Clinically, it has been shown that most tumor cell death following treatment with DNA damaging chemotherapeutics is due to the induction of DSB, and it is widely accepted that DSB are the most cytotoxic of DNA lesions (Khanna and Jackson 2001), so chemotherapeutics that can specifically induce DSB may be expected to be highly efficacious in cancer treatment. Indeed, treatment with CLM has been shown to increase survival in mice injected with tumor cell lines (Nicolaou, Smith et al. 1993). CLM linked to targeting antibodies has also been shown effective against acute myeloid leukemia, renal cell carcinoma and ovarian cancer (Elmroth, Nygren et al. 2003). As such, CLM is a specific inducer of DNA double strand breaks that is expected to be a highly valuable tool in the laboratory and in the clinic.

V. DSB Signaling and Response

Here we investigated the effects of calicheamicin treatment on DNA damage signaling and cellular response. We chose to measure seven signals (as allowed by our assay format, discussed in section VII) involved, or hypothesized to be involved in, the cellular signaling and response to DSB: phospho-ATM (Ser-1981), phospho-H2AX (Ser-139), phospho-Chk2 (Thr-68), phospho-p53 (Ser-15), phospho-p38 (Thr-182/Tyr-184), phospho-JNK (Thr-183/Tyr-185), and phospho-ERK (Thr-180/Tyr-182).

As discussed previously, ATM is a PI(3)Kinase-like kinase that is thought to be one of the most proximal signals activated following induction of IR-induced DSB (Burma, Chen et al. 2001). It is very important for primary signal transduction to effector kinases, such as Chk2, and to transcription factors, such as p53. ATM also phosphorylates H2AX on Ser-139 (Burma, Chen et al. 2001; Friesner, Liu et al. 2005). ATM deficient cells are highly sensitive to radiation and to chemotherapeutic agents that cause DSB (Taylor and Byrd 2005).

H2AX phosphorylation is one of the first measurable responses to DSB (Celeste, Fernandez-Capetillo et al. 2003). It becomes phosphorylated on Ser-139 and is incorporated into a 2Mb region surrounding a break and can be visualized in microscopic foci (Burma, Chen et al. 2001; Banath and Olive 2003). It is thought to be important in stabilizing the characteristic multi-protein complexes that form at sites of DSB. The stabilization of these foci is necessary for activation and coordination of repair and checkpoint proteins (Celeste, Fernandez-Capetillo et al. 2003; Mochan, Venere et al. 2004). Mice lacking H2AX have cell-cycle checkpoint defects and pre-disposition to cancer. H2AX is also located in a cytogenetic region that is commonly mutated in human cancers (11q23) (Bassing, Heikyung et al. 2003).

Chk2 is the primary effector kinase known to be activated by ATM by phosphorylation at Thr-68 (Matsuoka, Rotman et al. 2000; Zhou, Chaturvedi et al. 2000). As previously discussed, it is an important player in mediating cell cycle arrest in both G1 and G2/M via phosphorylation of CDC25 family members (O'Connell, Walworth et al. 2000). It has also been implicated in promoting apoptosis (Takai, Naka et al. 2002).

p53 is a transcription factor that is implicated both in promoting apoptosis in response to a wide variety of stresses, including genotoxic stress, and in maintenance of cell cycle arrest responses (Giaccia and Kastan 1998; Prives and Hall 1999; Vousden 2000). It is a substrate for ATM and ATR on Ser-15 and for Chk1 and Chk2 on Ser-20 (Caspari 2000).

p38, JNK and ERK kinases are all MAPK members of the MAPK (Mitogen Activated Protein Kinase) family. While MAPK family members are not traditionally thought of as part of the specific DNA damage, or DSB, response,

these important cellular proteins are widely accepted to be key elements in the regulation of cell fate decisions such as cell cycle control and apoptosis in nearly all cell types, and they undoubtedly play a role in regulation of cell fate following genotoxic stress. The MAPK family of signaling pathways is eukaryotic-specific and highly conserved (Orton, Sturm et al. 2005) (Chang and Karin 2001) (Sumbayev and Yasinska 2005). This family of signaling pathways consists of several specific pathways all sharing a general three-kinase signal cascade format in which a MAPKKK (MAPK kinase kinase) serine/threonine kinase is activated, dually phosphorylates and activates a MAPKK (MAPK kinase) dual specificity kinase, that, in turn, dually phosphorylates and activates a MAPK (MAP kinase) serine/threonine kinase on a TXY motif in the MAPK activation loop (Yung, Dolginov et al. 1997) (Chang and Karin 2001). MAPKs are serine-threonine kinases with a repertoire of at least 80 substrates consisting of transcription factors, protein kinases and cytoskeletal components (Fritz and Kaina 2005). There are relatively few MAPKs, just five, the best characterized in mammals being p38, JNK, and ERK1/2. However, they are involved in the mediation of such wide-ranging and key cellular processes as cellular growth, differentiation, adaptation to stress, survival and death in response to such diverse stimuli as growth factors, cytokines, cellular adherence status and hypoxic and genotoxic stress (Orton, Sturm et al. 2005) (Chang and Karin 2001). The ability of these few kinases to respond to such a wide variety of stimuli is not fully understood, but is probably facilitated by the MAPK cascade set-up and the ability of several MAPKKK to initiate each cascade (Chang and Karin 2001).

ERK(1/2) is the MAPK downstream in the three-kinase MAPK pathway consisting of Raf/MEK/ERK (Bose, Motiwale et al. 2005). ERK is activated by the MAPK kinases MEK1 and MEK2 in response to such growth factors as EGF and PDGF (Widmann, Gibson et al. 1999; Chang and Karin 2001). Its role in the regulation of cell proliferation and differentiation in response to various growth factors and mitogenic signals is well established (Bose, Motiwale et al. 2005). However, it is also implicated in both cell cycle control and protection from cell death in some cell types (Widmann, Gibson et al. 1999; Chang and Karin 2001), and it is activated in cells following treatment with several genotoxic agents (Solhaug, Refsnes et al. 2004) (Bose, Motiwale et al. 2005). We hypothesize that ERK participates in regulation of cell fate decisions regarding cell cycle control and cell death in response to the induction of DSB.

p38 is a MAPK family member that is activated by the MAPK kinases MEK3 and MEK6 (Widmann, Gibson et al. 1999) in response to cellular stresses, such as genotoxic and osmotic stress, and inflammatory cytokines, such as TNF-α and IL-1 (Deacon and Blank 1997). Its known substrates include the transcription factor ATF2 and the protein kinase MAPK activated protein kinase-2 (MAPKAPK2/Chk3) (Deacon and Blank 1997) (Manke, Nguyen et al. 2005). p38 has a role in mediating cytokine production and apoptosis (Chang and Karin 2001; Sumbayev and Yasinska 2005), as well as in cell cycle checkpoint induction and apoptosis following DNA damage (Manke, Nguyen et al. 2005)

(Fritz and Kaina 2005). We hypothesize that p38 participates in regulation of cell fate decisions regarding cell cycle control and cell death in response to the induction of DSB.

JNK is a MAPK family member that is activated by the MAPK kinases MEK4 and MEK7 (Widmann, Gibson et al. 1999) in response to such cellular stresses as genotoxic (eg UV light, γ-irradiation) and osmotic stess, and in response to inflammatory cytokines, such as TNF-α and IL-1) (Solhaug, Refsnes et al. 2004) (Bose, Motiwale et al. 2005) (Xia, Makris et al. 2000) (Sumbayev and Yasinska 2005) (Fritz and Kaina 2005). Its known substrates include the Jun-family transcription factors (c-Jun, c-Fos, ATF2) (Chang and Karin 2001; Fritz and Kaina 2005). JNK is implicated in the induction of apoptosis in several cell types (Sumbayev and Yasinska 2005) (Chang and Karin 2001) (Fritz and Kaina 2005). We hypothesize that JNK participates in regulation of cell fate decisions regarding cell death in response to the induction of DSB.

In addition to these cellular signals, we also measured the cellular response to CLM in several ways. We quantified the extent of cell death (cleaved caspase-3 detection and sub-G1 DNA content population) and cell cycle profiles (relative PI incorporation) in populations of cells following DSB induction. These cellular responses were measured by direct DNA or immuno-staining and subsequent FACS (fluorescence assisted cell sorting) analysis.

VI. In-Cell Western Assay (ICW)

Janes et al. gathered protein signaling data to build a data set appropriate for statistical modeling approaches such as partial least squares regression analysis (PLS) using several assay approaches, including kinase activity assays, quantitative immunoblots and antibody micro-arrays. There are several drawbacks to each of these approaches: Each of these assays requires several pre-processing steps before they may be performed, and are themselves non-trivial, multi-step protocols. Initial validation of kinase activity assays and of antibody micro-array assays is as well an arduous process, and all of these assay protocols require considerable amounts of biological material and reagents. The development of an alternative and/or additional assay for the rapid collection of quantitative, dynamic protein signaling data is highly desirable.

The In Cell Western (ICW) assay provides a high throughput way to gather quantitative, dynamic signaling data. This assay format allows for the measurement of up to 7 signals in triplicate, in response to up to three treatment regimes, or the measurement of up to 21 signals in triplicate after a single treatment. It offers distinct advantages over other assay systems which have been used in the measurement of signaling dynamics. Almost no pre-processing of the samples is required and the protocol itself consists of far fewer processing steps for each measurement than traditional western analysis or kinase activity

assays. Smaller reagent quantities and less biological material is required to obtain measurements.

In the ICW assay, cells are first seeded and grown in a 96-well plate format. Cells are treated with the appropriate cue, fixed, permeabilized and immuno-stained in the same 96-well plate. Bound primary antibodies are detected and prepared for visualization by incubation with IRDye 800CW-conjucated secondary antibodies, which are conjugated to dye molecules with absorption and emission maxima in the infrared range. Stained cells are then visualized using an Odyssey IR scanner. The scanner has two solid state lasers with excitation wavelengths of 680 and 780nm. Absorption maxima of the dyes conjugated to the secondary antibodies are closely matched to these excitation wavelengths (Alexa fluor-680 conjugated secondary antibodies and Topro-3 Iodide DNA stain are excited with the 680nm laser, with absorbance maxima respectively of 679nm and 642nm; IRDye800CW conjugated secondary antibodies are excited with the 800nm laser, with absorbance maxima at 774nm). Because the emission maxima of the dyes excited by the two lasers are narrow, and separated by about 100nm, signal overlap is minimized.

The two lasers simultaneously excite each point on the scanner bed surface during a scan. Light from both fluorescing infrared dyes is collected by a microscope objective focused on the point of excitation. Light is passed to a dichroic mirror that transmits light above 810nm and reflects light below 750nm to split the light into two signals. The two signals are then received by two physically separated silicon avalanche diodes. Each light signal is translated into a detectable current and given a pseudo-color intensity that is directly proportional to the measured current (red for the light collected from excitation with the 680nm laser and green for light collected from excitation with the 780nm laser) (LiCor Biosciences, 2005).

The ability of the Odyssey scanner to detect signal from dyes fluorescing in the IR range is directly responsible for its ability to deliver sensitive, quantitative and reliable data. Chemi-luminescent detection methods offer an indirect enzymatic detection of primary antibody bound. This detection is highly dependent upon both reaction start time and exposure time, preventing accurate quantitation of primary signal. In contrast, every IR-dye conjugated antibody fluoresces when excited by the Odyssey laser, allowing for a more linear response and accurate quantitation of signal (LiCor Biosciences, 2005). Use of IR wavelengths offers a distinct advantage over methods using fluorescence in the visible wavelengths, which are hampered by auto-fluorescence from both plates and cells.

We have validated this assay system for the simultaneous measurement of seven signals that are expected to be informative nodes in the cellular DSB response.

II. Materials and Methods

I. Antibodies and Reagants

Primary Phospho-Specific Antibodies:

Antigen detected, animal source, lot #, source, catalog #; dilution used

p38, Thr-180/Tyr-182, rabbit polyclonal, lot #14, CST, catalog #9211; 1:100
ATM, Ser-1981, mouse monoclonal, lot#24675, Upstate, catalog #05-740; 1:500
H2AX, Ser-139, rabbit polyclonal, lot #2, CST, catalog #2577; 1:200
Chk2, Thr-68, rabbit polyclonal, lot #5, CST, catalog #2661; 1:250
p53, Ser-15, rabbit polyclonal, lot #6, CST, catalog #9284; 1:500
JNK, Thr-183/Tyr-185, rabbit polyclonal, lot #8, CST, catalog #9251; 1:100
ERK, Thr-202/Tyr-204, rabbit monoclonal, lot #2, CST, catalog #4377; 1:100
H3, Ser-10, rabbit polyclonal, lot #, Upstate, catalog #, 1:

Primary Non-Phospho Antibodies:

Antigen detected, source; dilution used

Anti-Cleaved caspase-3, BD #559565;1:500

Secondary Antibodies:

Antigen detected, source; dilution used

800CW IR-Dye Goat anti-Rabbit, Rockland; 1:500
800CW IR-Dye Goat anti-Mouse, Rockland; 1:500
800CW IR-Dye Donkey anti-Mouse, Rockland; 1:500
Alexa fluor 647-conjugated Donkey anti-Rabbit IgG, Molecular Probes; 1:250
Alexa fluor 488-conjugated Goat anti-Rabbit IgG, Molecular Probes; 1:30

DNA Stain:

Topro-3 Iodide, Molecular Probes; 1:2500

Propidium Iodide (PI), Sigma (10mg/ml in PBS)

Other Reagants and Materials:

Calicheamicin (CLM), generous gift of Pete Dedon and M. DeMott (100uM in MeOH)
Doxorubicin, Sigma (10mM in water)
Odyssey Blocking Buffer, Licor
PMA, phorbol 12-myristate 13-acetate, Sigma (5mg/ml in EtOH)

II. Antibody Validation Experiments

Cell culture conditions for Ab dilution experiments (Fig. 3):

In order to determine optimal antibody concentrations for primary antibodies, tissue culture treated 96-well plates were seeded with U2OS cells at 10,000 cells per well in 200ul total volume of DME/HEP media supplemented with 10% FBS, 1% penicillin/streptomycin, and 1% glutamine (total media). Edge wells were not seeded with cells but received the same total volume of media as other wells. Wells were covered immediately with low-evaporation membranes in addition to plate tops and incubated overnight at 37°C.

Cell culture conditions for Cell number dilution experiments (Fig. 4):

In order to assay for linearity of primary antibody binding, tissue culture treated 96-well plates were seeded with U2OS cells as follows: Wells in Row B (wells B2-B11) were seeded at 10,000 cells per well in 200ul total volume of DME/HEP media supplemented with 10% FBS, 1% penicillin/streptomycin, and 1% glutamine (total media). Wells in Row C (wells C2-C11) were seeded at 8,000 cells per well in 200ul total media. Rows D, E, F and G were seeded at 6,000 cells/well, 4,000 cells/well, 2,000 cells/well and no cells respectively. Edge wells received the same total volume of media as other wells but were not seeded. Wells were covered immediately with low-evaporation membranes in addition to plate tops and incubated overnight at 37°C prior to experiments.

--Treatment and fixation—

ATM, Chk2, H2AX (100nM CLM):

In order to evaluate primary antibodies with specificity for active forms of ATM, Chk2 and H2AX, cells were treated with 100nM calicheamicin in total media or with control media and incubated at 37°C for 15 minutes before fixation with 4% formaldehyde in PBS. Briefly, 100uM calicheamicin (CLM) stock in a MeOH carrier was diluted 1000-fold in total media for a final treatment concentration of 100nM CLM. Control media consisted of an equivalent volume of 100% MeOH diluted in total media. Media was aspirated from two consecutive columns in a 96-well plate using an 8-channel manifold aspirator and replaced with 100ul control media, using an 8-channel pipette. Media was then aspirated

from two (or three) adjacent consecutive columns and replaced with 100ul 100nM CLM media. Plates were immediately returned to a 37°C incubator and incubated for 15 minutes before removing. Media from all wells was aspirated and replaced with 150ul 4% formaldehyde in PBS. Plates were then allowed to sit at room temperature, without shaking for 20 minutes.

p38, JNK (500mM NaCl):

In order to evaluate primary antibodies with specificity for active forms of p38 and JNK, cells were treated with 500mM NaCl in total media or with control media and incubated at 37°C for 30 minutes before fixation with 4% formaldehyde in PBS. Briefly, 5M NaCl stock in H20 was diluted 10-fold in total media for a final treatment concentration of 500mM NaCl. Control media consisted of total media. Media was aspirated from two (or three) consecutive columns in a 96-well plate using an 8-channel manifold aspirator and replaced with 100ul control media, using an 8-channel pipette. Media was then aspirated from three adjacent consecutive columns and replaced with 100ul 500mM NaCl media. Plates were immediately returned to a 37°C incubator and incubated for 30 minutes before removing. Media from all wells was aspirated and replaced with 150ul 4% formaldehyde in PBS. Plates were then allowed to sit at room temperature, without shaking for 20 minutes.

p53 (10μM DOX):

In order to evaluate primary antibodies with specificity for one active form of p53, cells were treated with 10uM doxorubicin (DOX) in total media or with control media and incubated at 37°C for 12-14hrs before fixation with 4% formaldehyde in PBS. Briefly, 10mM doxorubicin stock in H20 was diluted 1000-fold in total media for a final treatment concentration of 10uM doxorubicin. Control media consisted of total media. Media was aspirated from two (or three) consecutive columns in a 96-well plate using an 8-channel manifold aspirator and replaced with 100ul control media, using an 8-channel pipette. Media was then aspirated from three adjacent consecutive columns and replaced with 100ul 10uM doxorubicin media. Plates were immediately returned to a 37°C incubator and incubated for 12-14 hours before removing. Media from all wells was aspirated and replaced with 150ul 4% formaldehyde in PBS. Plates were then allowed to sit at room temperature, without shaking for 20 minutes.

ERK (100nM PMA):

In order to evaluate primary antibodies with specificity for the active form of ERK, cells were serum-starved over-night in DME/HEP media + 0.1% FBS + 1% penicillin/streptomycin + 1% glutamine. They were then treated with 100nM PMA in total media or with control media and incubated at 37°C for 10 minutes before fixation with 4% formaldehyde in PBS. Briefly, 8.1mM PMA stock in H_20 was diluted 81,000-fold in total media for a final treatment concentration of 100nM PMA. Control media consisted of total media. Media was aspirated from two (or three) consecutive columns in a 96-well plate using an 8-channel manifold aspirator and replaced with 100ul control media, using an 8-channel

pipette. Media was then aspirated from three adjacent consecutive columns and replaced with 100ul 100nM PMA media. Plates were immediately returned to a 37°C incubator and incubated for 10 minutes before removing. Media from all wells was aspirated and replaced with 150ul 4% formaldehyde in PBS. Plates were then allowed to sit at room temperature, without shaking for 20 minutes.

Immuno-staining and visualization was done as described in section VI (In-Cell Western Staining).

III. Time-course cellular signaling experiments

In order to investigate the time-dependent cellular signaling following CLM treatment, the following protocol was used.

Cell culture conditions for monitoring cellular signaling following CLM treatment (Fig. 5):
Tissue culture treated 96-well plates were seeded with U2OS cells at 6,000 cells per well in 200ul total volume of DME/HEP media supplemented with 10% FBS, 1% penicillin/streptomycin, and 1% glutamine (total media). Side edge wells were not seeded with cells but received the same total volume of media as other wells. Top and bottom edge wells were seeded as described. Wells were covered immediately with low-evaporation membranes in addition to plate tops and incubated overnight at 37°C.

--Treatment and fixation—

** We found that it was important that cells not be incubated for long periods with media containing CLM. Therefore, treatment of cells with CLM media was limited to a 15 minute period, at which point CLM media was replaced with fresh total media.

0 time-points:
0 time points correspond to no treatment. Briefly, media from all wells was aspirated and replaced with 150ul 4% formaldehyde in PBS. Plates were then allowed to sit at room temperature, without shaking for 20 minutes. 4% formaldehyde was then manually aspirated with an 8-channel pipette and replaced with 150ul PBS.

5 and 15 minute time-points:
Cells were treated with 50nM CLM in total media, 5nM CLM in total media or with control media. Plates were then returned to a 37°C incubator for 5 and 15 minute incubation times. Twenty seconds before each time-point, corresponding time-point plates were removed from incubator. Media from all wells was aspirated and replaced with 150ul 4% formaldehyde in PBS. Plates were then allowed to sit at room temperature, without shaking for 20 minutes. 4% formaldehyde was then manually aspirated with an 8-channel pipette and

replaced with 150ul PBS. Treatment media was not replaced with fresh total media before fixation for these time-point plates.

24h-30min time-points:

Plates were removed, treated and returned to a 37°C incubator in waves consisting of 3 plates each, beginning with latest time-point plates and excluding time-point plates below 30 minutes (Time-point plates from 24 hours to 30 minutes included). Cells were treated with 50nM CLM in total media, 5nM CLM in total media or with control media and incubated at 37°C for 15 minutes before replacement of treatment media with fresh total media in all wells, return to a 37°C incubator for the remainder of the incubation time set for each time-point plate, and fixation with 4% formaldehyde in PBS at the end of that incubation time. Briefly, 50uM CLM stock or 5uM CLM stock in MeOH was diluted 1000-fold in total media for final treatment concentrations of 50nM or 5nM CLM. Control media consisted of an equivalent volume of 100% MeOH diluted in total media. Media was aspirated from four consecutive columns (Columns 2-5) on each of three 96-well plates using an 8-channel manifold aspirator and replaced with 100ul control media, using an 8-channel pipette. Media was then aspirated from three adjacent consecutive columns (Columns 6-8) on each of the three 96-well plates and replaced with 100ul 5nM CLM media. Media was then aspirated from three adjacent consecutive columns (Columns 9-11) on each of the three 96-well plates and replaced with 100ul 50nM CLM media. Plates were immediately returned to a 37°C incubator and incubated in treatment media for 15 minutes. Treated plates were then removed in the same order, one wave at a time. Treatment media was aspirated from all wells in one plate in a wave at a time, beginning with latest time-point plates, and replaced with 200ul fresh total media. Plates were immediately returned to a 37°C incubator for the incubation time remaining for each time-point.

Twenty seconds before each time-point, corresponding time-point plates were removed from incubator. Media from all wells was aspirated and replaced with 150ul 4% formaldehyde in PBS. Plates were then allowed to sit at room temperature, without shaking for 20 minutes. 4% formaldehyde was then manually aspirated with an 8-channel pipette and replaced with 150ul PBS.

Immuno-staining and visualization was done as described in section VI (In-Cell Western Staining).

IV. Time-course cellular response experiments

In order to investigate the time-dependent cellular response to CLM treatment, the following protocol was used.

Cell culture conditions for monitoring cellular response following CLM treatment:

10cm plates were seeded with U20S cells at 1.3 x 10^6 cells per plate in 10ml total media and allowed to incubate overnight at 37°C prior to experiments.

--Treatment and fixation—

Previously seeded 10 cm plates were removed, treated with 50nM CLM in total media, 5nM CLM in total media or control media and returned to a 37°C incubator for 15 minutes. Plates were then removed and treatment media was replaced with 9ml fresh total media and returned to a 37°C incubator for the remaining incubation time set for each time-point. Treatment and replacement of treatment media with fresh total media was done in waves consisting of 6 plates each, beginning with plates to be collected at the latest time point. Each wave consisted of all plates to be collected at one of the three response time points: 12, 24 and 48 hours. 50nM and 5nM CLM treatment media and control media was made as described for time-course treatment of 96-well plates. Briefly, for each wave, six 10 cm plates were removed from 37°C incubator. Media was aspirated from two plates and replaced with 5ml of 50nM CLM media. Media was aspirated from two more plates and replaced with 5ml of 5nM CLM media. Media was aspirated from the final two plates in the wave and replaced with 5ml of control media. Plates were immediately returned to a 37°C incubator for 15 minutes. Plates from that wave were then removed. Media from those treated with 50nM CLM was aspirated and replaced with 9ml fresh total media. Media from those treated with 5nM CLM was aspirated and replaced with 9ml fresh total media. Finally, media from those treated with control media was aspirated and replaced with 9ml fresh total media. Plates were then returned to a 37°C incubator for the remaining incubation time set for that time-point.

Twenty seconds before each time-point all six plates to be collected were removed from 37°C incubator. Beginning with those treated with 50nM CLM media, media was removed from two like-treated plates and reserved in pre-labeled 15ml falcon tubes. Plates were then rinsed with 2ml PBS. PBS was removed and reserved in same pre-labeled 15ml tubes, then replaced with 1.5ml trypsin + 0.2%EDTA. Plates treated with 5nM CLM media and control media were treated in a like manner. All plates were then returned to a 37°C incubator for 2 minutes to allow for cell detachment, then removed. Beginning with those plates treated with 50nM CLM media, 10ml of reserved media from the corresponding pre-labeled 15ml tube was added to quench trypsin and completely detach cells. Media was pipetted up and down a couple of times to clear the whole plate and then returned to the corresponding 15ml falcon tube. Plates treated with 5nM CLM and control media were treated in a like manner.

All 15ml tubes were spun at 1000g for 5 minutes and the supernatant was aspirated. Cell pellets were resuspended in 400ul 4% formaldehyde in PBS, transferred to pre-labeled 1ml eppendorf tubes and allowed to sit at room temperature for 10-15 minutes. Tubes were spun 2 minutes at 4000rpm (all subsequent spins are at 4000rpm for 2 minutes, through staining procedure), supernatant was removed and cells were resuspended in 1ml PBS. Tubes were

spun, supernatant was removed and cells were resuspended in 400ul 100% MeOH. Tubes were stored at -20°C until staining for FACS analysis (cells can be stored for at least one week).

Immuno-staining and visualization was done as described in section VII (FACS Staining).

V. Positive control experiments (time course): positive controls used for normalization of time course experiments

In each experiment, it was necessary to establish positive controls for each of the signals measured for normalization purposes.

Treatment media and control media are all as described in Treatment procedure for validation experiments (section II).

ATM, CHK2, H2AX (Fig. 6):

Media from 5 consecutive columns (Columns 2-6) was aspirated and in only three rows (Rows 3-5) was replaced with 100ul control media using a one-channel pipette. Media from 5 adjacent consecutive columns (Columns 7-11) was aspirated and in only three rows (Rows 3-5) was replaced with 100ul 100nM CLM in total media. The plate was immediately returned to a 37°C incubator and incubated for 15 minutes before removing. Media from all wells was aspirated and replaced with 150ul 4% formaldehyde in PBS. The plate was then allowed to sit at room temperature, without shaking for 20 minutes. 4% formaldehyde was then manually aspirated with an 8-channel pipette and replaced with 150ul PBS.

p38, JNK (Fig. 7):

Media from 5 consecutive columns (Columns 2-6) was aspirated and in only two rows (Rows 3-4) was replaced with 100ul control media using a one-channel pipette. Media from 5 adjacent consecutive columns (Columns 7-11) was aspirated and in only two rows (Rows 3-4) was replaced with 100ul 500mM NaCl in total media. The plate was immediately returned to a 37°C incubator and incubated for 30 minutes before removing. Media from all wells was aspirated and replaced with 150ul 4% formaldehyde in PBS. The plate was then allowed to sit at room temperature, without shaking for 20 minutes. 4% formaldehyde was then manually aspirated with an 8-channel pipette and replaced with 150ul PBS.

p53, ERK (Fig. 8):

Media from 5 consecutive columns (Columns 2-6) was aspirated and in only one row (Row 3) was replaced with 100ul control media using a one-channel pipette. In one more row (Row 4) aspirated media was replaced with DME/HEP + 0.1% FBS + 1% penicillin/streptomycin + 1% glutamine (serum-starvation media). Media from 5 adjacent consecutive columns (Columns 7-11) was

aspirated and in only one row (Row 3) was replaced with 100ul 10uM doxorubicin in total media. In one more row (Row 4) aspirated media was replaced with DME/HEP + 0.1% FBS + 1% penicillin/streptomycin + 1% glutamine (serum-starvation media). The plate was immediately returned to a 37°C incubator and incubated for 12 hours (over-night) before removing. Media from Row 4, Columns 7-11 was aspirated and replaced with 100ul of 100nM PMA. The plate was returned to a 37°C incubator and incubated for 10 minutes before removing. Media from all wells was aspirated and replaced with 150ul 4% formaldehyde in PBS. The plate was then allowed to sit at room temperature, without shaking for 20 minutes. 4% formaldehyde was then manually aspirated with an 8-channel pipette and replaced with 150ul PBS.

Immuno-staining and visualization was done as described in section VI (In-Cell Western Staining).

VI. In-cell Western (ICW) Staining

For plates during time-courses: 4% formaldehyde was replaced with 200ul PBS and allowed to remain in PBS without shaking until at least 4 plates had been fixed and it was convenient to begin the triton permeabilization (usually after the 4 hour time-point has been collected). PBS was then aspirated and replaced with the first of five triton permeabilization solution changes (150ul 0.1% Triton in PBS). Remaining procedure is as described below.

For In-cell Western staining, 4% formaldehyde was manually aspirated from all wells with an 8-channel pipette and replaced with 150ul 0.1% Triton in PBS (triton permeabilization). All subsequent aspirations were done using an 8-channel manifold aspirator. Plates were gently shaken on a nutator for 5 minutes. Triton permeabilization solution was aspirated, replaced with 150ul fresh triton permeabilization solution and gently shaken for 5 minutes. Triton permeabilization solution changes were repeated for a total of 5 changes. Final triton permeabilization solution change was aspirated, replaced with 150ul Odyssey Blocking Buffer and gently shaken at room temperature for 1.5 hours. Odyssey Blocking Buffer was aspirated, replaced with 50ul primary antibody diluted in Odyssey Blocking Buffer, gently shaken at room temperature for 1 hour and then placed at 4°C overnight without shaking.

Primary antibody solution was aspirated, replaced with 150ul 0.1% Tween in PBS (tween wash) and gently shaken at room temperature for 5 minutes. Tween wash was aspirated, replaced with 150ul fresh tween wash and gently shaken for 5 minutes. Tween washes were repeated for a total of 4 washes. Final tween wash was aspirated and replaced with 50ul secondary antibody solution (secondary antibody (1:500 dilution)+ Topro-3 DNA stain (1:2500 dilution) diluted in Odyssey Blocking Buffer + 0.5% Tween). Plates were covered to protect from light and gently shaken at room temperature for 1 hour. Secondary antibody solution was aspirated, replaced with 150ul 0.1% Tween in PBS (tween wash)

and gently shaken at room temperature for 5 minutes. Tween wash was aspirated, replaced with 150ul fresh tween wash and gently shaken for 5 minutes. Tween washes were repeated for a total of 4 washes. Final tween wash was aspirated thoroughly. Plates were tapped upside down on an absorbent surface to remove any remaining moisture in the wells, covered to protect from light and placed at 4C until scanned.

ICW visualization and analysis:

Plates were scanned on an Odyssey Infrared Scanner and analyzed using Odyssey software.

VII. FACS Staining

In order to assay for apoptosis and cell cycle profile of cell populations from the same biological samples, the following protocol was used. Cells in 400ul 100% MeOH were resuspended by pipetting. 150ul from each sample was transferred to a pre-labelled 1ml eppendorf tube and both aliquots were returned to -20°C until stained for FACS. The 250ul aliquot from each biological sample was stained for cleaved caspase 3 to assay for apoptosis, and the 150ul aliquot was stained for phospho-H3 and with propidium iodide to assay for cell cycle profile of the population, using the following respective protocols below.

Cleaved Caspase-3

Cells were repelleted by spinning at 4000rpm for 2 minutes in a microcentrifuge, and methanol was removed. Cells were resuspended in 400ul PBS + 0.1% Tween (PBS-T). Cells were repelleted, PBS-T removed, and 100ul of primary antibody diluted in PBS-T +1% BSA (PBS-TB) added. Cells were resuspended by pipetting up and down and incubated with primary antibody for one hour at room temperature. 400ul PBS-T was added and cells were repelleted, supernatant was removed, and cells were resuspended in another 400ul PBS-T. Cells were repelleted, PBS-T wash was removed, resuspended in 100ul of secondary antibody diluted in PBS-TB, and incubated at room temperature for one hour, covered to protect from light. 400ul PBS-T was added and cells were repelleted. Supernatant was removed, cells were resuspended in another 400ul PBS-T and repelleted again. PBS-T wash was removed and cells were resuspended in 400ul of PBS-TB. Tubes were left overnight at 4°C, covered to protect from light, then transferred into FACS tubes for immediate analysis.

PI/Phospho-H3

Cells were repelleted by spinning at 4000rpm for 2 minutes in a microcentrifuge, methanol was removed, cells were resuspended in 1ml PBS and repelleted. Cells were washed once more in PBS, repelleted and resuspend in 400ul of PBS + 0.25% Triton for 15 minutes on ice. Cells were then repelleted and resuspended in 100ul PBS + 1% BSA + 0.75ug of anti-histone H3-phospho antibody and allowed to incubate for three hours at room temperature. Cells

were then repelleted, resuspended in 400ul PBS + 1% BSA then spun, resuspended in 100ul PBS + 1% BSA + goat anti-rabbit IgG FITC (Alexa fluor 488) at 1:30 and allowed to incubate at room temperature for 30 minutes covered to protect from life. Cells were then spun, washed with 1ml PBS and finally, resuspended in 600ul PBS + 50ug propidium iodide + 1mg RNase. Tubes were left overnight at 4°C, covered to protect from light, then transferred into FACS tubes for immediate analysis.

FACS data was acquired using CellQuest software and analyzed using FlowJo software.

III. Results and Discussion

Results

I. Experimental Design and Optimization of the In-Cell Western (ICW) assay

The goal of our work is to quantitatively monitor the activity of proteins that contribute to the DNA damage response. To further this aim, In-Cell Western (ICW) assays were developed to monitor the phosphorylation of p38, ATM, H2AX, Chk2, p53, JNK and ERK. The In-Cell Western assay was chosen because it provides a straightforward means of collecting multiple time-dependent data points. The In-Cell Western assay involves 6 steps that are schematicized in Fig. 5: i) cells are seeded in 96-well plates, ii) cells are treated with an agent of choice, iii) cells are fixed, permeabilized and blocked, iv) cells are immuno-stained with antibodies raised against proteins and/or phospho-proteins of interest, v)primary antibodies are detected using an IR Dye800CW-conjugated secondary antibody and a measure of cell density is achieved by staining DNA with Topro-3 Iodide and vi) experiments are visualized using the LiCor Odyssey IR Scanner.

Identification of antibodies suitable for monitoring DNA damage response protein phosphorylation by ICW

An essential preliminary step in the development of ICW assays is the indentification of antibodies for the phopho-proteins of interest. The antibodies must fulfill the following requirements: (i) these antibodies must bind their target with a sufficient affinity so as to be detectable by ICW, (ii) the antibodies must be highly specific for their target, such that changes in signal detection can be taken to be reflective of changes in target levels, (iii) the antibodies must detect their target over a wide range of target protein concentration, and (iv) the detection signal must be proportional to the concentration of target protein over a sufficient range of protein concentration range. Antibody specificity is critical in the ICW assay format because detected proteins can not be separated by molecular weight as is the case in the traditional Western assay format. For each of the proteins of interest (p38, ATM, H2AX, Chk2, p53, JNK and ERK), multiple commercially available phospho-specific antibodies were screened for use in the ICW format. A single high-affinity antibody for each phospho-protein was identified for use in subsequent experiments.

Commercial antibodies to be tested were chosen based upon Western blots provided by the manufacturer. Antibodies were chosen if they showed specificity for phosphorylated species over non-phosphorylated species, and a lack of background bands. The presence of background bands will decrease the ratio of signal between the background and the phosphoprotein of interest. The conditions under which proteins are detected in traditional and In-Cell Western

protocols differ dramatically, and as such, the availability of target epitopes will likewise differ between these protocols. Therefore, it is not expected that antibodies with sufficient affinity and specificity may be rigorously identified through examination of traditional Westerns alone. For example, in the case of one phospho-specific Akt antibody tested (CST #4056), no background bands were detected in traditional Western format, but this antibody showed high background in ICW format (Fig. 9, A and B). Nonetheless, the pre-screening process generally gave valuable information as to the suitability of a given antibody for use in the ICW assay.

Antibodies possessing these characteristics were tested for their ability to bind their target antigens with sufficient affinity and specificity in the ICW format. For antibodies with sufficient affinity and specificity, the optimal antibody concentration for target detection was determined.

Each antibody target was a protein modified by an activating phosphorylation or phosphorylations. In order to activate each protein of interest and induce these phosphorylations, cells were either treated or not treated with an agent known to lead to the modification of each of the respective proteins of interest (activating treatment). Following treatment and fixation, cells were immuno-stained in the In-cell Western format, with primary antibody dilutions of 1:50, 1:100, 1:250, 1:500, 1:1000, 1:2000 and 1:5000 (See Materials and Methods and Fig. 3 for a detailed explanation of Antibody dilution experiments). Sufficiency of specificity and affinity of each antibody for its target was determined by comparing the signal detected under treated (signal) and non-treated (background) conditions. The optimal antibody concentration was determined for those antibodies whose signal:background ratio was high. The optimal antibody concentration for each antibody was the concentration at which the signal:background ratio was maximized.

Determination of Dynamic Range and Linearity

Cell number dilution experiments were performed with antibodies for which the optimal antibody concentration had been determined. The goals of these experiments were to determine if the antibodies yield a detection signal over a sufficiently wide range of target protein concentration and to show that the signal is directly proportional to the concentration of target protein over a sufficiently wide range of target protein concentration.

In order to vary levels of protein concentration in the wells, cell density in the wells was varied. Cells were seeded at 10,000, 8,000, 6,000, 4,000, 2,000 and 0 cells per well (See Materials and Methods and Fig. 4 for a detailed explanation of Cell number dilution experiments). Differentially seeded wells were treated or not treated as in the antibody dilution experiments.

Antibodies were considered to have a sufficient dynamic range if signal was detected from the lowest concentration of target protein assayed (corresponding to 2,000 cells plated per well and treated with activating treatment) and if signal (signal detected from cells treated with activating treatment) was always above background (signal detected from cells not treated with activating treatment). Antibodies were considered to have a sufficient linear range if the detected signal was linear with respect to target protein concentration from the concentration of target protein represented by 0 cells plated per well to the concentration of target protein represented by 6,000 cells plated per well.

Phospho-ATM (Ser-1981)

ATM is phosphorylated on Serine 1981 following the induction of DNA double strand breaks, and this phosphorylation is a marker of ATM activation (Bakkenist and Kastan 2003). In the antibody validation experiments, ATM was activated by treating cells with 100nM calicheamicin for 15 minutes. Calicheamicin is a potent inducer of DNA double-strand breaks.

The Upstate antibody had a good signal:background ratio over the range of antibody concentrations assayed (Fig. 10A, pictured left panel, plotted A right panel). At an antibody dilution of 1:500 (corresponding to incubation of the wells with 0.1ug of antibody in 50ul total volume) signal:background is maximized with signal more than 6-fold greater than background (Fig 10A, right panel, arrow). A 1:500 dilution was considered to be the optimal antibody dilution for this antibody, and all subsequent experiments were performed using this dilution.

Using this optimal antibody dilution, signal was detected at the lowest concentration of target protein assayed (corresponding to 2,000 cells plated per well) and signal was always above background (Fig. 10B, pictured left panel, plotted right panel). Signal detected was linear with respect to target protein concentration, from the concentration of target protein represented by 0 cells plated per well, to the concentration of target protein represented by 8,000 cells plated per well (Fig. 10C, right panel). We considered that this antibody has sufficient dynamic and linear range to yield reliable, quantitative data that is directly reflective of levels of phospho-ATM. Above some protein concentration represented by 8,000 cells plated per well, antibody bound and detected was no longer linear and entered a plateau phase. Above this protein concentration, the antibody capture and detection step are unlikely to linearly report phospho-protein abundance in the wells.

Phospho-Chk2 (Thr-68)

Chk2 is phosphorylated on Threonine 68 following the induction of DNA double strand breaks, and this phosphorylation is a marker of Chk2 activation (Matsuoka, Rotman et al. 2000; Melchionna, Chen et al. 2000). Chk2 was

activated in antibody validation experiments by treating cells with 100nM CLM for 15 minutes.

The Cell Signaling Technologies antibody had a very good signal:background ratio over almost the whole range of antibody concentrations assayed and signal:background continued to increase with increasing antibody concentration (Fig. 11A, pictured left panel, plotted A right panel). At an antibody dilution of 1:250 (corresponding to incubation of wells with 0.02ug of antibody in 50ul total volume) signal:background is very high, with signal more than 10-fold greater than background (Fig 11A, right panel, arrow). Higher concentration of antibody (although somewhat further increasing the signal:background ratio) was considered unnecessary. A 1:250 dilution was considered to be the optimal antibody dilution for this antibody, and all subsequent experiments were performed using this dilution.

Using this optimal antibody dilution, signal was detected at the lowest concentration of target protein assayed (corresponding to 2,000 cells plated per well) and signal was always above background (Fig. 11B, pictured left panel, plotted right panel). Signal detected was linear with respect to target protein concentration, from the concentration of target protein represented by 0 cells plated per well, to the concentration of target protein represented by 6,000 cells plated per well (Fig. 11C, right panel). This antibody has sufficient dynamic and linear range to yield reliable, quantitative data that is directly reflective of levels of phospho-Chk2. Above a protein concentration represented by 6,000 cells plated per well, antibody bound and detected was no longer linear and entered a plateau phase. Above this protein concentration, the antibody capture and detection step is unlikely to linearly report phospho-protein abundance in the wells.

Phospho-H2AX (Ser-139)

H2AX is phosphorylated on Serine 139 following the induction of DNA double strand breaks, and this phosphorylation is a marker of activation (Burma, Chen et al. 2001; Mochan, Venere et al. 2004; Friesner, Liu et al. 2005). H2AX was activated in Antibody dilution experiments by treating cells with 100nM CLM for 15 minutes.

The Cell Signalling Technologies antibody had a good signal:background ratio over a large range of antibody concentrations assayed and signal:background always increased with increasing antibody concentration (Fig. 12A, pictured left panel, plotted A right panel). At an antibody dilution of 1:200 (corresponding to incubation of wells with 0.025ug of antibody in 50ul total volume) signal:background is very high, with signal more than 10-fold greater than background (Fig 12A, right panel, arrow). Higher concentration of antibody (although further increasing the signal:background ratio) was considered unnecessary. A 1:200 dilution was considered to be the optimal antibody dilution

for this antibody, and all subsequent experiments were performed using this dilution.

Using this optimal antibody dilution, signal was detected at the lowest concentration of target protein assayed (corresponding to 2,000 cells plated per well) and signal was always above background (Fig. 12B, pictured left panel, plotted right panel). Signal detected was linear with respect to target protein concentration, from the concentration of target protein represented by 0 cells plated per well, to the concentration of target protein represented by 6,000 cells plated per well (Fig. 12C, right panel). This antibody has sufficient dynamic and linear range to yield reliable, quantitative data that is directly reflective of levels of phospho-H2AX. Above a protein concentration represented by 6,000 cells plated per well, antibody bound and detected was no longer linear and entered a plateau phase. Above this protein concentration, the antibody capture and detection step is unlikely to linearly report phospho-protein abundance in the wells.

Phospho-JNK (Thr-183/Tyr-185)

JNK is dually phosphorylated on Threonine 183 and Tyrosine 185 following various cellular stresses, including osmotic stress. Phosphorylation is a marker of JNK activation (Deacon and Blank 1997; Yung, Dolginov et al. 1997). JNK was activated in Antibody dilution experiments by treating cells with 500mM NaCl for 30 minutes.

The Cell Signaling Technologies antibody exhibits a lower absolute signal than Phospho-ATM, Chk2 or H2AX antibodies. However, it had acceptable signal:background ratio over almost the whole range of antibody concentrations assayed (Fig. 13A, pictured left panel, plotted A right panel). At an antibody dilution of 1:100 (corresponding to incubation of wells with 0.05ug of antibody in 50ul total volume) signal to background ratio is close to its consistent maximum with signal more than 3-fold greater than background (Fig 13A, right panel, arrow). At this dilution, absolute signal was significantly higher than that detected using lower antibody concentrations. A 1:100 dilution was considered to be the optimal antibody dilution for this antibody, and all subsequent experiments were performed using this dilution.

Using this optimal antibody dilution, signal was detected at the lowest concentration of target protein assayed (corresponding to 2,000 cells plated per well) and signal was always above background (Fig. 13B, pictured left panel, plotted right panel). Signal detected was linear with respect to target protein concentration, from the concentration of target protein represented by 0 cells plated per well, to the concentration of target protein represented by 6,000 cells plated per well (Fig. 13C, right panel). This antibody has sufficient dynamic and linear range to yield reliable, quantitative data that directly reports levels of phospho-JNK. Above a protein concentration represented by 6,000 cells plated

per well, the amount of antibody bound and detected was no longer linear and entered a plateau phase. Above this protein concentration, the antibody capture and detection step cannot be relied upon to linearly reflect phospho-protein abundance in the wells.

Phospho-p38 (Threonine 180/Tyrosine 182)

p38 is dually phosphorylated on Threonine 180 and Tyrosine 182 following various cellular stresses, such as osmotic stress, and this phosphorylation is a marker of p38 activation (Deacon and Blank 1997; Yung, Dolginov et al. 1997). p38 was activated in Antibody dilution experiments by treating cells with 500mM NaCl for 30 minutes.

The Cell Signaling Technologies phospho-p38 antibody had a lower absolute signal than phospho-ATM, phospho-Chk2 or phospho-H2AX antibodies. However, it had acceptable signal:background ratio over a limited range of antibody concentrations assayed (Fig. 14A, pictured left panel, plotted right panel). At an antibody dilution of 1:100 (corresponding to incubation of wells with 0.05ug of antibody in 50ul total volume) signal:background is maximum with signal more than 3-fold greater than background (Fig 14A, right panel, arrow). A 1:100 dilution was considered to be the optimal antibody dilution for this antibody, and all subsequent experiments were performed using this dilution.

Using this optimal antibody dilution, signal was detected at the lowest concentration of target protein assayed (corresponding to 2,000 cells plated per well) and signal was always above background (Fig. 14B, pictured left panel, plotted right panel). Signal detected was linear with respect to target protein concentration, from the concentration of target protein represented by 0 cells plated per well, to the concentration of target protein represented by 8,000 cells plated per well (Fig. 14C, right panel). This antibody has sufficient dynamic and linear range to yield reliable, quantitative data that is directly reflective of levels of phospho-JNK. Above a protein concentration represented by 8,000 cells plated per well, the amount of antibody bound and detected was no longer linear and entered a plateau phase. Above this protein concentration, the antibody capture and detection step can not be relied upon to linearly reflect phospho-protein abundance in the wells.

Phospho-ERK (Threonine 182/Tyrosine 184)

ERK is dually phosphorylated on Threonine 182 and Tyrosine 184 following stimulation with various cytokines and growth factors. This phosphorylation is a marker of ERK activation (Deacon and Blank 1997; Yung, Dolginov et al. 1997; Orton, Sturm et al. 2005). The activating treatment used in validating phopho-ERK antibodies is overnight serum starvation followed by treatment of cells with 100nM phorbol 12-myristate 13-acetate (PMA, a diacylglycerol (DAG) analog) for 5 minutes.

The Cell Signaling Technologies antibody had a lower absolute signal than Phospho-ATM, Chk2 or H2AX antibodies. However, it had acceptable signal:background ratio over a limited range of antibody concentrations assayed (Fig. 15A, pictured left panel, plotted right panel). At an antibody dilution of 1:100 (corresponding to incubation of wells with 0.05ug of antibody in 50ul total volume) signal:background is close to its maximum with signal more than 3-fold greater than background (Fig 15A, right panel, arrow). A 1:100 dilution was considered to be the optimal antibody dilution for this antibody, and all subsequent experiments were performed using this dilution.

Using this optimal antibody dilution, signal was detected at the lowest concentration of target protein assayed (corresponding to 2,000 cells plated per well) and signal was always above background (Fig. 15B, pictured left panel, plotted right panel). Signal detected was linear with respect to target protein concentration, from the concentration of target protein represented by 0 cells plated per well, to the concentration of target protein represented by 6,000 cells plated per well (Fig. 15C, right panel). This antibody has sufficient dynamic and linear range to yield reliable, quantitative data that is directly reflective of levels of phospho-ERK. Above a protein concentration represented by 6,000 cells plated per well, antibody bound and detected was no longer linear and entered an exponential rise phase. Above this protein concentration, the antibody capture and detection step can not be relied upon to linearly reflect phospho-protein abundance in the wells.

p53 (Serine 15)

p53 is phosphorylated on Serine 15 following induction of general DNA damage. This phosphorylation is a marker of p53 activation (Caspari 2000; Appella and Anderson 2001). The activating treatment used in validation experiments for the phospho-p53 antibody is treatment of cells with 10uM doxorubicin (DOX) for 12 hours.

The Cell Signaling Technologies antibody had a lower absolute signal than phospho-ATM, phospho-Chk2 or phospho-H2AX antibodies. Treatment with DOX, in addition to activating p53, is pro-apoptotic and leads to apoptosis in some percentage of treated cells. U2OS cells become non-adherent when they are apoptotic, and it is difficult to retain these cells for staining in the In-cell Western format. As a result, there are fewer cells available for staining in the treated populations than in the untreated populations and so the detected signal must be normalized based on this reduced number of cells. In order to accommodate this requirement, treated and untreated cells were stained concurrently with a DNA stain (for cell number normalization) and immunologically for phospho-p53 (Fig. 16A and B, left and middle panels). In wells containing treated cells, as opposed to in wells containing untreated cells, significantly fewer cells remained following fixation and staining (compare Fig.

16A, middle panel, (-) and (+) and Fig. 16B, middle panel, (-) and (+)). Following normalization of signal to DNA present, it was found that this antibody had acceptable signal:background ratio over a limited range of antibody concentrations assayed (Fig. 16A, pictured left and center panel, plotted right panel). At an antibody dilution of 1:500 (corresponding to incubation of wells with 0.01ug of antibody in 50ul total volume) signal:background is maximum with signal nearly 10-fold greater than background (Fig 16A, right panel, arrow). A 1:500 dilution was the optimal antibody dilution for this antibody, and all subsequent experiments were performed using this dilution.

Using this optimal antibody dilution, signal was detected at the lowest concentration of target protein assayed (corresponding to 2,000 cells plated per well) and signal was always above background (Fig. 16B, pictured left and center panel, plotted right panel). Signal detected was linear with respect to target protein concentration, from the concentration of target protein represented by 0 cells plated per well, to the concentration of target protein represented by 6,000 cells plated per well (Fig. 16C, right panel). This antibody has sufficient dynamic and linear range to yield reliable, quantitative data that is directly reflective of levels of phosphorylation of p53. Above a protein concentration represented by 6,000 cells plated per well, antibody bound and detected was no longer linear and entered a plateau phase. Above this protein concentration, we considered that the antibody capture and detection step can not be relied upon to linearly reflect phospho-protein abundance in the wells.

Antibodies incompatible with the ICW format

Antibodies tested but not selected based on failure of one or more of these conditions are listed in Table 2

Table 2.

Target protein	**Manufacturer**	**Mode of failure**
Phospho-JNK	Biosource	High background
Phospho-ATM, Ser-1981	Rockland	Low signal
Phospho-Akt	CST #4056	High background
Phospho-ERK	CST #4376	High background
Phospho-p38	CST #9216	High background
Phospho-MK2	CST	High background
Phospho-MK2	CST	High background
Phospho-hsp27	CST	High background
Phospho-p53, Ser-15	Calbiochem	High background
Phospho-p53, Ser-20	Calbiochem	Low signal
Phospho-p53, Ser-20	CST	High background
p53, total	CST	High background

Experimental Considerations

As was the case for the activating treatment used in the validation of the phospho-p53 antibody, many treatments will lead to apoptosis in some percentage of the population. Because of this, it is necessary to normalize the signal to the cell number present. Therefore, in all subsequent experiments, In-cell Western staining consisted of concurrent staining with DNA stain (for cell number normalization) and immunological staining for target protein.

For each antibody validated for use in subsequent experiments, the amount of antibody bound was not linear above some protein concentration in the wells. In this non-linear range, the antibody capture and detection step can not be relied upon to linearly reflect phospho-protein abundance. The threshold for non-linear antibody binding varied among antibodies, but was never lower than a protein concentration represented by 6,000 cells plated per well. Therefore, in all subsequent experiments, cells were seeded at 6,000 cells per well in order to ensure linearity of detection and to maintain a parallel and consistent seeding step.

Experiments were highly reproducible and intra-assay error was almost always ≤ 10%. As such, the high throughput ICW assays are capable of providing reproducible, quantitative measurements of levels of target proteins modified with activating phosphorylations.

II. Analysis of the calicheamicin-induced DSB response

U2OS cells are a p53 wild type human osteosarcoma cell line that die in response to ionizing radiation (IR)-induced double strand breaks (DSB). We determined that U2OS cells also die in response to DSB induced by the enidyne antibiotic agent, calicheamicin (CLM), and that the extent of this response is highly dose-dependent (Fig. 20). We also determined that U2OS cells exhibit severe cell cycle phenotypes in response to CLM-induced DSB and that the cell-cycle phenotype exhibited varies dramatically in a dose-dependent manner (Fig. 21, 22). Based on these results, we set out to investigate the differential signaling dynamics, following treatment with various doses of CLM, which might be involved in mediating these dramatic dose-dependent phenotypic differences.

U2OS cells were treated with 0nM, 5nM or 50nM CLM in triplicate well samples per experiment, over two separate experiments (Fig. 5), and formaldehyde fixed for signal analysis at 12 time points over 27 hours. There is a very fast (on the order of minutes) response to the induction of DSB in the cell and there is an early-phase of activity in which protein kinetics are expected to be quite rapid; this fast response is followed by a later, longer and more sustained period of response and repair (Appella and Anderson 2001; Celeste, Fernandez-Capetillo et al. 2003; Kastan and Bartek 2004). It has also been observed that repair of CLM-induced DSB follows biphasic kinetics, consisting of an early fast repair period (completed within the two hours following lesion induction) and a late, long repair period that is sustained through a 24 hour period following lesion

induction (Elmroth, Nygren et al. 2003). Based upon this knowledge, time points were most densely sampled in the first 2 hours (Fig. 17, left panels). Levels of activated ATM, Chk2, H2AX, JNK, p38, ERK and p53 were measured at these time-points, in triplicate, using the high-throughput ICW assays (Fig. 17, right panels). In order to compare the dose-dependent signaling differences, we performed a three way comparison for each target protein under 50nM, 5nM and 0nM CLM treatment (Fig. 18).

Response measurement time-points were collected in duplicate at three time-points over 48 hours (12, 24 and 48h). Cell death in the population was measured by FACS detection of cleaved caspase-3 (representative data shown in Fig. 19, quantified in Fig. 20) and by sub-G1 PI incorporation (Fig. 22). Cell cycle profile in the population was also measured by FACS detection of relative PI incorporation (Fig. 21, 22).

Cellular signaling

Time-course of signaling

All protein activation levels were normalized to their measured activation levels at time 0 (corresponding to no treatment, n = 9, triplicate samples on three separate plates). Fold activation at each time-point is reported with respect to this measured level of activation. Cells treated with 0nM CLM served as a negative control in these experiments.

Except in the case of ATM, following the negative control treatment of 0nM CLM, protein activation levels never deviated from the no-treatment activation levels by more than +/- 60%, (Fig. 17A, right panel). ATM activation levels increased significantly from no-treatment activation levels following treatment with 0nM CLM at late time-points. ATM activation levels jumped to 4.6 fold activation at 12 hours. This high activation level at 12 hours is followed by a dip to a 2.8 fold activation level at 16 hours, and climbs again to a 5.4 fold activation level at the latest time-point of 26.5 hours (Fig. 17A, right panel).

Following treatment with 5nM CLM, protein activation levels of all proteins, except H2AX and ATM, remained low over the full time-course, never exceeding a 2-fold activation level (Fig. 17B, right panel). H2AX activation levels peaked quickly, reaching a maximum activation of more than 8-fold at 30 minutes. This high activation level is not sustained and dropped quickly to just above 5-fold activation by 90 minutes (Fig. 17B, left panel). H2AX activation levels decreased slowly over the rest of the time-course and returned to no-treatment levels by 26.5 hours (Fig. 17B, right panel). ATM levels also peaked quickly, reaching a maximum activation of 3.8-fold activation at 30 minutes and remained at this level through 1 hour, before dropping to just above 2-fold activation levels by 90 minutes (Fig. 17B, left panel). Activation levels of ATM rose again to just above 3-fold by 2 hours and then decreased slowly to just above 2-fold activation levels

by 8 hours (Fig. 17B, right panel). By 12 hours, ATM's measured level of activation was nearly 5-fold. This activation level is similar to the activation levels found for ATM at this time following 0nM CLM treatment. This high activation level for ATM persisted for the remainder of the time-course (through 26.5 hours) (Fig. 17B, right panel).

Following 50nM CLM treatment, protein activation levels of H2AX and ATM were again highly activated, but to an even larger extent than following 5nM CLM treatment. H2AX activation levels peaked at more than 12-fold at just 15 minutes following treatment, dropped to 9-fold by 90 minutes, and recovered to another peak of 12.5-fold activation at 2 hours (Fig. 17C, left panel). Following this peak, H2AX activation levels decreased sharply to 7.6-fold by 6 hours, and rose once more to 9.5-fold, before decreasing slowly over the remainder of the time-course to just above 3-fold at 26.5 hours (Fig. 17C, right panel). Similar to its behavior following 5nM CLM treatment, ATM activation levels once again peaked by 30 minutes following 50nM CLM treatment, although this time at a much higher activation level of 7-fold (Fig. 17C, left panel). This activation level dropped slightly to 6-fold by 90 minutes, before recovering to another peak of activation of 7.4-fold by 2 hours (Fig. 17C, left panel). This peak was followed by a sharp decline in activation level to 4.7-fold by 6 hours and, as is seen in both the 0nM and 5nM CLM treated populations, ATM activation levels once again rose to very high levels at 12 hours following treatment (6.9-fold) and remained high for the remainder of the time-course (Fig. 17C, right panel).

In contrast to their lack of significant activation following 5nM CLM treatment, Chk2 and p38 are highly activated following 50nM CLM treatment (Fig. 18A, right panel, Fig. 18C, left panel). Chk2 activation levels increased to 3.3-fold by 30 minutes following 50nM CLM treatment (Fig. 17C, left panel). This Chk2 activation level was maintained through 90 minutes. Activation levels increased to greater than 4-fold at 2 hours, and this activation level was maintained through 4 hours, at which point Chk2 activation levels decreased quickly to 2.6 fold at 6 hours and continued to decrease slowly for the remainder of the time-course. Chk2 activation levels reached as low as 1.5-fold at 26.5 hours following treatment (Fig. 17C, right panel). The initial rise in p38 activation levels following 50nM CLM treatment was delayed with respect to the initial activation of H2AX, ATM, and Chk2 (Figure 17C, left panel). Activation levels of p38 rose quickly at 2 hours following 50nM CLM treatment and reached a peak activation level of 3.5-fold at 4 hours following treatment (Fig. 18C, left panel). Activation levels of p38 dropped quickly back to 1.6-fold by 6 hours and continued to slowly decline over the remainder of the time-course to 1.2-fold at 26.5 hours (Fig. 17C, right panel).

Similar to their behavior following 5nM CLM treatment, the remaining proteins, including p53, JNK and ERK remained at low levels of activation following 50nM CLM treatment, never exceeding a 2-fold activation level (Fig. 18D and Fig. 18B and 18C, right panels, respectively).

Dose-dependent signaling

While H2AX and ATM are highly activated following both 5nM and 50nM CLM treatment, there is a significant dose-dependence in the extent of this activation. Both initial activation peaks and maximal activation peaks are dramatically higher following 50nM CLM treatment than following 5nM CLM treatment (Fig. 18A and 18B, left panels). The initial activation peak of H2AX following 5nM CLM treatment reaches 8.1-fold, while the initial activation peak following 50nM CLM treatment reaches 12.1-fold (Fig. 18B, left panel). The initial activation peak of ATM following 5nM CLM treatment reaches 3.8-fold, while the initial activation peak following 50nM CLM treatment reaches 7-fold (Fig. 18A, left panel).

The trajectories of activation of both Chk2 and p38 following 5nM and 50nM CLM treatment are clearly qualitatively, as well as quantitatively, different. Neither Chk2 nor p38 are significantly activated following treatment with 5nM CLM. However, both are significantly activated following treatment with 50nM CLM. Chk2 reaches a maximal activation level of 4.6-fold at 4 hours following treatment (Fig. 18A, right panel), while p38 reaches a maximal activation level of 3.5-fold also 4 hours following treatment (Fig. 18C, left panel).

Neither ERK nor JNK show any significant activation over the 26.5 hours following treatment with either 5nM or 50nM CLM. The activation level of these proteins following treatment with 0nM, 5nM and 50nM CLM never exceeds 1.6-fold. Additionally, the trajectories of activation of ERK following treatment with 0nM, 5nM and 50nM CLM, as well as those of JNK following treatment with 0nM, 5nM and 50nM CLM, are virtually super-imposable (Fig. 18B and 18C, right panels).

The activation level of p53 never exceeds 1.7-fold activation following 5nM or 50nM CLM treatment. However, while the trajectories of activation of p53 following 5nM or 50nM CLM are virtually identical, these trajectories differ from that of p53 activation following treatment with 0nM CLM (Fig. 18D). Maximal activation levels of p53 following both 5nM and 50nM CLM treatment are reached at 8 hours following treatment and correspond to 1.6- and 1.7-fold activation respectively, while the activation level measured following 0nM treatment remains flat at 1.

Cellular response

Microscopic analysis

Cell populations were observed under a light microscope at 12, 24 and 48 hours following treatment with no, low and high dose CLM. At 12 hours, following both 5 and 50nM treatment, cells morphology was large, flat, and

spread out with large flat nuclei as compared to the control cells. In addition, while control populations had a large number of cells observably undergoing mitosis (twinned cells lifted up off the plate surface), in both treated populations there was no observable mitosis.

After 24 hours, untreated populations had noticeably fewer observably mitotic cells than after 12 hours, which is to be expected as cells at this point are fairly confluent and somewhat contact inhibited. Cell populations treated with the low dose of CLM have no observable mitosis. Cell populations treated with the high dose of CLM display a very large number of cells observably in the mitotic state (twinned cells lifted up off the plate surface).

After 48 hours, the untreated populations display virtually no observable mitosis (as previously discussed, this is due to contact inhibition, which is quite extensive at this point). Low dose-treated populations show a large number of cells observably in the mitotic state, and high dose-treated populations consist of nearly all floating or apoptotic cells, as assessed by nuclear blebbing (data not shown).

Cell-cycle profiling

Cell cycle profiles were determined at 12, 24 and 48 hours following treatment with no, low and high dose CLM by FACS based detection of relative propidium iodide (PI) incorporation. Figure 21 shows sample cell-cycle data from each of these time and treatment points. Figure 22 shows an average of cell-cycle data collected at each of these time and treatment points over four individual experiments (Fig. 21, 22). Cells treated with 0nM CLM served as a negative control in this experiment.

At 12 hours following treatment with 0nM CLM, cell populations displayed population percentages in G1, S and G2/M phases of 46+/-3%, 18+/-0.6% and 23+/-1% respectively (Fig. 22, top left). This population distribution is consistent with widely accepted distributions for normal cell populations of population percentages in G1, S and G2/M phases of 50%, 20% and 20% respectively. This population distribution is preserved at 24 hours following treatment in the 0nM CLM treated population (Fig. 22, top middle). At 48 hours, the percentage of the population in G1 has increased (46+/-3% at 12 hours, 54+/-2% at 48 hours) and the percentage of the population in G2/M has decreased (23+/-1% at 12 hours, 13+/-4% at 48 hours) (Fig. 22, top left and top right). These shifts in population percentages in cell populations treated with 0nM CLM reflects an expected adjustment to slower population proliferation rates as cell density on the plate becomes very high.

At 12 hours following treatment with 5nM CLM, cell populations displayed population percentages in G1, S and G2/M phases of 30+/-2%, 27+/-2% and 34+/-2% respectively (Fig. 22, middle left) indicating an increase in the G2/M

population over control population distributions, a possible increase in the S phase populations over control population distributions, and a decrease in G1 population. At 24 hours following treatment with 5nM CLM, cell populations displayed population percentages in G1, S and G2/M phases of 8+/-2%, 23+/-8% and 54+/-6% respectively (Fig. 22, center). This distribution is dramatically different from that displayed by control cell populations. It indicates a greatly increased G2/M population (54+/-6% in 5nM-treated population, 19+/-4% in 0nM treated population) and a nearly abolished G1 population (8+/-2% in 5nM-treated population, 48+/-4% in 0nM-treated population) (Fig. 22, center and top middle). The S phase population, at 23+/-8% of the population, is consistent with control cell population distributions. At 48 hours following treatment with 5nM CLM, cell populations displayed population percentages in G1, S and G2/M phases of 6+/-0.7%, 14+/-5% and 49+/-1% respectively (Fig. 22, middle right), indicating a decrease in the S phase population. Additionally, the population distribution includes a small sub-G1 population of 5+/-0.1%, indicating a small amount of cell death, and a large aneuploid population of 26+/-7% (versus 14+/-5% in control populations; Fig. 22, top right).

At 12 hours following treatment with 50nM CLM, cell populations displayed population percentages in G1, S and G2/M phases of 39+/-3%, 24+/-1% and 28+/-3% respectively (Fig. 22, bottom left), indicating a decrease in the G1 population from control population distributions (46+/-3% in 0nM-treated populations, Fig. 22, top left). At 24 hours following treatment with 50nM CLM, cell populations displayed population percentages in G1, S and G2/M phases of 31+/-3%, 24+/-1% and 31+/-3% respectively (Fig. 22, bottom middle), indicating a further decrease in G1 population and an increase in the G2/M population over that that found in control cell populations (31+/-3% in 50nM-treated, 19+/-4% in 0nM-treated). At 48 hours following treatment with 50nM CLM, cell populations displayed population percentages in G1, S and G2/M phases of 13+/-0.1%, 10+/-0.4% and 20+/-4% respectively (Fig. 22, bottom right), with a large sub-G1 population of 45+/-8%, indicating a large amount of cell death. This distribution indicates a dramatic decrease in G1 and S phase populations, as well as a subsequent decrease in the G2/M population following the previous increase in this population above control levels observed at 24 hours following treatment (31+/-4% at 24 hours, 20+/-4% at 48 hours, Fig. 22, bottom right and bottom middle).

Apoptotic measurements

Apoptosis in treated and untreated populations was measured by FACS detection cleaved caspase-3, an early apoptotic effector molecule. Apoptosis in populations treated with 5nM CLM was not found to be significantly elevated above levels in untreated populations at 24 or 48 hrs. Apoptosis in populations treated with 50nM CLM was found to be dramatically elevated above levels in untreated populations at 24 and 48 hours (>24% at 24 hours and >60% at 48 hours).

Discussion

In-cell Western Assay

Intra-assay variation

A major component of this work was the validation of the In-cell Western as a technique for monitoring the phosphorylation state of proteins involved in DNA damage signaling. As such, it is pertinent to consider the shortcomings of this assay.

Systematic error in quantifying protein activation levels from plate to plate in the ICW assay is a concern. The inclusion of both a positive and negative control for each protein activation level, on each plate in the time-course, would allow for very rigorous checks on such systematic error. This is not possible in the format of the ICW assay. However, the low level of deviation of protein activation data in the negative control-treated population (0nM CLM treatment) across all plates in the time-course (time-points: 5min to 26.5h) from the level of protein activation following no treatment (time-point: 0min, measured in triplicate on three separate plates), demonstrates that systematic error is not a confounding element in this data collection method (Fig. 17A).

ATM: is intra-assay variation a fact or an artefact?

We did observe a significant deviation of protein activation levels for ATM in the 0nM CLM-treated population, from the level of protein activation following no treatment, at late time-points (12 hours and later) (Fig. 17A, right panel). This deviation is unexpected. It appears to be artefactual and raises questions as to the reliability of the phospho-ATM antibody used in these assays.

The unexpected activation of ATM following treatment with 0nM CLM is observed only at late time-points (compare Fig. 17A left panel and right panel), at which point, cell density is very high. It is known that many cell processes shift dramatically at high cell density and that protein activation levels, specifically of known tumor suppressors and cell-cycle regulators, differ from activation levels observed at low cell density (Kammouni, Ramakrishna et al. 2002; Bar, Cohen-Noyman et al. 2004; Uegaki, Kanamori et al. 2005). It is possible that the unexpected levels of measured ATM activation in this assay are not artefactual, and instead represent real changes in ATM activation that occur at high cell density. These findings require further investigation.

Cellular Signaling

The conclusions described below are based on In-cell Western data alone. All of these data would benefit by initial additional validation by quantitative western blot.

As expected, ATM, H2AX and Chk2 were all highly activated immediately following treatment with high dose (50nM) CLM (Fig. 17, B and C, left panels). ATM and H2AX are both activated following low dose (5nM) CLM treatment, though not to the extent that they are activated following high dose treatment (Fig. 17B). Unexpectedly, Chk2 is not highly activated following low dose treatment with CLM (Fig. 17B, left and right panels). Following 5nM treatment, Chk2 shows only subtle quantitative differences in trajectory as compared to control (no treatment), with activation never exceeding 2-fold. It seems unlikely that Chk2 does not play a role in the DSB response following low dose CLM treatment as ATM is quite highly activated, and Chk2 is a well-established substrate of ATM (Matsuoka, Rotman et al. 2000; Zhou, Chaturvedi et al. 2000). Therefore it is possible that these subtle quantitative differences are critical for Chk2's role in low dose response.

p38 was highly activated following high dose CLM treatment (Fig. 17C, right panel) although with largely different and far slower kinetics. As compared to ATM, H2AX and Chk2, which all reach an initial peak in activation by 30 minutes following treatment with 50nM CLM, p38 reached a peak of 3.5-fold activation only by 4 hours following treatment (Fig. 18C, left panel). Additionally, p38 is not activated in response to low dose CLM (Fig. 17B). Taken together, these results suggest a role for p38 in DSB response that is related to longer term effector responses, rather than initial lesion sensing and immediate response.

We did not observe a dramatic activation of p53 (Fig. 17B and C, right panels). Trajectories of activation for p53 in cells following 5nM and 50nM CLM treatment are nearly identical (Fig. 18D, left panel), despite the highly divergent cellular apoptotic response at these doses. 5nM CLM treatment elicited a very low level of apoptosis in treated cell populations (~ 5% by 48 hours), and 50nM CLM treatment elicited a very strong apoptotic response in treated cell populations (>20% at 24 hours, >60% at 48 hours) (Fig. 20). Nearly identical trajectories of activation of p53 in cell populations following 5nM and 50nM CLM treatment, correspond to dramatically divergent apoptotic outcomes in these differentially treated populations. These observations are interesting in light of the well-established role of p53 in promoting apoptosis, and suggest the possibility of a p53-independent apoptotic response following CLM treatment. Indeed, other groups have found that CLM may induce apoptosis in a p53-independent manner (Prokop, Wrasidlo et al. 2003), consistent with data presented here.

Trajectories of JNK and ERK activation following low or high dose CLM treatment are nearly super-imposable with control levels (Fig. 18B and C, right panels). This may imply that these signaling pathways are not highly utilized in the DSB response. It is possible that it is necessary to measure activation levels at time-points later than 27 hours following induction of DNA damage to catch

late variations in activation of these signals that might be important in mediating cell fate. There are conflicting reports regarding the timing of MAPK (ERK, JNK and p38) activation following genotoxic stress with hints that significant activation does not occur before 48 hours following DNA damage (Bose, Motiwale et al. 2005). However, Fritz et al. recently reported that JNK is activated, to levels up to 2.5-fold over saline-treated controls, by specific types of DNA damage within 8 hours of damage induction by alkylating agents such as MMS (Fritz and Kaina 2005). In light of this, the absence of any significant observed JNK activation in this experiment set is troubling and leads to concerns over the reliability and sensitivity of the antibodies used to detect activated JNK and ERK proteins.

Cellular Response

Changes in cell-cycle profile of cell populations treated with 5nM and 50nM CLM were dramatic. In cells treated with 5nM CLM, the dramatic increase in the G2/M population and the near abolition of the G1 population at 24 hours following treatment (Fig. 22, middle left and middle center), taken together, suggest the initiation of a strong G2/M checkpoint in these populations.

In cells treated with 50nM CLM, these same trends in G1 and G2/M populations present themselves at 24 hours following treatment, though the shifts in population percentages are far less dramatic than those in the 5nM CLM-treated populations (Fig. 22, bottom left and bottom middle). These population shifts again suggest the initiation of a G2/M checkpoint in cell populations treated with 50nM CLM. The lack of as dramatic a build-up in the G2/M population and decrease in G1 population in the 50nM CLM-treated population as in the 5nM CLM-treated population, despite this G2/M checkpoint, suggests that a G1 cell-cycle checkpoint may also be active in cell populations treated with 50nM CLM.

At 48 hours following treatment with 50nM CLM, G1, S and G2/M population percentages dramatically deceased from levels at 24 hours following treatment (Fig. 22, bottom right and bottom middle). Additionally, a very large sub-G1 population developed (45% of the population), indicating a large amount of cell death in these populations. Taken together, these trends suggest that all cell-cycle checkpoints are over-ridden by 48 hours following treatment in cell populations treated with 50nM CLM, allowing cells to either proceed through the cell cycle to mitosis before dying by mitotic catastrophe, or to exit the cell cycle directly to die.

These observations are interesting. They suggest that low dose CLM is capable of strongly inducing a G2/M checkpoint. Also suggested is that the high dose of CLM is capable of inducing both G2/M and G1-phase checkpoints, but that no checkpoints are maintained by 48 hours in populations treated with 50nM CLM. The induction of cell cycle checkpoints is a rapid process mediated by signaling transduced by post translational modifications (O'Connell, Walworth et al. 2000). This response is strongly activated by both low and high dose CLM.

However, maintenance of cell cycle checkpoints requires transcription and translation of new proteins, especially the p21 cdk inhibitor (Yoon, Chen et al. 2003). CLM-treated cells may well be unable to support such transcription due to lesions created in the genome that are critical for such transcription (eg at the p21 locus) (Khanna and Jackson 2001). Such an inability to transcribe key checkpoint maintenance factors would plausibly account for the inability of CLM-treated cells to maintain cell cycle checkpoints.

It is also interesting to note the dramatic difference in cell death induced by low (5nM) and high (50nM) CLM-treatment (5% in 5nM, 45% in 50nM, as compared to 3% in untreated populations at 48 hours following treatment) (Fig. 20). However, there is a large buildup in the aneuploid population in cell populations treated with 5nM CLM (26% in 5nM, 12% in 50nM populations, versus 14% in untreated populations) (Fig. 22B, right panel). It has been observed that cells may die by mitotic catastrophe following induction of DNA double-strand breaks (DSB), both in vitro and in vivo, and that death by this route is preceded by several abnormal mitoses without cell division, leading to aneuploid cells (Mekid, Tounekti et al. 2003). This may explain the microscopically observed high levels of mitotic cells in the treated populations at differential time points and suggests that this aneuploid population is on its way to death via mitotic catastrophe. If this hypothesis is correct, we would predict that a similar build up in aneuploid cells occurred in the 50nM population preceeding the observed high levels of cell death, most likely occurring at a timepoint shortly after 24 h (the time at which high levels of mitosis were observed).

Future Work

The response to a cytotoxic lesion such as a DSB requires that cell processes come to a halt (i.e. that cell cycle, cell growth, general protein translation and other metabolic activities stop) and drastically switch focus to allow for repair processes and subsequent re-entry into the cell-cycle, or death (Bose, Motiwale et al. 2005). The signal transduction mechanisms that must coordinate such a drastic rewiring and return, or end, of so many cellular processes are incredibly complex.

It will be very interesting to learn how information flow through these networks mediates the drastically various responses. We will initially attempt a partial least squares (PLS)-based analysis of this data in order to extract novel relationships between signaling parameters and/or groups of signaling parameters and response. In the future, we plan to expand data collection by high throughput In-cell western. Signals to be measured will be expanded to include several more key network signaling components (eg MAPKAPK2/Chk3, CDC25 family members, Cdks, Akt (see Fig.1)). These proteins are known to play an important role in mediating such cell fate decisions cell cycle arrest (cdks) and survival (Akt). The signaling and response to a broader range of cues

will be measured in order to stretch the dynamic range of both signaling and response values in the context of this network and to better train a robustly predictive model. The development of predictive tests for cell response to DSB from such a model would be extremely relevant to cancer therapy as such tests would help to identify agents that are potentially effective and those that will most likely not be effective, or have too great a potential for insupportable side-effects. Finally, the relationships we are able to identify from these statistical models will allow us to contruct new deterministic physico-chemical models of this system and/or to improve such existing models.

VI. Acknowledgements

This work was funded by ICBP grant 1 P50 CA112967.

I would like to thank the many people who provided invaluable help and advice to me in completing this work. Thanks to:

Michael Yaffe for always expecting the best

Forest White for always being supportive

Doug Lauffenburger for help in guiding the initial direction of this research and support along the way

Mary Stewart for being the reagent fairy (and more)!

Gerry Ostheimer for all his help, especially in the editing and revision of this manuscript

Graduate Group Club members: Duaa, Sarah, Drew (and sometimes even Jes!)

Shark tank dwellers and the entire Yaffe lab for advice, reagents, support, laughs, and for being a great lab to be a part of

Kevin Janes, John Albeck, Suzanne Gaudet, Gordon Klu, Paul Jasper, and the entire CDP sub-group for reagents, protocols, advice, and a great environment in which to share ideas and work, and to ask questions

Alan Grodzinsky for encouragement and support

White lab members for support and a fresh perspective

Glen Paradis

CCR 5th floor members

ICBP DNA damage group members

Ericka Noonan
Josh Apgar
Hyung-do Kim
Jason Wyman

My roommates, Rana, Tammy and Safa
and my family

V. Figure Captions

Figure 1. DNA damage signaling network

Figure 2.
(A) Chemical structure of calicheamicin (CLM). High-lighted in red is the 10-member enediyne ring structure. This enediyne structure is thought to undergo the Bergman cyclization reaction in B, below, following a nucleophilic attack on the central sulfur in the methyl trisulfide substituent group in CLM (illustration taken from the faculty website of Liang, Z.-X. Assistant Professor, NTU School of Biological Sciences. 2005).
(B) Schematic for the thermal cycloaromatization reaction of enediynes, first characterized by Bergman. One of the intermediates in this reaction (2) is a highly reactive di-radical species. It is this species that is thought to be responsible for the ability of CLM to simultaneously abstract hydrogen atoms from opposite DNA strands at sufficiently close proximity to result in a DNA double-strand break (illustration taken from Nicolaou and Yue, 1993).

Figure 3. Antibody Dilution Experimental Set-up, Determining the optimal antibody dilution of up to two antibodies simultaneously
(A) U2OS cells were seeded at 10,000 cells per well in a total volume of 200ul of total media in 96-well tissue-culture treated plates, all wells on the edge of the plate were filled with an equal volume of media, but were not seeded
(B) Following overnight incubation at 37°C, cells were treated or not with activating treatments as described in Materials and Methods for each antibody, and according to the above schematic
(C) Following fixation, cells were immuno-stained with antibody dilutions ranging from 1:50 to 1:5000 (1:50, 1:100, 1:250, 1:500, 1:1000, 1:2000, 1:5000 and 0) as described in Materials and Methods and according to the above schematic

Figure 4. Cell Number Dilution Experimental Set-up, Determining Linear Range of detection for up to two antibodies simultaneously
(A) U2OS cells were seeded in dilutions ranging from 10,000 cells/well to 2,000 cells/well (10,000, 8,000, 6,000, 4,000, 2,000 and 0) in a total volume of 200ul of total media in 96-well tissue-culture treated plates according to the above schematic, all wells on the edge of the plate were filled with an equal volume of media, but were not seeded
(B) Following overnight incubation at 37°C, cells were treated or not with activating treatments as described in Materials and Methods for each antibody, and according to the above schematic
(C) Following fixation, cells were immuno-stained with antibody at the optimal antibody concentration determined from previous Antibody Dilution experiments

Figure 5. Time-course Cellular Signaling Experiments: Time-point Experimental Set-up for up to seven antibodies simultaneously

(**A**) U2OS cells were seeded at 6,000 cells per well in a total volume of 200ul of total media in 96-well tissue-culture treated plates, all wells in the first and last column of the plate were filled with an equal volume of media, but were not seeded
(**B**) Following overnight incubation at 37°C, cells were treated with 0, 5 or 50nM calicheamicin (CLM) as described in Materials and Methods and according to the above schematic
(**C**) Following fixation, cells were immuno-stained with antibodies at their respective optimal dilutions previously determined from Antibody Dilution experiments, according to the above schematic

Figure 6. Positive Control Experimental Set-up for phospho-ATM, Chk2, and H2AX
(**A**) U2OS cells were seeded at 6,000 cells per well across only three rows, excluding edge wells according to the above schematic, all remaining wells were filled with an equal volume of media, but were not seeded
(**B**) Following overnight incubation at 37°C, cells were treated or not for 15 minutes with 100nM CLM (the activating treatment corresponding to these target phospho-proteins, as described in Materials and Methods)
(**C**) Following fixation, cells were immuno-stained with phospho-ATM, Chk2 or H2AX antibodies at their respective optimal dilutions

Figure 7. Positive Control Experimental Set-up for phospho-JNK and p38
(**A**) U2OS cells were seeded at 6,000 cells per well across only two rows, excluding edge wells, according to the above schematic, all remaining wells were filled with an equal volume of media, but were not seeded
(**B**) Following overnight incubation at 37°C, cells were treated or not for 30 minutes with 500mM NaCl (the activating treatment corresponding to these target phospho-proteins, as described in Materials and Methods)
(**C**) Following fixation, cells were immuno-stained with phospho-JNK or p38 antibodies at their respective optimal dilutions

Figure 8. Positive Control Experimental Set-up for phospho-p53 and ERK
(**A**) U2OS cells were seeded at 6,000 cells per well across only two rows, excluding edge wells, according to the above schematic, all remaining wells were filled with an equal volume of media, but were not seeded
(**B**) Following overnight incubation at 37°C, cells in the first row were treated or not for 12 hours with 10uM doxorubicin (DOX), (the activating treatment corresponding to the target phospho-protein, phospho-p53, as described in Materials and Methods), while cells in the second row were serum starved for 12 hours and then treated or not for 10 minutes with 100nM PMA (the activating treatment corresponding to the target phospho-protein, phospho-ERK, as described in Materials and Methods)
(**C**) Following fixation, cells in the first and second row were respectively immuno-stained with phospho-p53 and phospho-ERK antibodies at their respective optimal dilutions

Figure 9. Traditional Western Blots are not sufficient to ensure Antibody specificity and affinity in the In-Cell Western Format

(**A**) Traditional western blot with phospho-Akt antibody from CST, #4056, shows high specificity and affinity for phospho-Akt
(**B**) In-cell western using the same phospho-Akt antibody (CST #4056), shows high background, indicates that this antibody lacks sufficient specificity to be a useful reagent for detection of phospho-Akt in this assay format

Figure 10. Phospho-ATM antibody validation
(**A**) Antibody dilution experiments:
left panel: Cells untreated (-) or treated (+) with activating treatment for phospho-ATM, immuno-stained with primary antibody dilutions of phospho-ATM antibody (pictured, from top: 1:50, 1:100, 1:250, 1:500, 1:5000, 0) and secondary antibody (IRDye 800CW Donkey anti-Mouse, at 1:500), detected on the Odyssey Scanner in the 800nm channel, pseudo-colored green;
right panel: Data from the image in the left panel, quantified and plotted, shows the Antibody signal intensity, in arbitrary units, as a function of the amount of antibody in the well in both untreated (-) and treated (+) cell populations. Antibody signal intensity indicates the Raw Integrated Intensity of signal detected in the well in the 800nm channel at each antibody dilution, minus the Raw Integrated Intensity of signal detected in the 800nm channel in wells with no primary antibody, to correct for background effects. The **arrow** indicates the point of optimal antibody amount in the well for this antibody (where the rate of increase in signal to background is maximum) and corresponds to an optimal antibody dilution of 1:500 for the phospho-ATM antibody of original concentration 1ug/ul
(**B**) Cell number dilution experiments:
left panel: Cell dilutions untreated (-) or treated (+) with activating treatment for phospho-ATM, immuno-stained with primary antibody at the optimal antibody dilution of 1:500, determined in A above (pictured, from top: 10,000, 8,000, 6,000, 4,000, 2,000 and 0 cells plated per well) and secondary antibody (IRDye 800CW Donkey anti-Mouse, at 1:500), detected on the Odyssey Scanner in the 800nm channel, pseudo-colored green;
right panel: Data from the image in the left panel, quantified and plotted, shows the Antibody signal intensity, in arbitrary units, as a function of the cell number plated per well in untreated (-) and treated (+) cell populations. Antibody signal intensity indicates the Raw Integrated Intensity of signal detected in the well in the 800nm channel at each cell number dilution, minus the Raw Integrated Intensity of signal detected in the 800nm channel in wells with no cells plated, to correct for background effects.
(**C**)Antibody signal intensity as a function of the cell number plated per well in the treated cell population only. The R^2 value of 0.9883 for the linear fit demonstrates linearity of detected signal with respect to target protein concentration in the wells over the range of protein concentration represented by 0 to 8,000 cells plated per well

Figure 11. Phospho-Chk2 antibody validation
(**A**) Antibody dilution experiments:
left panel: Cells not treated (-) or treated (+) with activating treatment for phospho-Chk2, immuno-stained with primary antibody dilutions of phospho-Chk2 antibody (pictured, from top: 1:50, 1:100, 1:250, 1:500, 1:5000 and 0) and secondary antibody

(IRDye 800CW Goat anti-Rabbit, at 1:500), detected on the Odyssey Scanner in the 800nm channel, pseudo-colored green;
right panel: Data from the image in the left panel, quantified and plotted, showing the Antibody signal intensity, in arbitrary units, as a function of the amount of antibody in the well in both untreated (-) and treated (+) cell populations. Antibody signal intensity indicates the Raw Integrated Intensity of signal detected in the well in the 800nm channel at each antibody dilution, minus the Raw Integrated Intensity of signal detected in the 800nm channel in wells with no primary antibody, to correct for background effects. The **arrow** indicates the point of optimal antibody amount in the well for this antibody (where the rate of increase in signal to background is maximum) and corresponds to an optimal antibody dilution of 1:250 for the phospho-Chk2 antibody of original concentration 0.1ug/ul
(**B**) Cell number dilution experiments:
left panel: Cell dilutions untreated (-) or treated (+) with activating treatment for phospho-Chk2, immuno-stained with primary antibody at the optimal antibody dilution of 1:250, determined in A above (pictured, from top: 10,000, 8,000, 6,000, 4,000, 2,000 and 0 cells plated per well) and secondary antibody (IRDye 800CW Goat anti-Rabbit, at 1:500), detected on the Odyssey Scanner in the 800nm channel, pseudo-colored green;
right panel: Data from the image in the left panel, quantified and plotted, showing the Antibody signal intensity, in arbitrary units, as a function of the cell number plated per well in untreated (-) and treated (+) cell populations. Antibody signal intensity indicates the Raw Integrated Intensity of signal detected in the well in the 800nm channel at each cell number dilution, minus the Raw Integrated Intensity of signal detected in the 800nm channel in wells with no cells plated, to correct for background effects.
(**C**) Antibody signal intensity as a function of the cell number plated per well in the treated cell population only. The R^2 value of 0.9992 for the linear fit demonstrates linearity of detected signal with respect to target protein concentration in the wells over the range of protein concentration represented by 0 to 6,000 cells plated per well

Figure 12. Phospho-H2AX antibody validation
(**A**) Antibody dilution experiments:
left panel: Cells not treated (-) or treated (+) with activating treatment for phospho-H2AX, immuno-stained with primary antibody dilutions of phospho-H2AX antibody (pictured, from top: 1:50, 1:100, 1:250, 1:500, 1:5000 and 0) and secondary antibody (IRDye 800CW Goat anti-Rabbit, at 1:500), detected on the Odyssey Scanner in the 800nm channel, pseudo-colored green;
right panel: Data from the image in the left panel, quantified and plotted, showing the Antibody signal intensity, in arbitrary units, as a function of the amount of antibody in the well in both untreated (-) and treated (+) cell populations. Antibody signal intensity indicates the Raw Integrated Intensity of signal detected in the well in the 800nm channel at each antibody dilution, minus the Raw Integrated Intensity of signal detected in the 800nm channel in wells with no primary antibody, to correct for background effects. The **arrow** indicates the point of optimal antibody amount in the well for this antibody (where the rate of increase in signal to background is maximum) and corresponds to an optimal antibody dilution of 1:200 for the phospho-H2AX antibody of original concentration 0.1ug/ul

(**B**) Cell number dilution experiments:
left panel: Cell dilutions untreated (-) or treated (+) with activating treatment for phospho-H2AX, immuno-stained with primary antibody at the optimal antibody dilution of 1:200, determined in A above (pictured, from top: 10,000, 8,000, 6,000, 4,000, 2,000 and 0 cells plated per well) and secondary antibody (IRDye 800CW Goat anti-Rabbit, at 1:500), detected on the Odyssey Scanner in the 800nm channel, pseudo-colored green;
right panel: Data from the image in the left panel, quantified and plotted, showing the Antibody signal intensity, in arbitrary units, as a function of the cell number plated per well in untreated (-) and treated (+) cell populations. Antibody signal intensity indicates the Raw Integrated Intensity of signal detected in the well in the 800nm channel at each cell number dilution, minus the Raw Integrated Intensity of signal detected in the 800nm channel in wells with no cells plated, to correct for background effects.
(C)Antibody signal intensity as a function of the cell number plated per well in the treated cell population only. The R^2 value of 0.967 for the linear fit demonstrates linearity of detected signal with respect to target protein concentration in the wells over the range of protein concentration represented by 0 to 6,000 cells plated per well

Figure 13. Phospho-JNK antibody validation
(**A**) Antibody dilution experiments:
left panel: Cells not treated (-) or treated (+) with activating treatment for phospho-JNK, immuno-stained with primary antibody dilutions of phospho-JNK antibody (pictured, from top: 1:50, 1:100, 1:250, 1:500, 1:5000 and 0) and secondary antibody (IRDye 800CW Goat anti-Rabbit, at 1:500), detected on the Odyssey Scanner in the 800nm channel, pseudo-colored green;
right panel: Data from the image in the left panel, quantified and plotted, showing the Antibody signal intensity, in arbitrary units, as a function of the amount of antibody in the well in both untreated (-) and treated (+) cell populations. Antibody signal intensity indicates the Raw Integrated Intensity of signal detected in the well in the 800nm channel at each antibody dilution, minus the Raw Integrated Intensity of signal detected in the 800nm channel in wells with no primary antibody, to correct for background effects. The **arrow** indicates the point of optimal antibody amount in the well for this antibody (where the rate of increase in signal to background is maximum) and corresponds to an optimal antibody dilution of 1:100 for the phospho-JNK antibody of original concentration 0.1ug/ul
(**B**) Cell number dilution experiments:
left panel: Cell dilutions untreated (-) or treated (+) with activating treatment for phospho-JNK, immuno-stained with primary antibody at the optimal antibody dilution of 1:100, determined in A above (pictured, from top: 10,000, 8,000, 6,000, 4,000, 2,000 and 0 cells plated per well) and secondary antibody (IRDye 800CW Goat anti-Rabbit, at 1:500), detected on the Odyssey Scanner in the 800nm channel, pseudo-colored green;
right panel: Data from the image in the left panel, quantified and plotted, showing the Antibody signal intensity, in arbitrary units, as a function of the cell number plated per well in untreated (-) and treated (+) cell populations. Antibody signal intensity indicates the Raw Integrated Intensity of signal detected in the well in the 800nm channel at each cell number dilution, minus the Raw Integrated Intensity of signal detected in the 800nm channel in wells with no cells plated, to correct for background effects.

(**C**) Antibody signal intensity as a function of the cell number plated per well in the treated cell population only. The R^2 value of 0.9913 for the linear fit demonstrates linearity of detected signal with respect to target protein concentration in the wells over the range of protein concentration represented by 0 to 6,000 cells plated per well

Figure 14. Phospho-p38 antibody validation
(**A**) Antibody dilution experiments:
left panel: Cells not treated (-) or treated (+) with activating treatment for phospho-p38, immuno-stained with primary antibody dilutions of phospho-p38 antibody (pictured, from top: 1:50, 1:100, 1:250, 1:500, 1:5000 and 0) and secondary antibody (IRDye 800CW Goat anti-Rabbit, at 1:500), detected on the Odyssey Scanner in the 800nm channel, pseudo-colored green;
right panel: Data from the image in the left panel, quantified and plotted, showing the Antibody signal intensity, in arbitrary units, as a function of the amount of antibody in the well in both untreated (-) and treated (+) cell populations. Antibody signal intensity indicates the Raw Integrated Intensity of signal detected in the well in the 800nm channel at each antibody dilution, minus the Raw Integrated Intensity of signal detected in the 800nm channel in wells with no primary antibody, to correct for background effects. The **arrow** indicates the point of optimal antibody amount in the well for this antibody (where the rate of increase in signal to background is maximum) and corresponds to an optimal antibody dilution of 1:100 for the phospho-p38 antibody of original concentration 0.1ug/ul
(**B**) Cell number dilution experiments:
left panel: Cell dilutions untreated (-) or treated (+) with activating treatment for phospho-p38, immuno-stained with primary antibody at the optimal antibody dilution of 1:100, determined in A above (pictured, from top: 10,000, 8,000, 6,000, 4,000, 2,000 and 0 cells plated per well) and secondary antibody (IRDye 800CW Goat anti-Rabbit, at 1:500), detected on the Odyssey Scanner in the 800nm channel, pseudo-colored green;
right panel: Data from the image in the left panel, quantified and plotted, showing the Antibody signal intensity, in arbitrary units, as a function of the cell number plated per well in untreated (-) and treated (+) cell populations. Antibody signal intensity indicates the Raw Integrated Intensity of signal detected in the well in the 800nm channel at each cell number dilution, minus the Raw Integrated Intensity of signal detected in the 800nm channel in wells with no cells plated, to correct for background effects.
(**C**) Antibody signal intensity as a function of the cell number plated per well in the treated cell population only. The R^2 value of 0.9915 for the linear fit demonstrates linearity of detected signal with respect to target protein concentration in the wells over the range of protein concentration represented by 0 to 8,000 cells plated per well

Figure 15. Phospho-ERK antibody validation
(**A**) Antibody dilution experiments:
left panel: Cells not treated (-) or treated (+) with activating treatment for phospho-ERK, immuno-stained with primary antibody dilutions of phospho-ERK antibody (pictured, from top: 1:50, 1:100, 1:250, 1:500, 1:5000 and 0) and secondary antibody (IRDye 800CW Goat anti-Rabbit, at 1:500), detected on the Odyssey Scanner in the 800nm channel, pseudo-colored green;

right panel: Data from the image in the left panel, quantified and plotted, showing the Antibody signal intensity, in arbitrary units, as a function of the amount of antibody in the well in both untreated (-) and treated (+) cell populations. Antibody signal intensity indicates the Raw Integrated Intensity of signal detected in the well in the 800nm channel at each antibody dilution, minus the Raw Integrated Intensity of signal detected in the 800nm channel in wells with no primary antibody, to correct for background effects. The **arrow** indicates the point of optimal antibody amount in the well for this antibody (where the rate of increase in signal to background is maximum) and corresponds to an optimal antibody dilution of 1:100 for the phospho-ERK antibody of original concentration 0.1ug/ul

(**B**) Cell number dilution experiments:

left panel: Cell dilutions untreated (-) or treated (+) with activating treatment for phospho-ERK immuno-stained with primary antibody at the optimal antibody dilution of 1:100, determined in A above (pictured, from top: 10,000, 8,000, 6,000, 4,000, 2,000 and 0 cells plated per well) and secondary antibody (IRDye 800CW Goat anti-Rabbit, at 1:500), detected on the Odyssey Scanner in the 800nm channel, pseudo-colored green;

right panel: Data from the image in the left panel, quantified and plotted, showing the Antibody signal intensity, in arbitrary units, as a function of the cell number plated per well in untreated (-) and treated (+) cell populations. Antibody signal intensity indicates the Raw Integrated Intensity of signal detected in the well in the 800nm channel at each cell number dilution, minus the Raw Integrated Intensity of signal detected in the 800nm channel in wells with no cells plated, to correct for background effects.

(**C**) Antibody signal intensity as a function of the cell number plated per well in the treated cell population only. The R^2 value of 0.9795 for the linear fit demonstrates linearity of detected signal with respect to target protein concentration in the wells over the range of protein concentration represented by 0 to 8,000 cells plated per well

Figure 16. Phospho-p53 antibody validation

(**A**) Antibody dilution experiments:

left panel: Cells not treated (-) or treated (+) with activating treatment for phospho-p53, concurrently stained with Topro-3 Iodide DNA stain (1:2500 dilution) and immuno-stained with primary antibody dilutions of phospho-p53 antibody (pictured, from top: 1:50, 1:100, 1:250, 1:500, 1:5000 and 0) and secondary antibody (IRDye 800CW Goat anti-Rabbit, at 1:500); p53 immuno-stain is detected on the Odyssey Scanner in the 800nm channel, pseudo-colored green;

middle panel: Cells not treated (-) or treated (+) with activating treatment for phospho-p53, concurrently stained with Topro-3 Iodide DNA stain (1:2500 dilution) and immuno-stained with primary antibody dilutions of phospho-p53 antibody (pictured, from top: 1:50, 1:100, 1:250, 1:500, 1:5000 and 0) and secondary antibody (IRDye 800CW Goat anti-Rabbit, at 1:500); Topro-3 Iodide DNA stain is detected on the Odyssey Scanner in the 700nm channel, pseudo-colored red;

right panel: Data from the image in the left panel, quantified and plotted, showing the Antibody signal intensity, in arbitrary units, as a function of the amount of antibody in the well in both untreated (-) and treated (+) cell populations. Antibody signal intensity indicates the Raw Integrated Intensity of signal detected in the well in the 800nm channel at each antibody dilution, minus the Raw Integrated Intensity of signal detected in the

800nm channel in wells with no primary antibody, to correct for background effects, and normalized to amount of DNA detected in the wells, to correct for cell number variation in wells containing treated vs. untreated cells. The **arrow** indicates the point of optimal antibody amount in the well for this antibody (where the rate of increase in signal to background is maximum) and corresponds to an optimal antibody dilution of 1:500 for the phospho-p53 antibody of original concentration 0.1ug/ul
(**B**) Cell number dilution experiments:
left panel: Cell dilutions untreated (-) or treated (+) with activating treatment for phospho-p53 concurrently stained with Topro-3 Iodide DNA stain (1:2500 dilution) and immuno-stained with primary antibody at the optimal antibody dilution of 1:500, determined in A above (pictured, from top: 10,000, 8,000, 6,000, 4,000, 2,000 and 0 cells plated per well) and secondary antibody (IRDye 800CW Goat anti-Rabbit, at 1:500); p53 immuno-stain is detected on the Odyssey Scanner in the 800nm channel, pseudo-colored green;
middle panel: Cell dilutions untreated (-) or treated (+) with activating treatment for phospho-p53 concurrently stained with Topro-3 Iodide DNA stain (1:2500 dilution) and immuno-stained with primary antibody at the optimal antibody dilution of 1:500, determined in A above (pictured, from top: 10,000, 8,000, 6,000, 4,000, 2,000 and 0 cells plated per well) and secondary antibody (IRDye 800CW Goat anti-Rabbit, at 1:500); Topro-3 Iodide stain is detected on the Odyssey Scanner in the 700nm channel, pseudo-colored red;
right panel: Data from the image in the left panel, quantified and plotted, showing the Antibody signal intensity, in arbitrary units, as a function of the cell number plated per well in untreated (-) and treated (+) cell populations. Antibody signal intensity indicates the Raw Integrated Intensity of signal detected in the well in the 800nm channel at each cell number dilution, minus the Raw Integrated Intensity of signal detected in the 800nm channel in wells with no cells plated, to correct for background effects, and normalized to amount of DNA detected in the wells, to correct for cell number variation in wells containing treated vs. untreated cells..
(**C**) Antibody signal intensity as a function of the cell number plated per well in the treated cell population only. The R^2 value of 0.9969 for the linear fit demonstrates linearity of detected signal with respect to target protein concentration in the wells over the range of protein concentration represented by 0 to 6,000 cells plated per well

Figure 17. Time-course of cellular signaling (fold activation of phospho-proteins) for cells treated with 0, 5 or 50nM CLM. Fold activation indicates the fold increase in phospho-protein level over the phospho-protein level detected at time 0 (corresponding to no treatment, see Materials and Methods).
(**A**) 0nM CLM treatment:
left panel: early time-points (0-240 minutes)
right panel: full time-course (0-26.5 hours)
For each of the phospho-proteins (except phospho-ATM), each point represents the average of eight biological replicates from two experiments separated in time. For phospho-ATM, each point represents the average of four biological replicates from one experiment.
(**B**) 5nM CLM treatment:

left panel: early time-points (0-240 minutes)
right panel: full time-course (0-26.5 hours)
For each of the phospho-proteins (except phospho-ATM), each point represents the average of six biological replicates from two experiments separated in time. For phospho-ATM, each point represents the average of three biological replicates from one experiment.
(**C**) 50nM CLM treatment:
left panel: early time-points (0-240 minutes)
right panel: full time-course (0-26.5 hours)
For each of the phospho-proteins (except phospho-ATM), each point represents the average of six biological replicates from two experiments separated in time. For phospho-ATM, each point represents the average of three biological replicates from one experiment.

Figure 18. Dose-responsive Cellular-signaling, comparing the fold activation of phospho-proteins in cells treated with 0, 5 and 50nM CLM. Fold activation indicates the fold increase in phospho-protein level over the phospho-protein level detected at time 0 (corresponding to no treatment, see Materials and Methods).
(**A**) **left panel**: phospho-ATM, **right panel**: phospho-Chk2
(**B**) **left panel**: phospho-H2AX, **right panel**: phospho-JNK
(**C**) **left panel**: phospho-p38, **right panel**: phospho-ERK
(**D**) **left panel**: phospho-p53

Figure 19. FACS-based cleaved caspase-3 detection as a read-out for apoptosis (representative plots). The horizontal pink line in each plot separates cell populations with low cleaved caspase-3 (viable) from cell populations with high cleaved caspase-3 (apoptotic).
Upper left: cells treated with 0nM CLM after 12 hours (negative control), 99.3% of the population is viable
Lower left: cells treated with 50nM CLM after 12 hours, 2.6% of the population is apoptotic
Lower middle: cells treated with 50nM CLM after 24 hours, 24.2% of the population is apoptotic
Lower right: cells treated with 50nM CLM after 48 hours, 59.9% of the population is apoptotic

Figure 20. FACS-based cleaved caspase-3 detection as a read-out for apoptosis, for cells treated with 0, 5 and 50nM CLM at 12, 24 and 48 hours. Data from plots is quantified and plotted.

Figure 21. Example of cell-cycle profiles determined by relative propidium iodide incorporation in the population for cells treated with 0, 5 or 50nM CLM at 12, 24 and 48 hours following treatment. Plots are based on whole cell data only (debris gated out) and, within this population, all cells are expected to fall into one of five classes: the sub-G1 population (dead), the G1 population (2N), the S phase population, the G2/M population (4N) or the aneuploid population (> 4N). Each plot is explicitly divided into four areas

that are quantified and represent, from left, the sub-G1 population (dead), the G1 population (2N), the G2/M population (4N) and the aneuploid population (> 4N). The percentage of the total cell population in S phase was determined by subtracting the percentages of cells in all other populations from 100 percent.

Figure 22. Cumulative analysis of cell-cycle profiles from four separate experiments as determined by relative propidium iodide incorporation in the population for cells treated with 0, 5 or 50nM CLM at 12, 24 and 48 hours following treatment. Data from the plots (Figure 21) is quantified and visualized.

VI. References

Allan, J. and L. Travis (2005). "Mechanisms of therapy-related carcinogenesis." Nature Reviews Cancer **5**(12): 943-55.

Appella, E. and C. Anderson (2001). "Post-translational modifications and activation of p53 by genotoxic stresses." European Journal of Biochemistry **268**(10): 2764-72.

Bakkenist, C. J. and M. B. Kastan (2003). "DNA damage activates ATM through intermolecular autophosphorylation and dimer dissociation." Nature **421**(6922): 499-506.

Baldwin, E. and N. Osheroff (2005). "Etoposide, topoisomerase II and cancer." Current Med Chem Anti-Canc Agents **5**(4): 363-72.

Banath, J. and P. Olive (2003). "Expression of phosphorylated histone H2AX as a surrogate of cell killing by drugs that create double-strand breaks." Cancer Research, Advances in brief **3**: 4346-4350.

Bar, J., E. Cohen-Noyman, et al. (2004). "Attenuation of the p53 response to DNA damage by high cell density." Oncogene **23**(12): 2128-37.

Bartek, J. and J. Lukas (2003). "Chk1 and Chk2 kinases in checkpoint control and cancer." Cancer Cell **2**(5): 421-9.

Bassing, C., S. Heikyung, et al. (2003). "Histone H2AX: A dosage-dependent suppressor of oncogenic translocations and tumors." Cell **114**: 359-370.

Bose, B., L. Motiwale, et al. (2005). "DNA damage and G2/M arrest in Syrian hamster embryo cells during malachite green exposure are associated with elevated phosphorylation of ERK1 and JNK1." Cancer Letters **230**: 260-70.

Bulavin, D., S. Amundson, et al. (2002). "p38 and Chk1 kinases: different conductors for the G(2)/M checkpoint symphony." Current Opinion in Genetics and Development **12**(1): 92-7.

Burma, S., B. Chen, et al. (2001). "ATM phosphorylates histone H2AX in response to DNA double-strand breaks." Journal of Biological Chemistry **276**(45): 42462-7.

Caspari, T. (2000). "How to activate p53." Current Biology **10**(8): R3115-7.

Celeste, A., O. Fernandez-Capetillo, et al. (2003). "Histone H2AX phosphorylation is dispensable for the initial recognition of DNA breaks." Nat Cell Biol **5**(7): 675-9.

Chang, L. and M. Karin (2001). "Mammalian MAP kinase signalling cascades." Nature **410**(6824): 37-40.

Chen, B., T. Bohnert, et al. (2004). "5'-(2-phosphoryl-1,4-dioxobutane) as a product of 5'-oxidation of deoxyribose in DNA: elimination as trans-1,4-dioxo-2-butene and approaches to analysis." Chemical Research in Toxicology **17**(11): 1406-13.

Cliby, W., C. Roberts, et al. (1998). "Overexpression of a kinase-inactive ATR protein causes sensitivity to DNA-damaging agents and defects in cell cycle checkpoints." EMBO Journal **17**(1): 159-69.

Cobb, J., T. Schleker, et al. (2005). "Replisome instability, fork collapse, and gross chromosomal rearrangements arise synergistically from Mec1 kinase and RecQ helicase mutations." Genes and Development **19**(24): 3055-69.

Cortez, D., S. Guntuku, et al. (2001). "ATR and ATRIP: partners in checkpoint signaling." Science **294**(5547): 1713-6.

Deacon, K. and J. Blank (1997). "Characterization of the mitogen-activated protein kinase kinase 4 (MKK4)/c-Jun NH2-terminal kinase 1 and MKK3/p38 pathways regulated by MEK kinases 2 and 3." Journal of Biological Chemistry **272**(22): 14489-96.

Elmroth, K., J. Nygren, et al. (2003). "Cleavage of Cellular DNA by calicheamicin gamma-1." DNA Repair **2**: 363-374.

Friesner, J., B. Liu, et al. (2005). "Ionizing radiation-dependent gamma-H2AX focus formation requires ataxia telangiectasia mutated and ataxia telangiectasia mutated and Rad3-related." Molecular Biology of the Cell **16**: 2566-2576.

Fritz, G. and B. Kaina (2005). "Late activation of stress kinases (SAPK/JNK) by genotoxins requires the DNA repair proteins DNA-PKcs and CSB." Molecular Biology of the Cell **Epub ahead of print**.

Gaudet, S., K. Janes, et al. (2005). "A compendium of signals and responses triggered by prodeath and prosurvival cytokines." Molecular and Cellular Proteomics.

Giaccia, A. and M. Kastan (1998). "The complexity of p53 modulation: emerging patterns from divergent signals." Genes and Development **12**(19): 2973-83.

Ho, C., W. Siu, et al. (2005). "The relative contribution of CHK! and CHK2 to Adriamycin-induced checkpoint." Exp Cell Res **304**(1): 1-15.

Ismail, I., S. Nystrom, et al. (2005). "Activation of Ataxia Telangiectasia Mutated by DNA Strand Break-inducing agents correlates closely with the number of DNA Double Strand Breaks." Journal of Biological Chemistry **280**(6): 4649-4655.

Janes, K., J. Albeck, et al. (2003). "A High-throughput quantitative multiplex kinase assay for monitoring information flow in signaling networks." Molecular and Cellular Proteomics.

Janes, K., J. Kelly, et al. (2004). "Cue-Signal response analysis of TNF-induced apoptosis by partial least squares regression of dynamic multivariate data." Journal of Computational Biology **11**(4): 544-561.

Jeong, S., A. Kumagai, et al. (2003). "Phosphorylated Claspin interacts with a phosphate-binding site in the kinase domain of Chk1 during ATR-mediated activation." Journal of Biological Chemistry **278**(47): 46782-8.

Kammouni, W., G. Ramakrishna, et al. (2002). "Increased K-ras protein and activity in mouse and human lung epithelial cells at confluence." Cell Growth and Differentiation **13**(9): 441-8.

Kastan, M. and J. Bartek (2004). "Cell-cycle checkpoints and cancer." Nature **432**: 316-323.

Khanna, K. and S. Jackson (2001). "DNA double-strand breaks: signaling, repair and the cancer connection." Nature Getnetics **27**(3): 247-54.

Kim, S., D. Lim, et al. (1999). "Substrate specificities and identification of putative substrates of ATM kinase family members." Journal of Biological Chemistry **274**(53): 37538-43.

Klein, A. d., M. Muijtjens, et al. (2000). "Targeted disruption of the cell-cycle checkpoint gene ATR leads to early embryonic lethality in mice." Current Biology **10**(8): 479-82.

Lee, J., D. Gold, et al. (2005). "Roles of replication fork-interacting and Chk1-activating domains from Claspin in a DNA replication checkpoint response." Molecular and Cellular Biology **16**(11): 5269-82.

Liang, Z.-X. Assistant Professor, NTU School of Biological Sciences. **2005**.

Lopez-Girona, A., K. Tanaka, et al. (2001). "Serine-345 is required for Rad3-dependent phosphorylation and function of checkpoint kinase Chk1 in fission yeast." PNAS **98**(20): 11289-94.

Lopez-Larraza, D., K. Moore, et al. (2001). "Thiols alter the partitioning of calicheamicin-induced deoxyribose 4'-oxidation reactions in the absence of DNA radical repair." Chemical Research in Toxicology **14**(5): 528-35.

Manke, I., A. Nguyen, et al. (2005). "MAPKAP Kinase-2 is a cell cycle checkpoint kinase that regulates the G2/M transition and S phase progression in response to UV irradiation." Molecular Cell **17**: 37-48.

Matsuoka, S., G. Rotman, et al. (2000). "Ataxia telangiectasia-mutated phosphorylates Chk2 in vivo and in vitro." PNAS **97**(19): 10389-94.

Mekid, H., O. Tounekti, et al. (2003). "In vivo evolution of tumour cells after the generation of double-strand DNA breaks." British Journal of Cancer **88**: 1763-1771.

Melchionna, R., X. Chen, et al. (2000). "Threonine 68 is required for radiation-induced phosphorylation and activation of Cds1." Nat Cell Biol **2**(10): 762-5.

Mochan, T., M. Venere, et al. (2004). "53BP1, an activator of ATM in response to DNA damage." DNA Repair (Amst.) **3**(8-9): 945-52.

Nicolaou, K., A. Smith, et al. (1993). "Chemistry and biology of natural and designed enediynes." PNAS **90**: 5881-5888.

O'Connell, M., N. Walworth, et al. (2000). "The G2-phase DNA-damage checkpoint." Trends in Cell Biology **10**(7): 296-303.

Orton, R., O. Sturm, et al. (2005). "Computational modelling of the receptor-tyrosine-kinase-activated MAPK pathway." Biochemical Journal **392**(part 2): 249-61.

Prives, C. and P. Hall (1999). "The p53 pathway." Journal of Pathology **187**(1): 112-26.

Prokop, A., W. Wrasidlo, et al. (2003). "Induction of apoptosis by enediyne antibiotic calicheamicin gammaII proceeds through a caspase-mediated mitochondrial amplification loop in an entirely Bax-dependent manner." Oncogene **22**: 9107-9120.

Solhaug, A., M. Refsnes, et al. (2004). "Role of cell signalling involved in induction of apoptosis by benzo[a]pyrene and cyclopenta[c,d]pyrene in Hepa1c1c7 cells." Journal of Cellular Biochemistry **93**: 1143-1154.

Sumbayev, V. and I. Yasinska (2005). "Regulation of MAP kinase-dependent apoptotic pathway: implication of reactive oxygen and nitrogen species." Archives of Biochemistry and Biophysics **436**(2005): 406-12.

Takai, H., K. Naka, et al. (2002). "Chk2-deficient mice exhibit radioresistance and defective p53-mediated transcription." EMBO Journal **21**(19): 5195-205.

Taylor, A. and P. Byrd (2005). "Molecular pathology of ataxia telangiectasia." Journal of Clinical Pathology **58**(10): 1009-15.

Tibbetts, R., K. Brumbaugh, et al. (1999). "A role for ATR in the DNA damage-induced phosphorylation of p53." Genes and Development **13**(2): 152-7.

Tobias, R. D. "An introduction to partial least squares regression."

Uegaki, K., Y. Kanamori, et al. (2005). "PTEN is involved in the signal transduction pathway of contact inhibition in endometrial cells." Cell Tissue Research **E-pub ahead of print**: 1-6.

Unsal-Kacmaz, K. and A. Sancar (2004). "Quaternary structure of ATR and effects of ATRIP and replication protein A on its DNA binding and kinase activities." Molecular and Cellular Biology **24**(3): 1292-300.

Vousden, K. (2000). "p53: death star." Cell **103**(5): 691-4.

Widmann, C., S. Gibson, et al. (1999). "Mitogen-activated protein kinase: conservation of a three-kinase module from yeast to human." Physiology Review **79**(1): 143-80.

Xia, Y., C. Makris, et al. (2000). "MEK kinase 1 is critically required for c-Jun N-terminal kinasse activation by proinflammatory stimuli and growth factor-induced cell migration." PNAS **97**(10): 5243-8.

Yoon, H., X. Chen, et al. (2003). "Kruppel-like factor 4 mediates p53-dependent G1/S cell cycle arrest in response to DNA damage." Journal of Biological Chemistry **278**(4): 2101-5.

Yoon, H. and V. Yang (2004). "Requirement of Kruppel-like factor 4 in preventing entry into mitosis following DNA damage." Journal of Biological Chemistry **279**(6): 5035-5041.

Yung, Y., Y. Dolginov, et al. (1997). "Detection of ERK activation by a novel monoclonal antibody." FEBS Letters **408**(3): 292-6.

Zhao, H. and H. Piwnica-Worms (2001). "ATR-mediated checkpoint pathways regulate phosphorylation and activation of human Chk1." Molecular and Cellular Biology **21**(13): 4129-39.

Zhou, B. and J. Bartek (2004). "Targeting the checkpoint kinases: chemosensitization versus chemoprotection." Nature Reviews **4**.

Zhou, B., P. Chaturvedi, et al. (2000). "Caffeine abolishes the mammalian G(2)/M DNA damage checkpoint by inhibiting ataxia-telangiectasia-mutated activity." Journal of Biological Chemistry **275**(14): 10342-8.

Zou, L. and S. Elledge (2003). "Sensing DNA damage through ATRIP recognition of RPA-ssDNA complexes." Science **300**(5625): 1542-8.

Figure 1

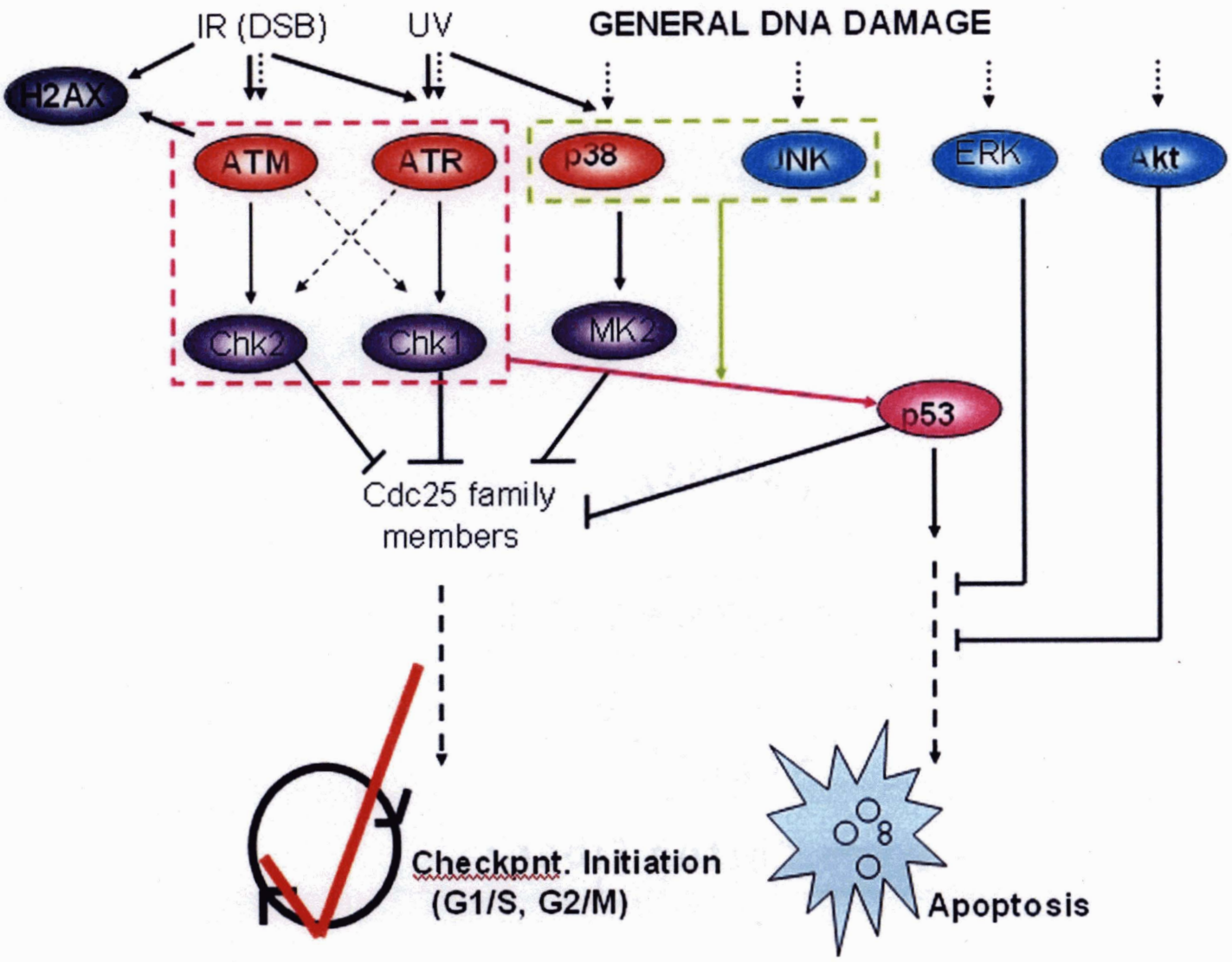
IR (DSB)
UV
GENERAL DNA DAMAGE
H2AX
ATM
ATR
p38
JNK
ERK
Akt
Chk2
Chk1
MK2
p53
Cdc25 family members
Checkpnt. Initiation (G1/S, G2/M)
Apoptosis

Figure 2

A

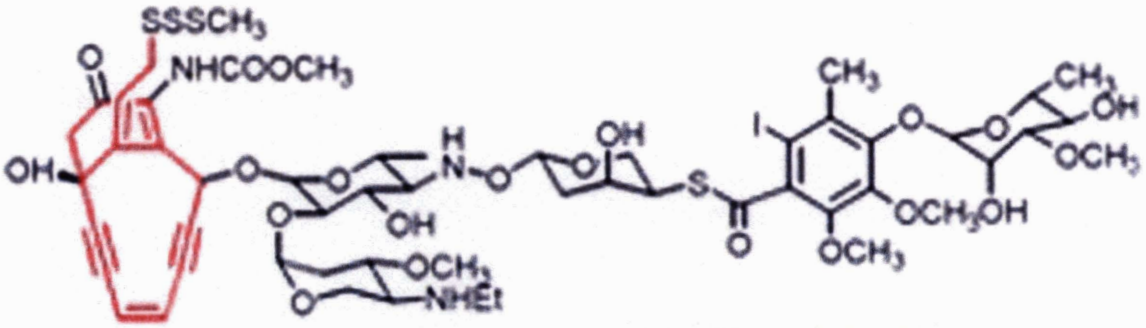

Calicheamicin (1)

B

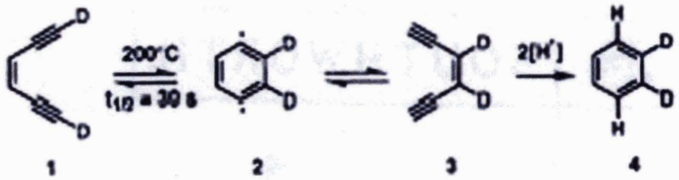

Figure 3

A

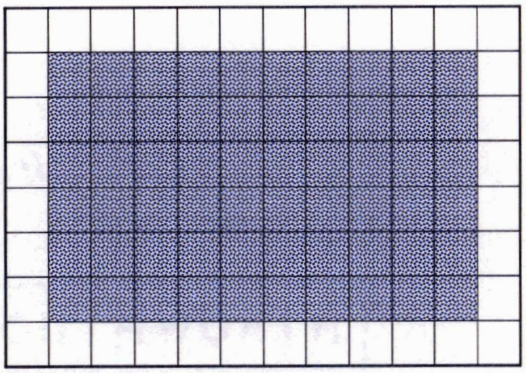

1. seed at 10,000 cells per well in 200ul total volume

B

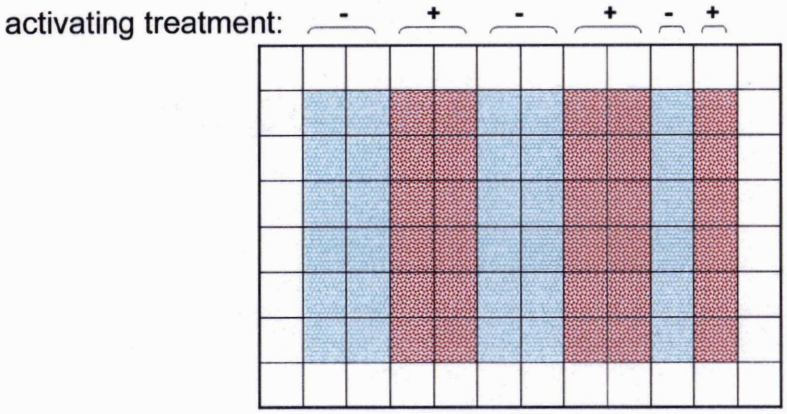

2. treat or not with activating treatment

C

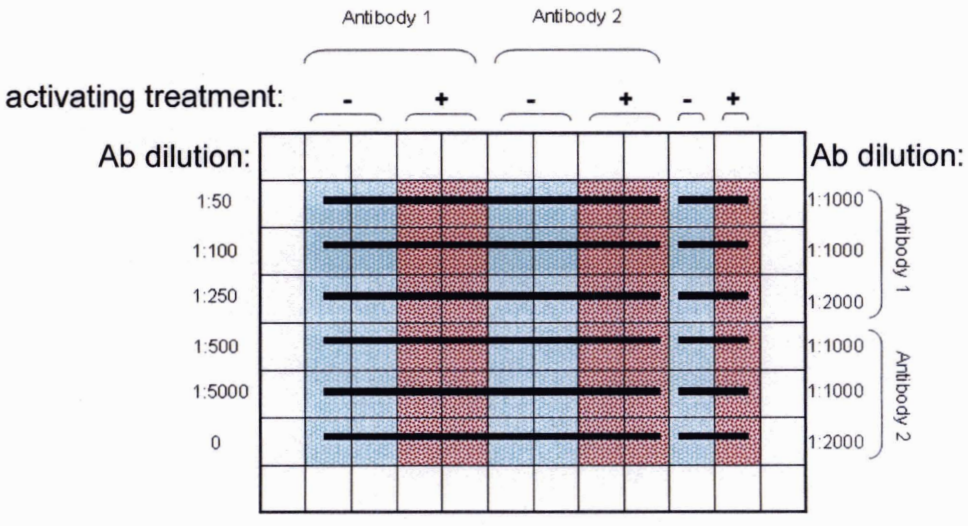

3. immuno-stain using antibody dilutions ranging from 1:50 to 1:5000

Figure 4

A

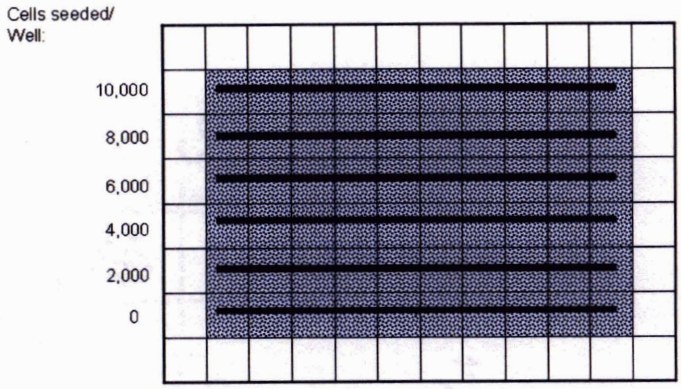

1. seed a dilution of cells, from 10,000 cells seeded per well to 2,000 cells seeded per well

B

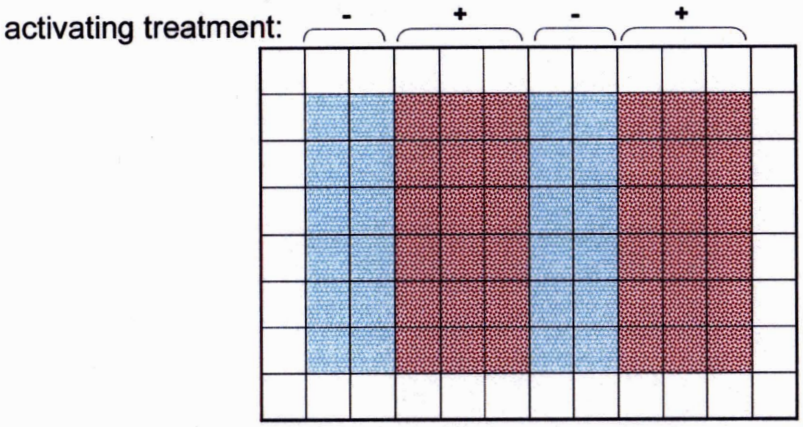

2. treat or not with activating treatment

C

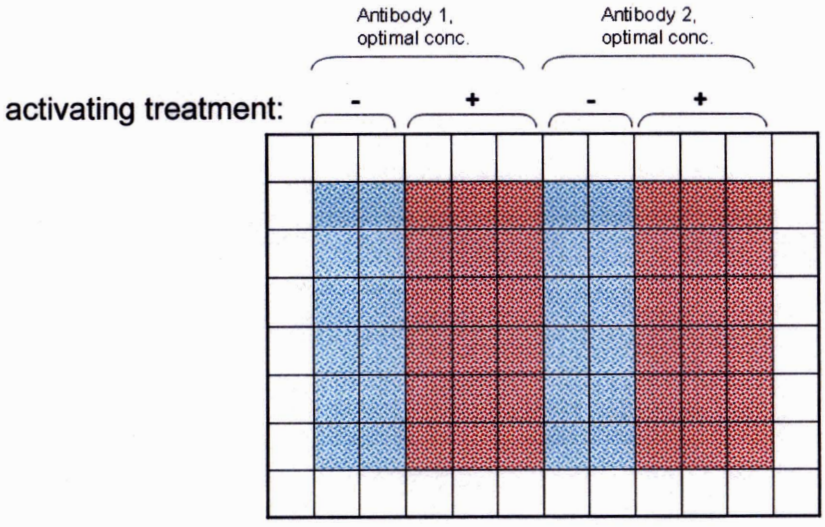

3. immuno-stain with antibody using optimal antibody dilution determined in Antibody dilution experiments

Figure 5

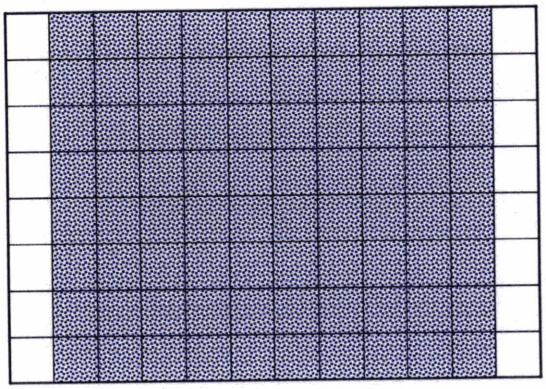

seed (6,000 cells/well),
incubate O/N, 37C

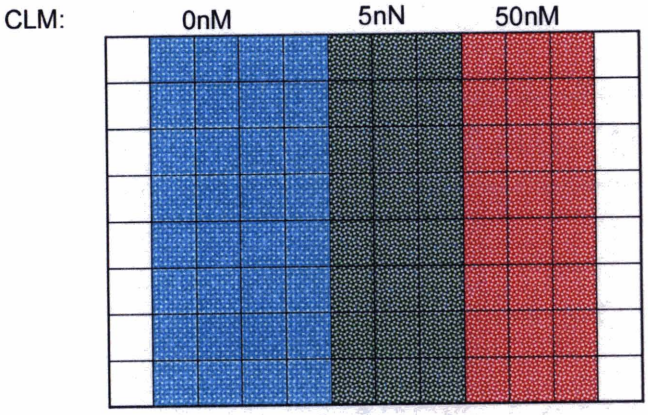

treatments

(fix, permeabilize, block)

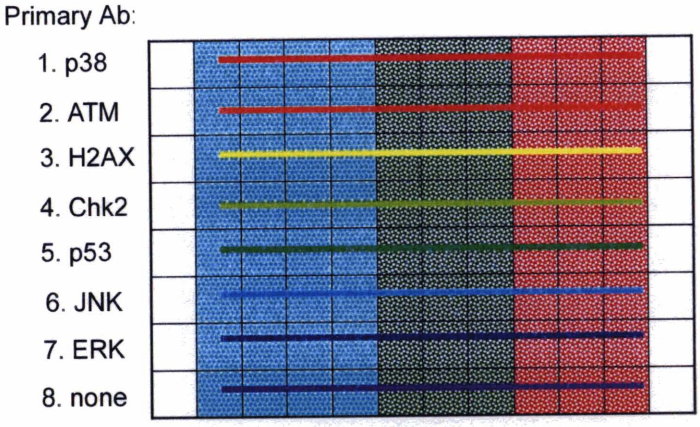

primary incubation

secondary incubation, visualize (scan)

Figure 6

A

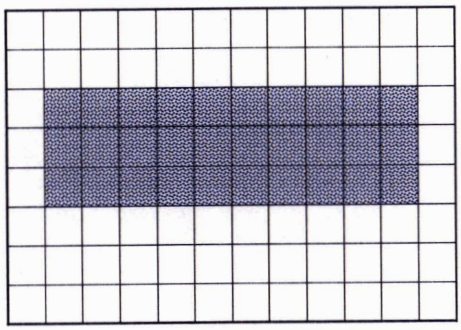

1. seed at 6,000 cells per well

B

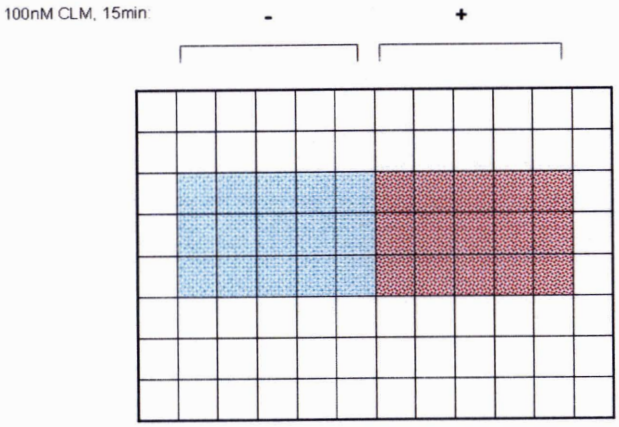

2. treat or not for 15 minutes with 100nM CLM

C

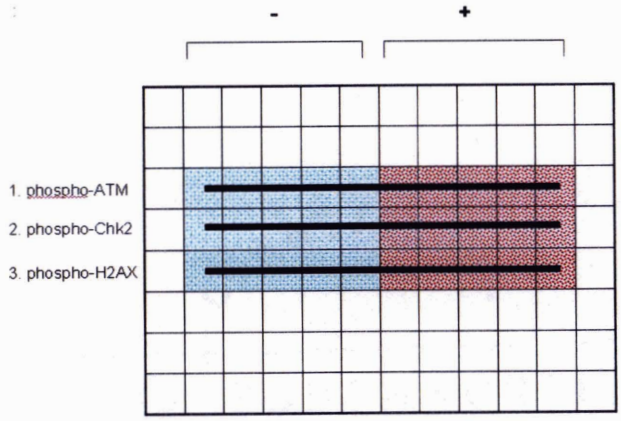

3. immuno-stain with phospho-ATM, Chk2 and H2AX antibodies

Figure 7

A

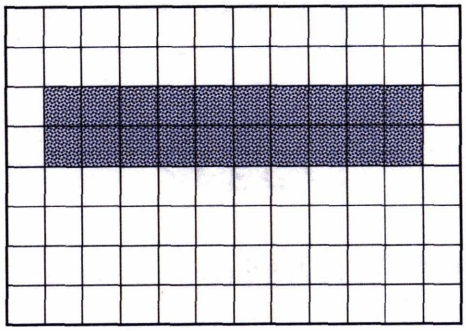

1. seed cells at 6,000 cells per well

B

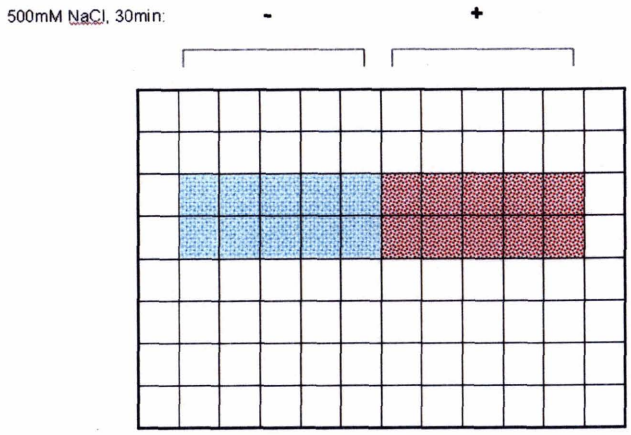

2. treat cells for 30 minutes with 500mM NaCl

C

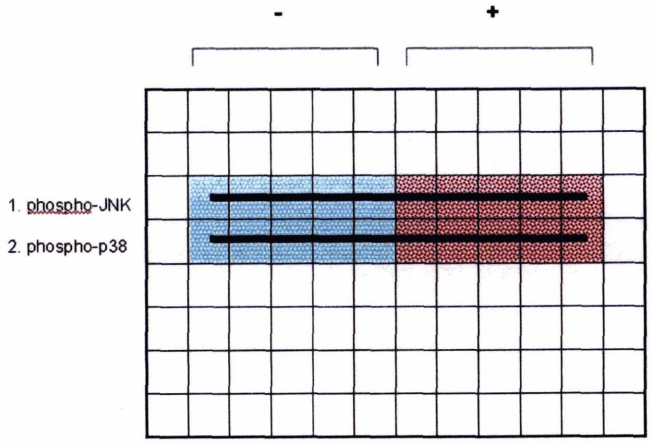

3. immuno-stain with phospho-JNK and p38 antibodies

Figure 8

A

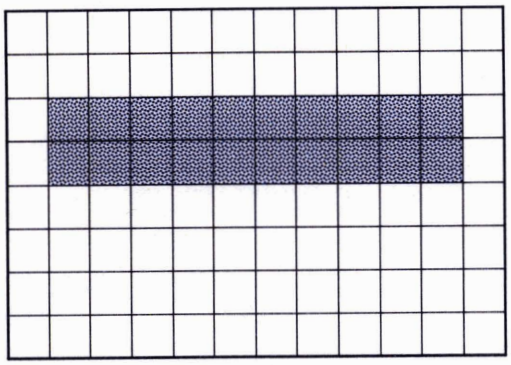

1. seed cells at 6,000 cells per well

B

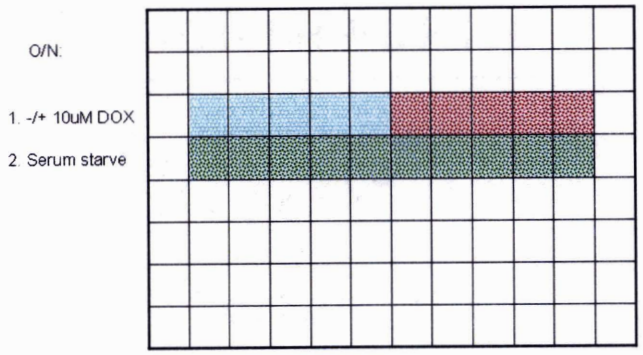

2. treat or do not treat in one row with DOX for 12 hours; replace media in remaining row with serum starvation media (0.1% FBS)

C

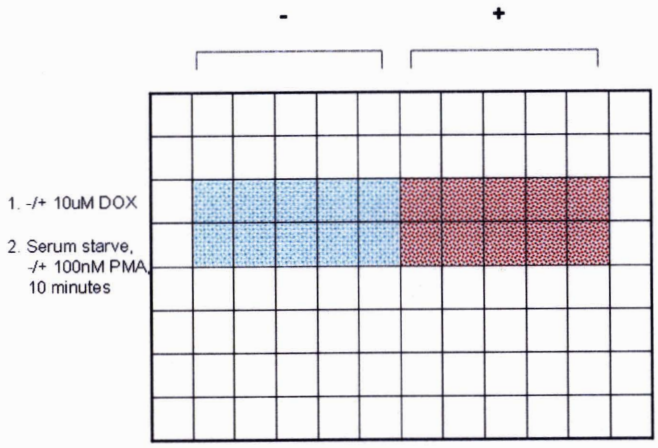

3. treat or do not treat serum starved cells with 10uM PMA for 10 minutes

D

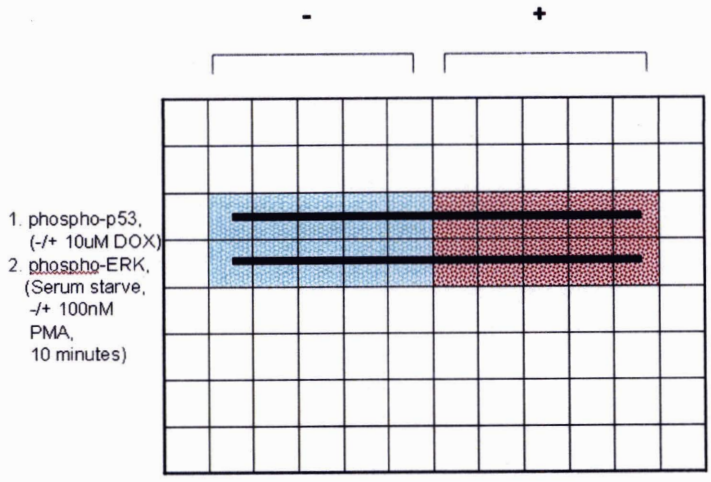

4. immuno-stain DOX (+/-) treated with phospho-p53 antibody; immuno-stain PMA (+/-) treated with phospho-ERK antobody

Figure 9

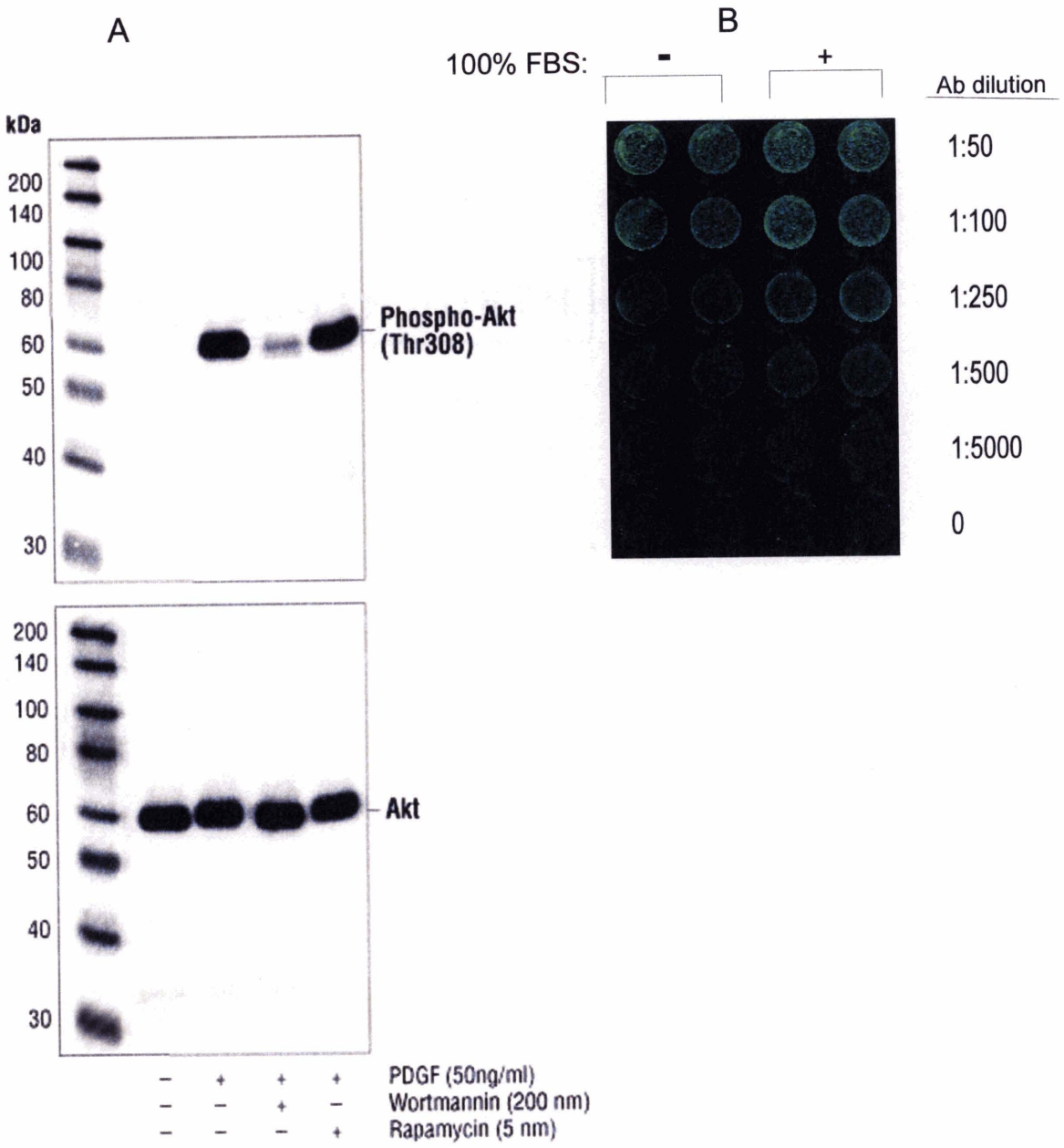
A
B
kDa
200
140
100
80
60
50
40
30
Phospho-Akt
(Thr308)
Akt
PDGF (50ng/ml)
Wortmannin (200 nm)
Rapamycin (5 nm)
100% FBS:
-
+
Ab dilution
1:50
1:100
1:250
1:500
1:5000
0

Figure 10

A

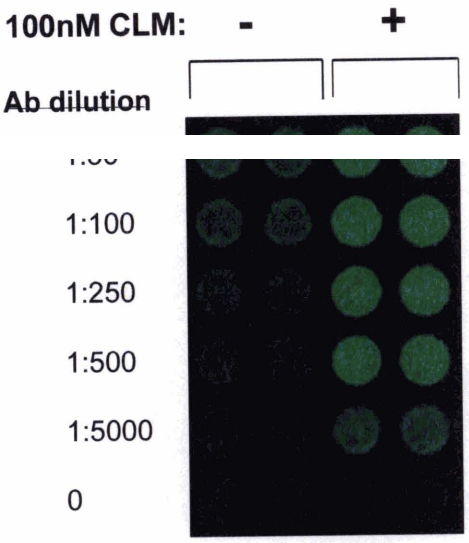

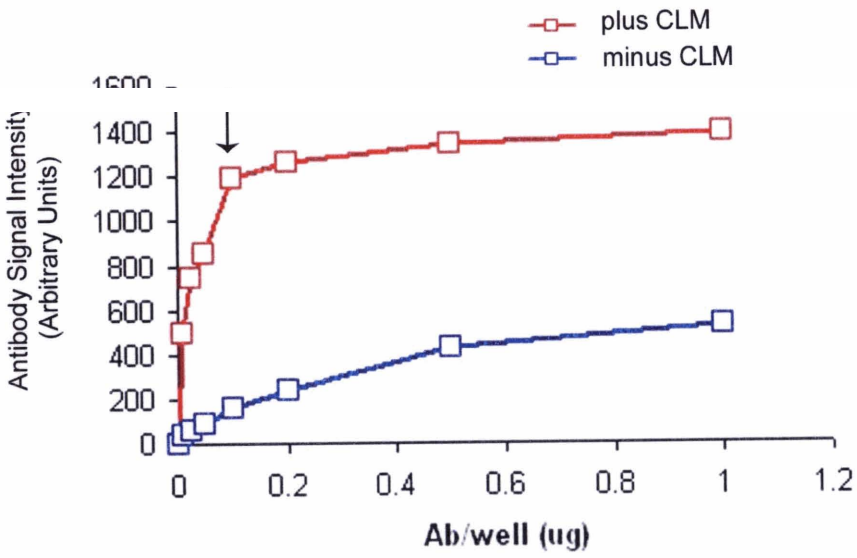

B

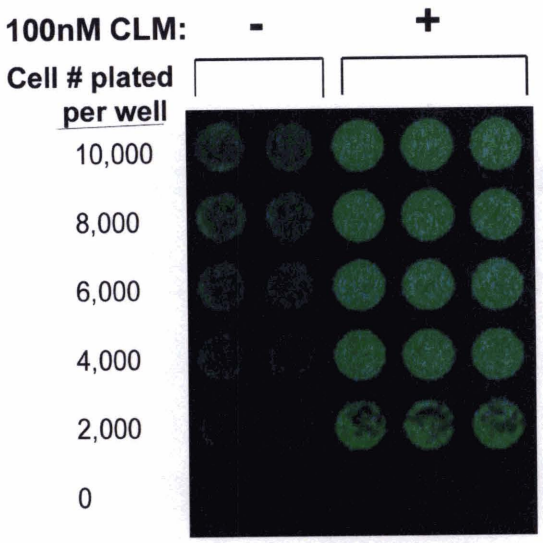

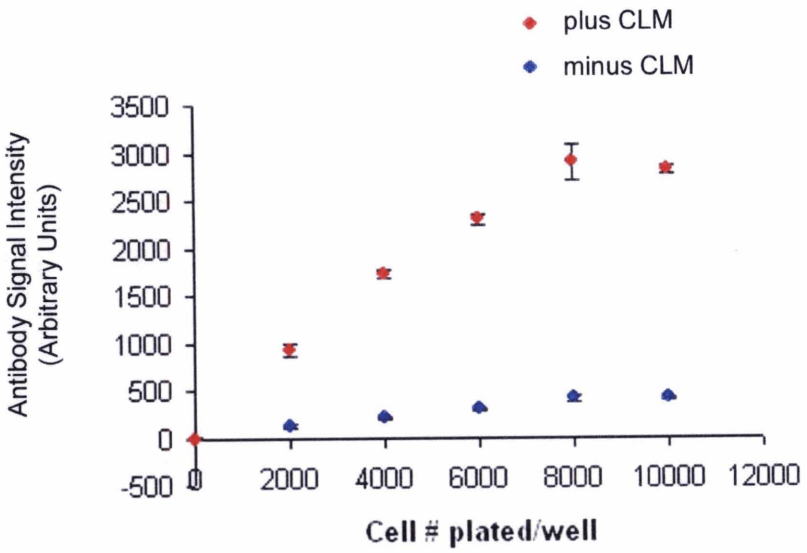

C

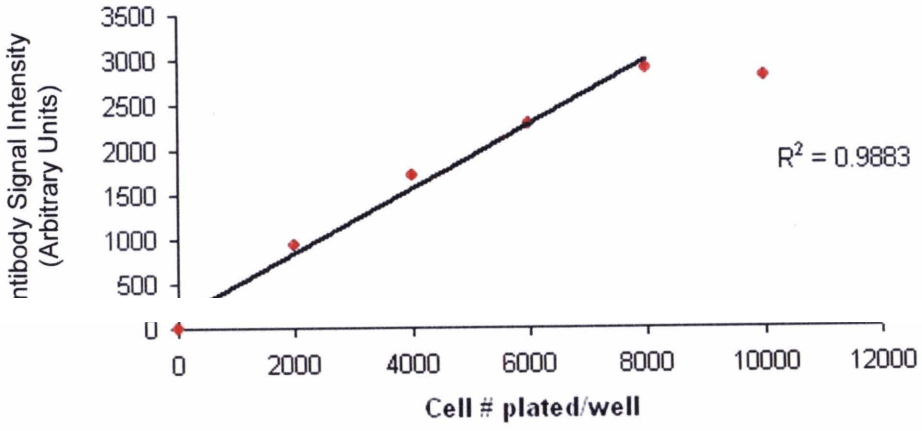

Figure 11

A

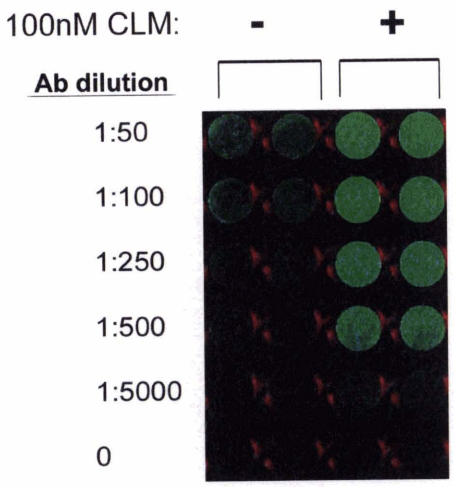

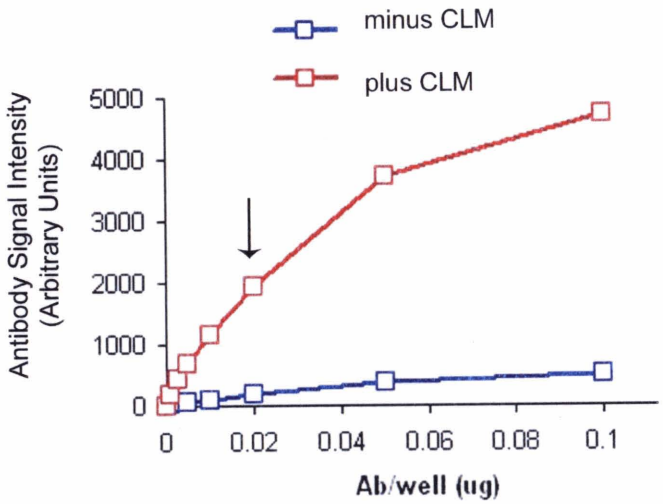

B

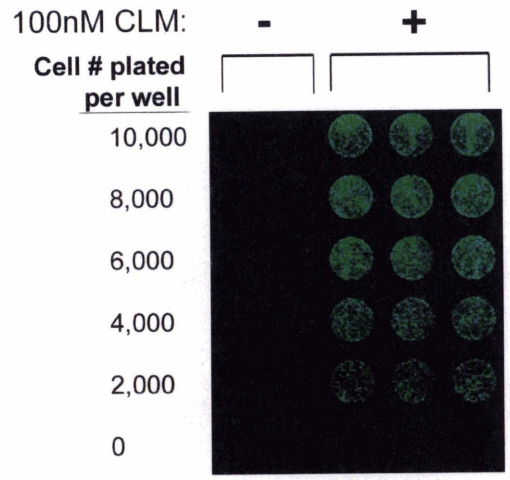

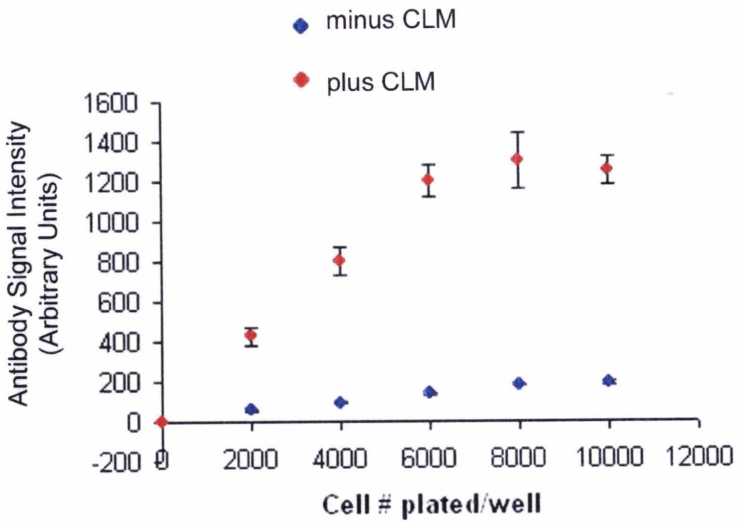

C

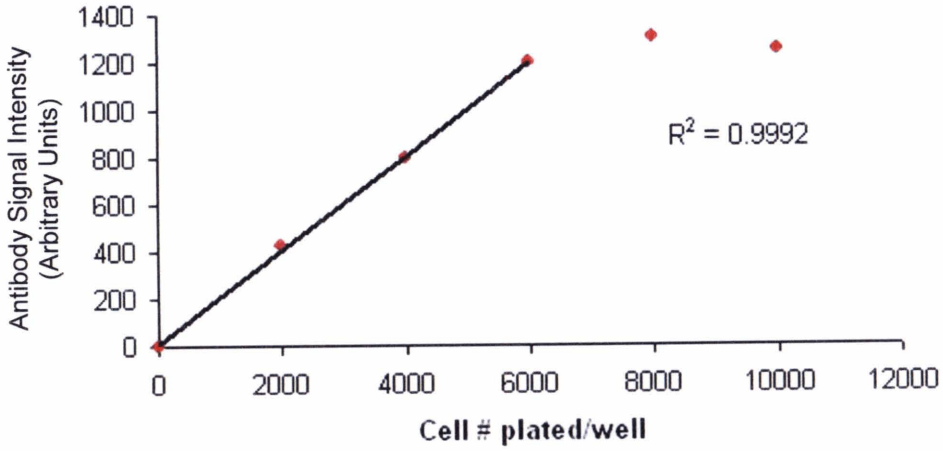

Figure 12

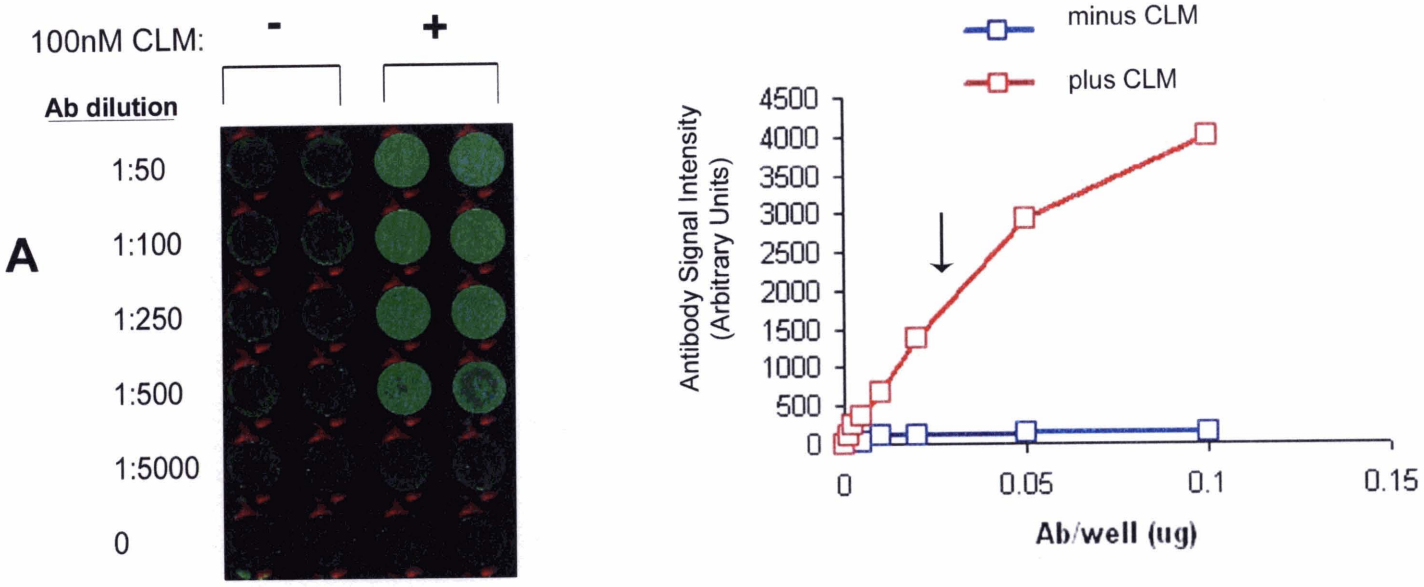
A
100nM CLM:
-
+
Ab dilution
1:50
1:100
1:250
1:500
1:5000
0
minus CLM
plus CLM
Antibody Signal Intensity (Arbitrary Units)
4500
4000
3500
3000
2500
2000
1500
1000
500
0
0
0.05
0.1
0.15
Ab/well (ug)

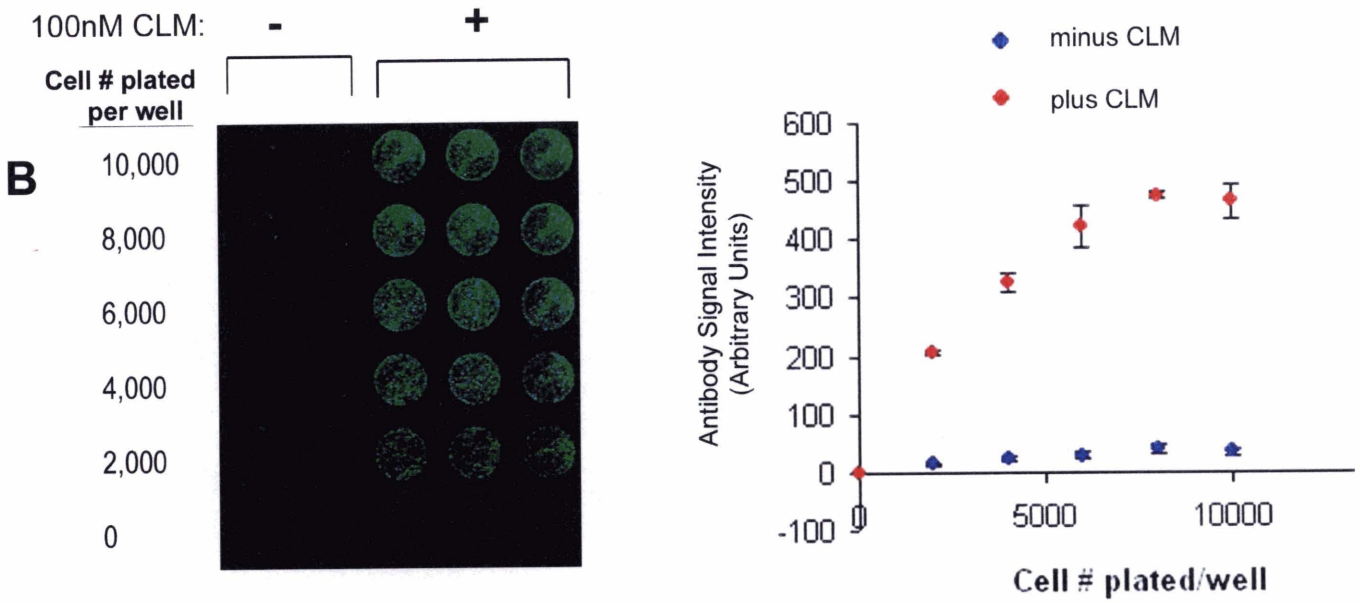
B
100nM CLM:
-
+
Cell # plated per well
10,000
8,000
6,000
4,000
2,000
0
minus CLM
plus CLM
Antibody Signal Intensity (Arbitrary Units)
600
500
400
300
200
100
0
-100
0
5000
10000
Cell # plated/well

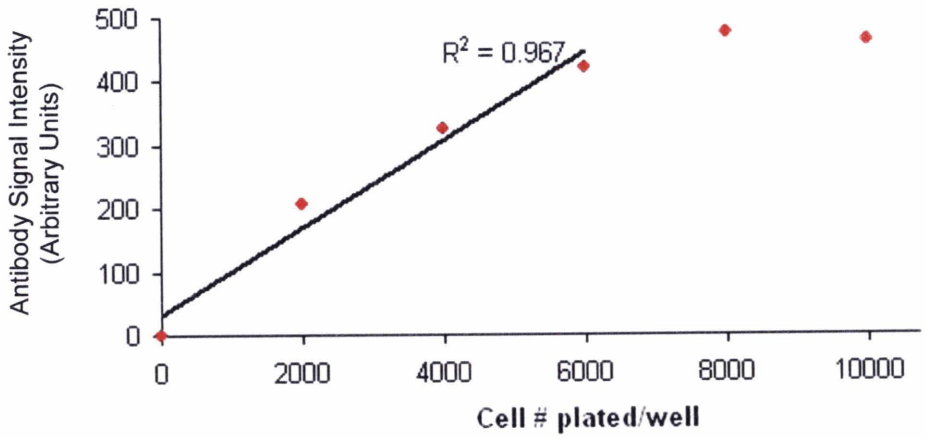
C
Antibody Signal Intensity (Arbitrary Units)
500
400
300
200
100
0
R2 = 0.967
0
2000
4000
6000
8000
10000
Cell # plated/well

Figure 13

A

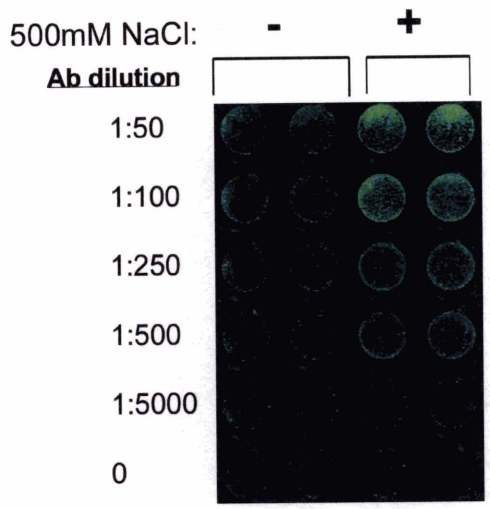

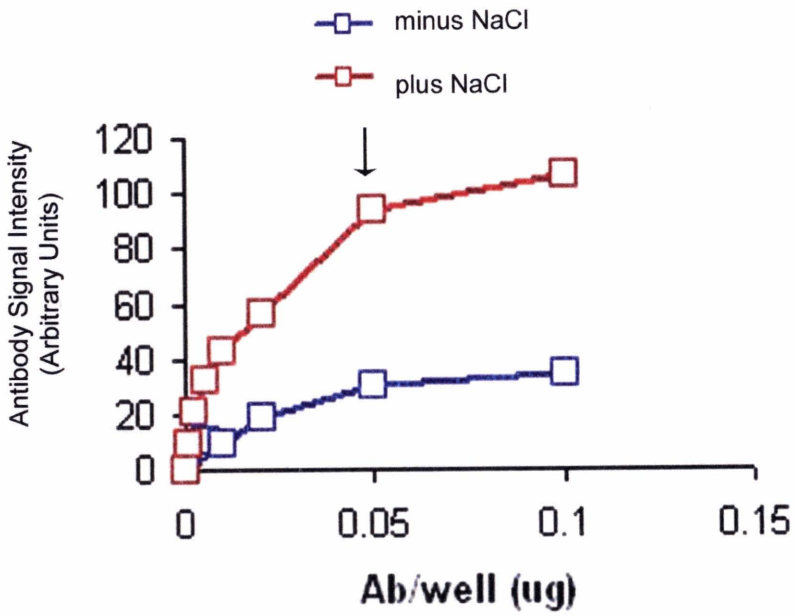

B

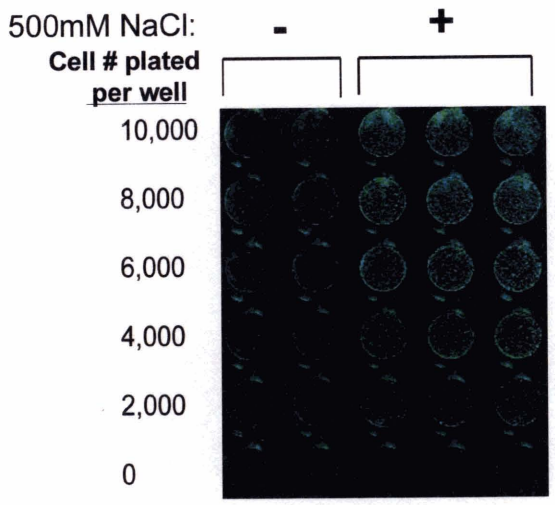

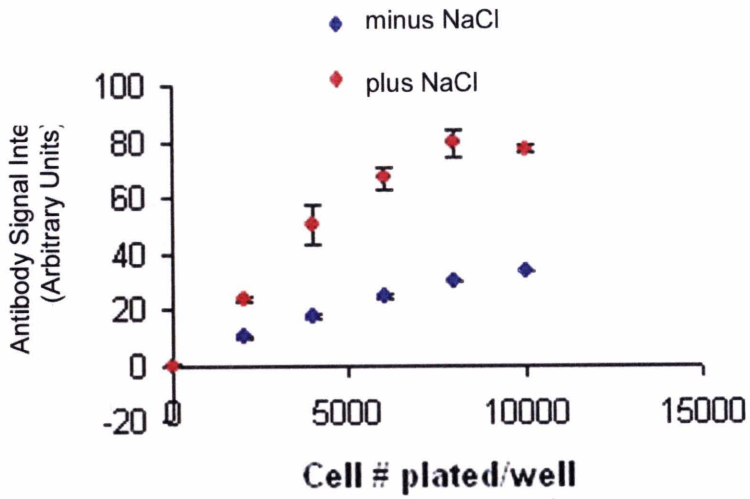

C

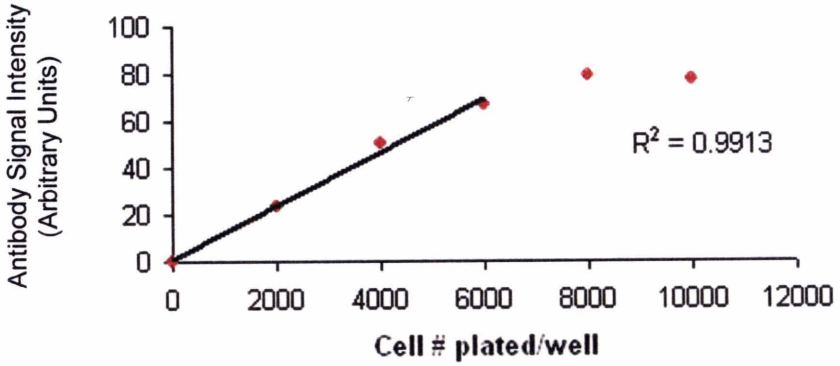

Figure 14

A

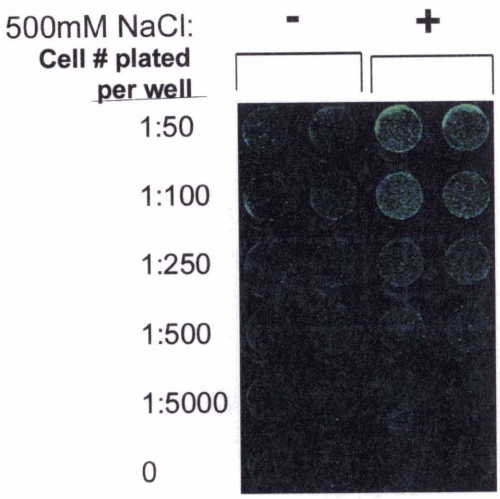

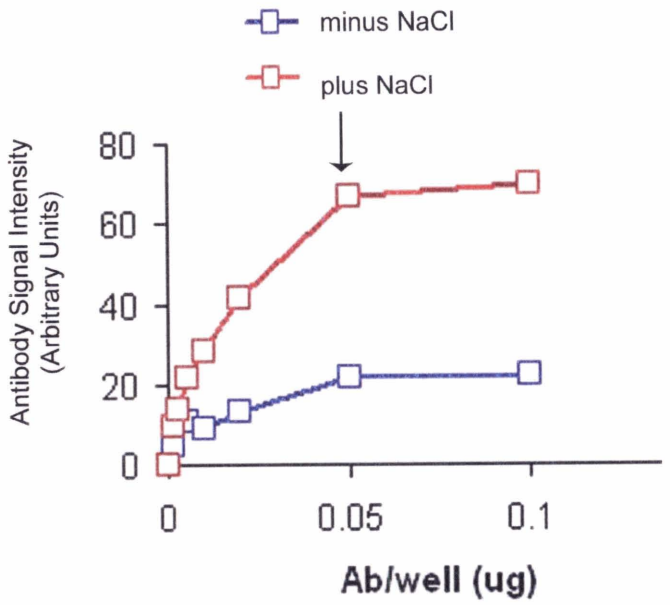

B

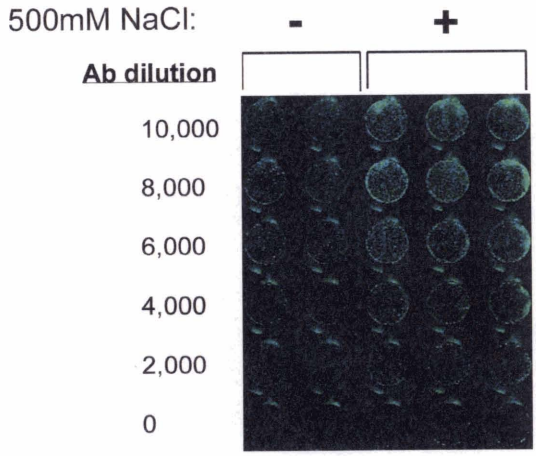

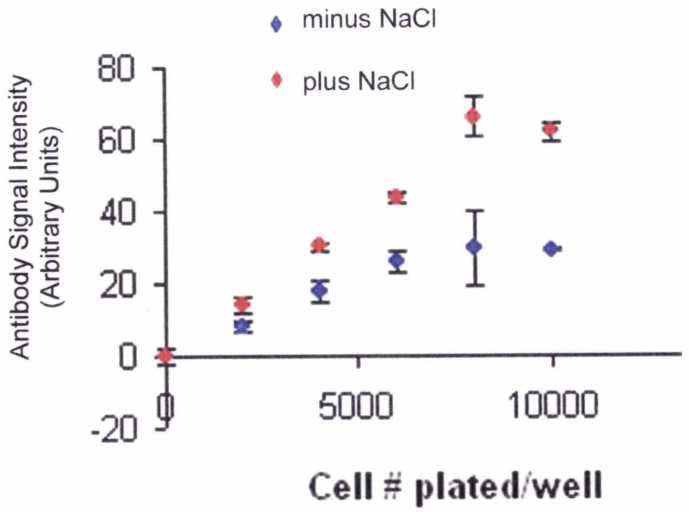

C

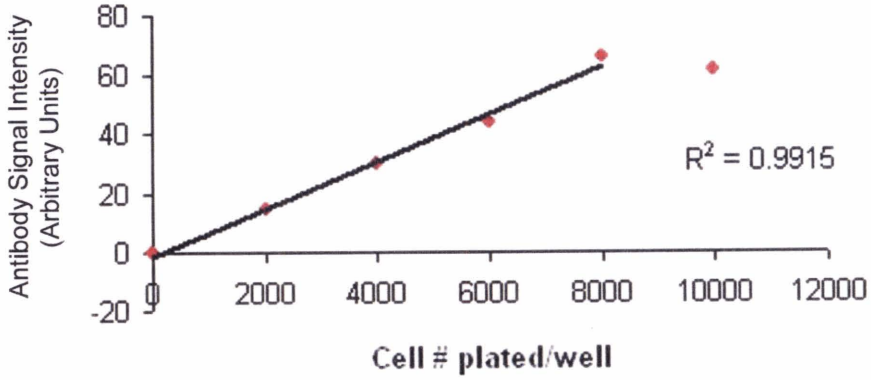

Figure 15

A

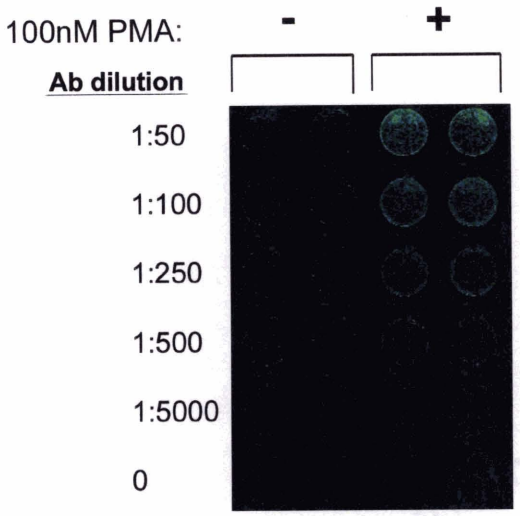

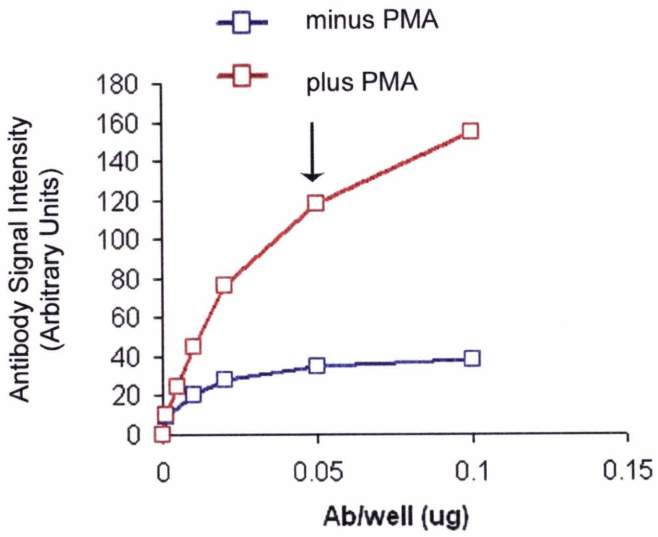

B

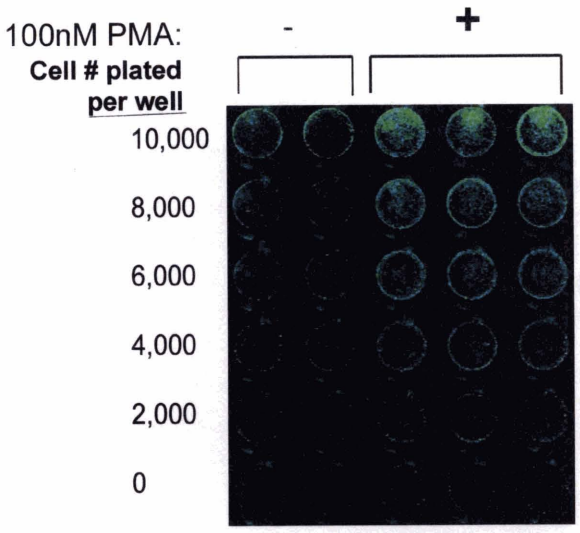

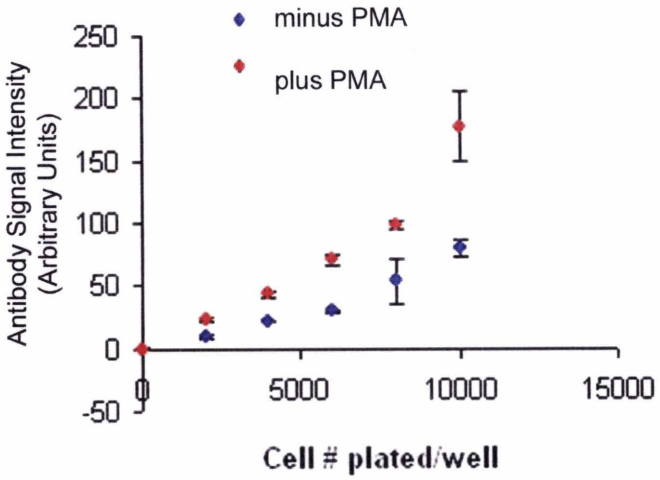

C

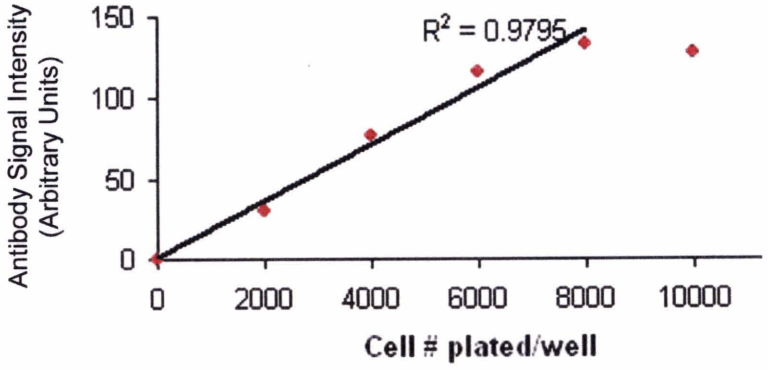

Figure 16

A

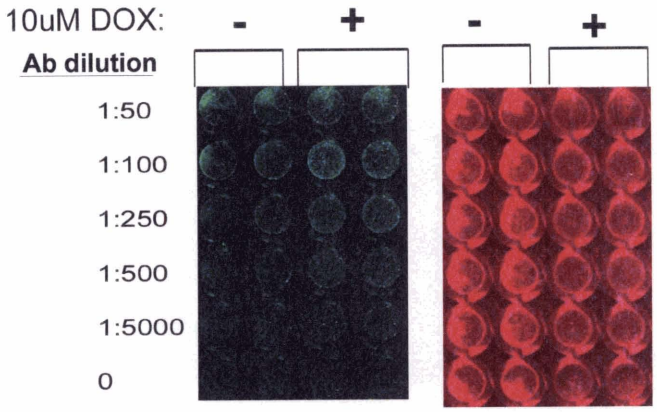

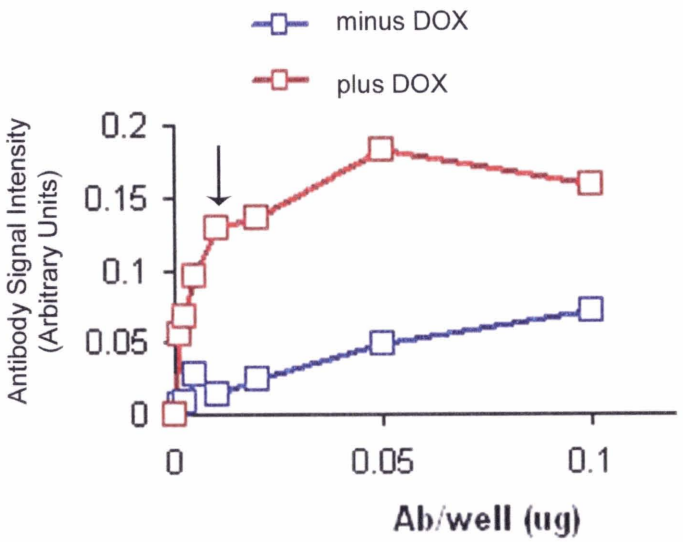

B

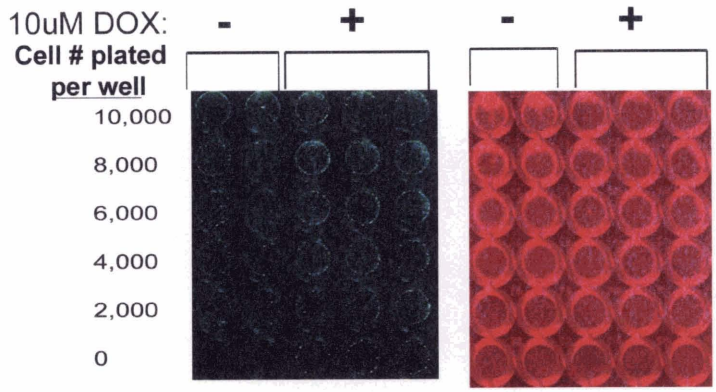

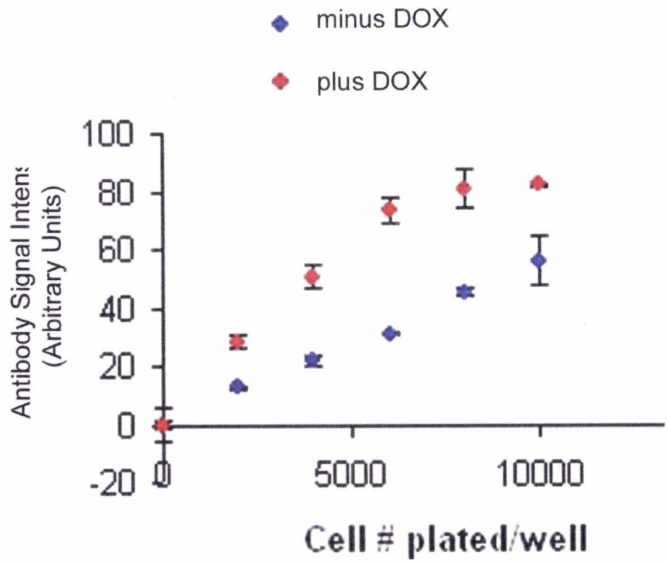

C

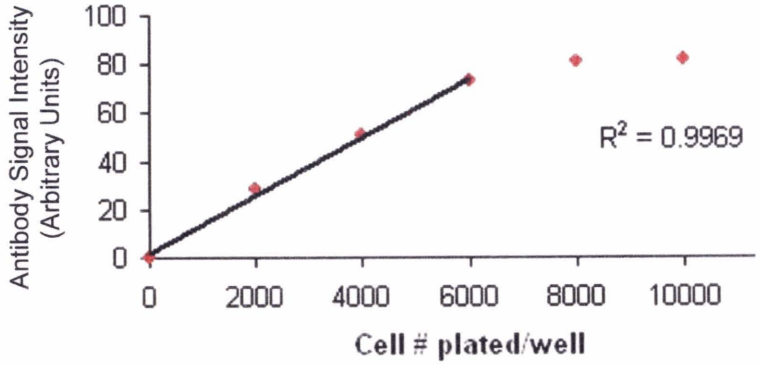

Figure 17

early time-points

all time-points

A 0nM CLM

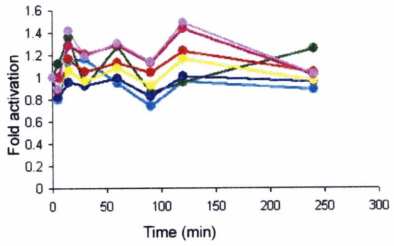

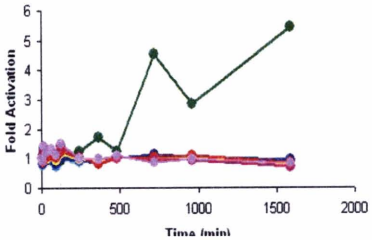

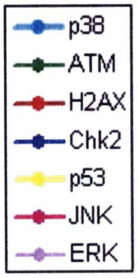

B 5nM CLM

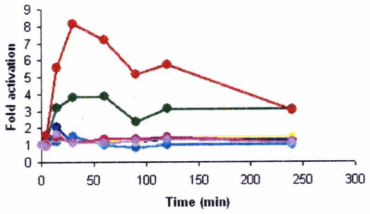

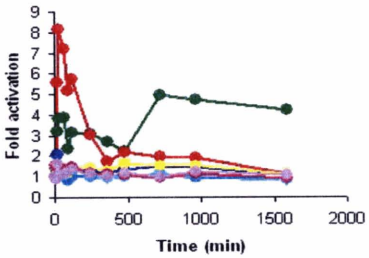

C 50nM CLM

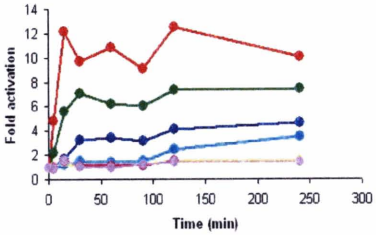

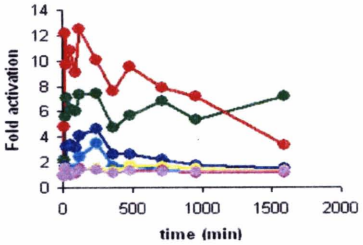

Figure 18

A

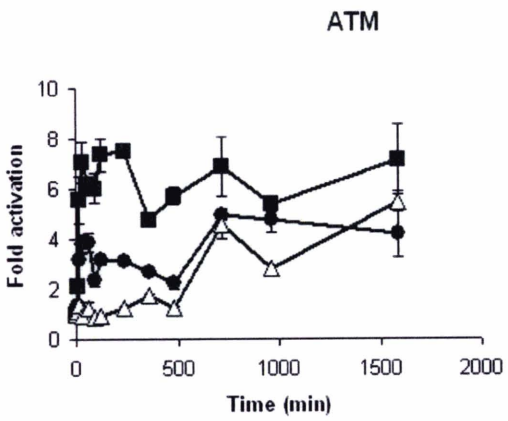

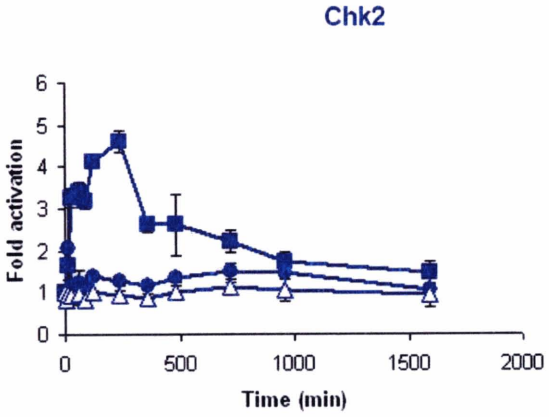

B

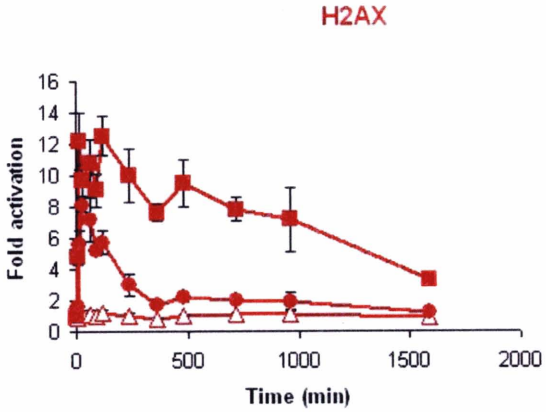

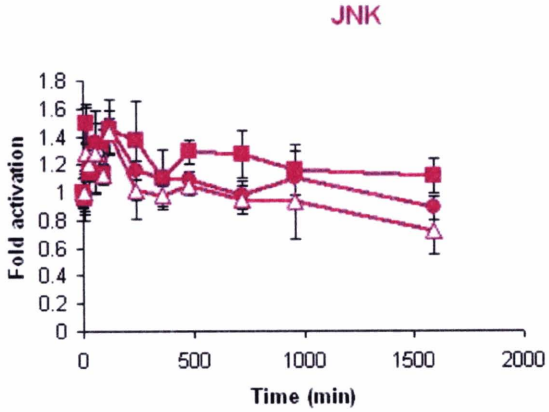

C

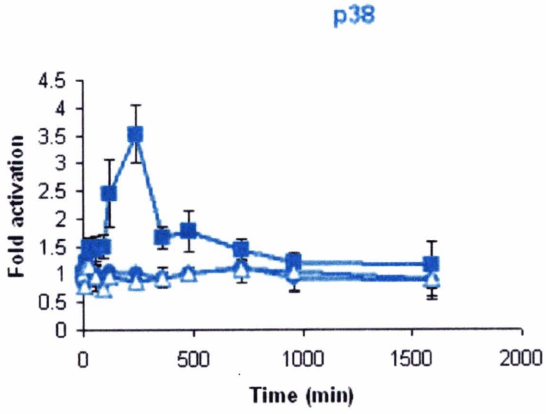

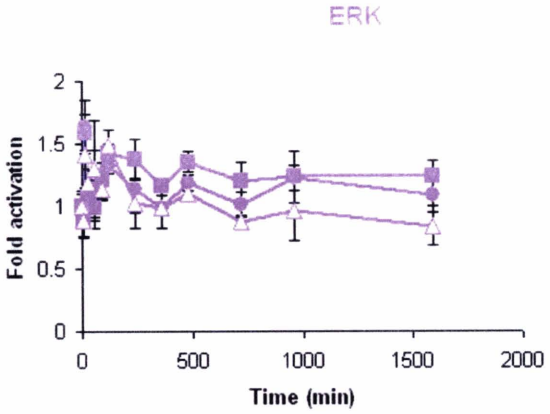

D

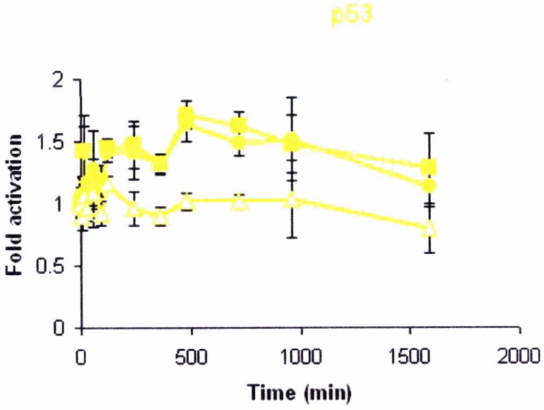

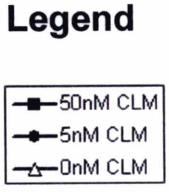

Figure 19

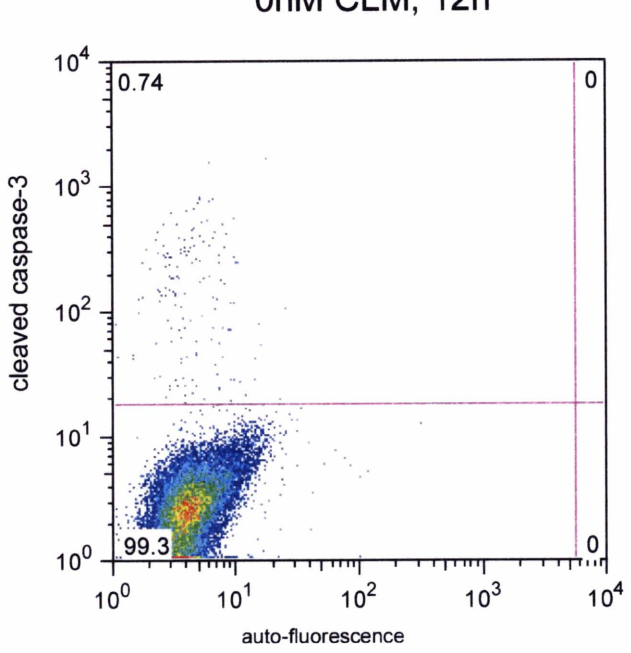
0nM CLM, 12h
0.74
99.3
0
0
cleaved caspase-3
auto-fluorescence

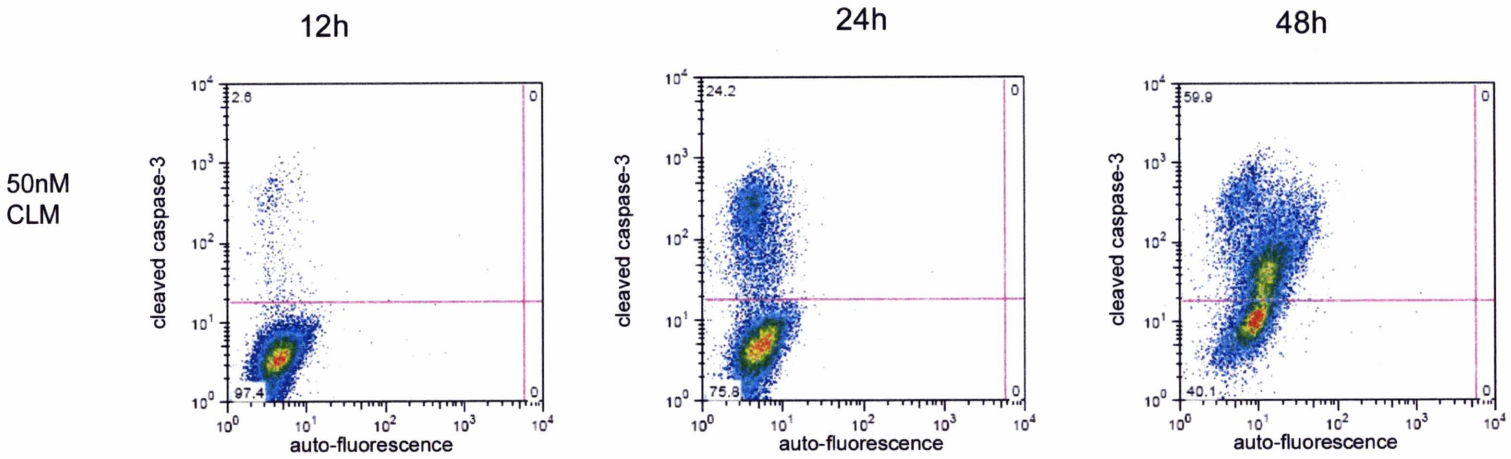
12h
24h
48h
50nM CLM
2.6
97.4
24.2
75.8
59.9
40.1
cleaved caspase-3
auto-fluorescence

Figure 20

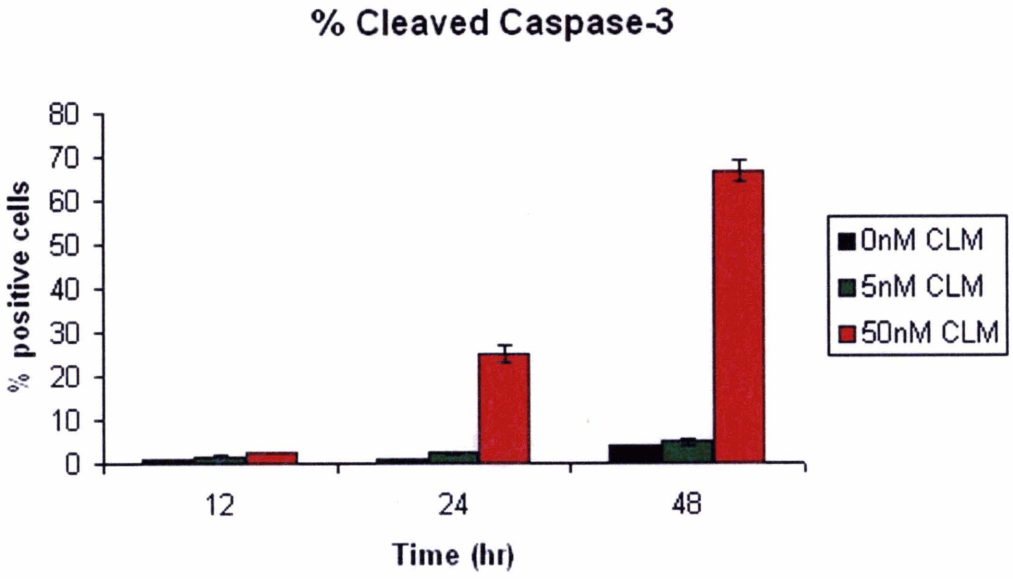
% Cleaved Caspase-3
% positive cells
80
70
60
50
40
30
20
10
0
12
24
48
Time (hr)
0nM CLM
5nM CLM
50nM CLM

Figure 21

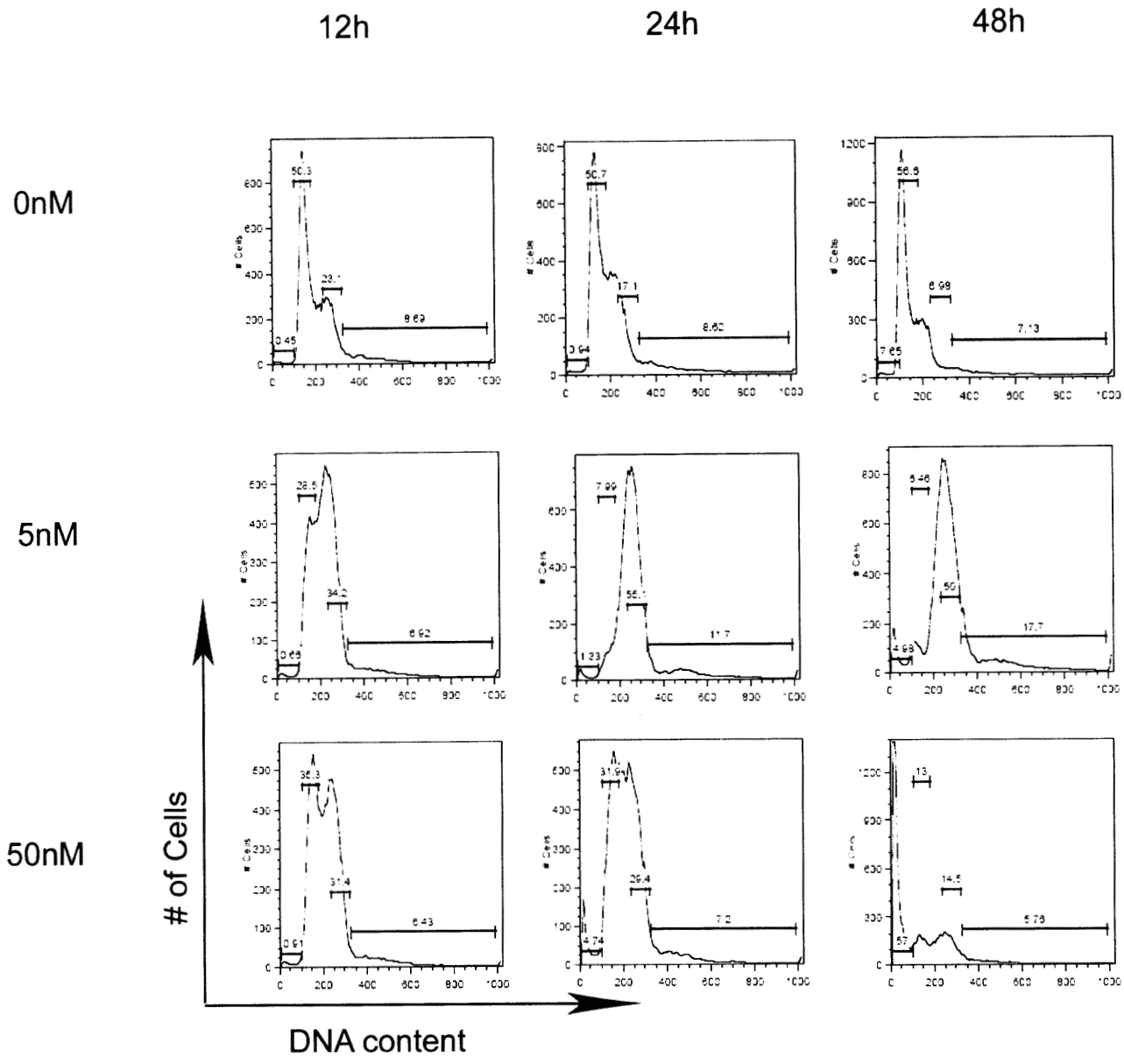

Figure 22

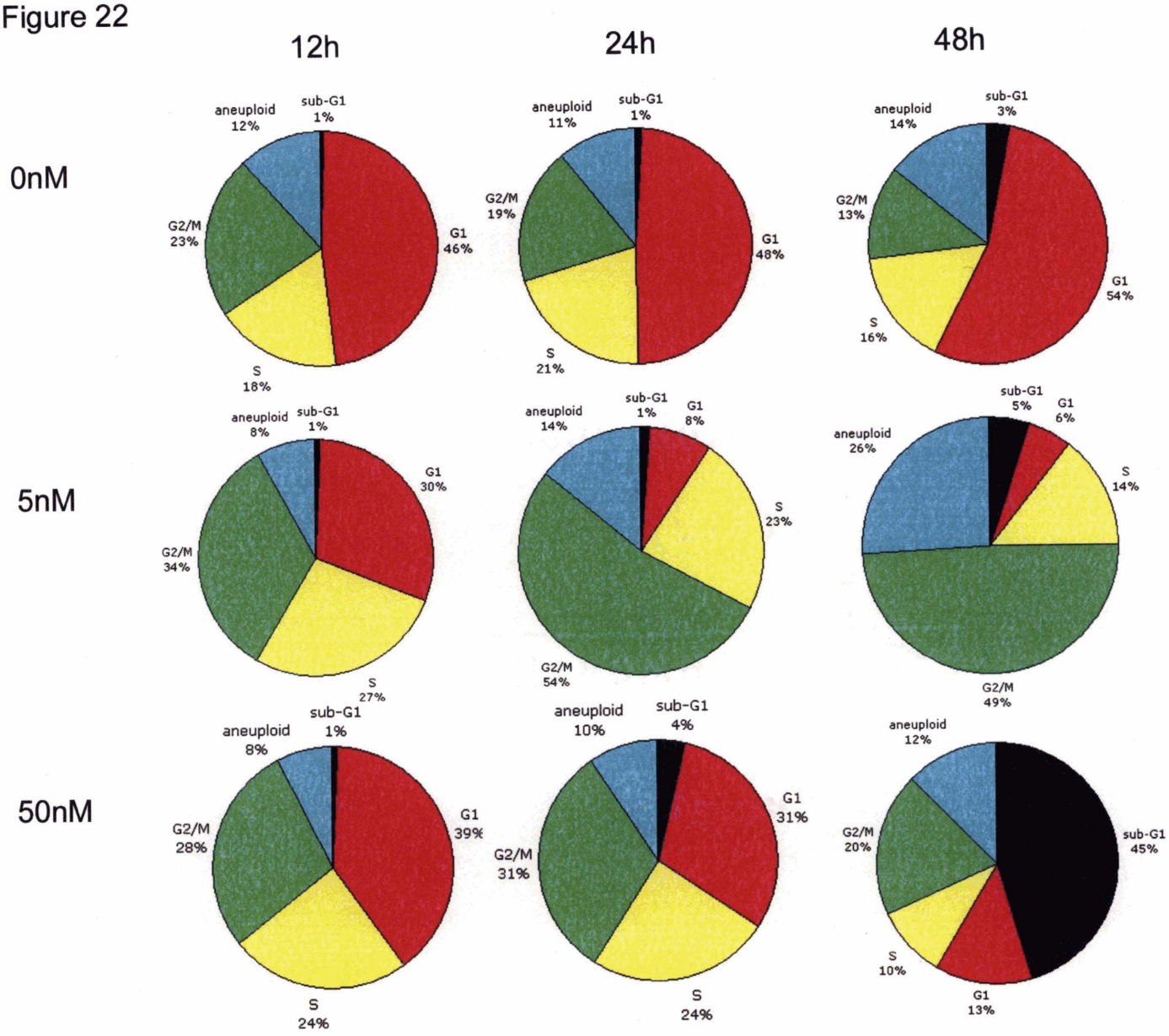
12h
24h
48h
0nM
5nM
50nM
aneuploid 12%
sub-G1 1%
G1 46%
S 18%
G2/M 23%
aneuploid 11%
sub-G1 1%
G1 48%
S 21%
G2/M 19%
aneuploid 14%
sub-G1 3%
G1 54%
S 16%
G2/M 13%
aneuploid 8%
sub-G1 1%
G1 30%
S 27%
G2/M 34%
aneuploid 14%
sub-G1 1%
G1 8%
S 23%
G2/M 54%
aneuploid 26%
sub-G1 5%
G1 6%
S 14%
G2/M 49%
aneuploid 8%
sub-G1 1%
G1 39%
S 24%
G2/M 28%
aneuploid 10%
sub-G1 4%
G1 31%
S 24%
G2/M 31%
aneuploid 12%
sub-G1 45%
G1 13%
S 10%
G2/M 20%